

**LINEAR STABILITY ANALYSIS OF CIRCULAR JETS:
INTEGER, FRACTIONAL, AND MULTIPLE MODE EXCITATION**

by

Matthew Pancoast Leimkuhler

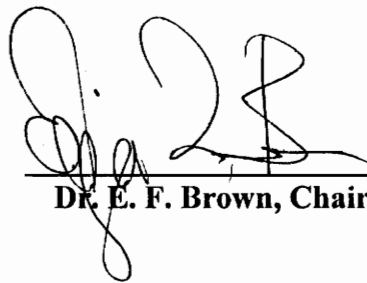
Thesis submitted to the Faculty of the
Virginia Polytechnic Institute and State University
in partial fulfillment of the requirements for the degree of

Master of Science

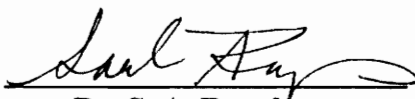
in

Mechanical Engineering

APPROVED:



Dr. E. F. Brown, Chairman



Dr. S. A. Ragab



Dr. U. Vandsburger

December, 1995

2

LD
5655
V855
1995
L467
C.2

LINEAR STABILITY ANALYSIS OF CIRCULAR JETS: INTEGER, FRACTIONAL, AND MULTIPLE MODES

by

Matthew Pancoast Leimkuhler

Committee Chairman: Eugene F. Brown

Department of Mechanical Engineering

(ABSTRACT)

The linear stability analysis of Huang [1995] has been adapted to ignore the effects of swirl, and to allow calculation of the eigenvalues and eigenfunctions for integer, fractional, and multiple modes of excitation. The investigation was intended to be exploratory; to gain the best possible insights into the flow characteristics from analysis of the linearized Euler equations. All of the azimuthal modes investigated (one-half, one, three-halves, and two) were found to lead to the continuous, helical, vortical structure evolution in the streamwise direction of the jet. The analysis for fractional modes of excitation predicted aphysical behavior near the jet center that has been attributed to unresolved questions in the mathematical analysis of the problem. Multiple mode excitation at the axisymmetric mode and one or more azimuthal modes were found to result in un-even, periodic, vortex-ring growth in the shear layer. An argument was presented for the axisymmetric mode ($m=0$) resulting in the highest levels of entrainment for all integer, fractional, and multiple modes of excitation. Finally the importance of the azimuthal

component of vorticity in the entrainment process was identified.

ACKNOWLEDGMENTS:

First, I would like to thank Dr. Brown for his instruction and guidance throughout this undertaking. I would also like to thank Dr. S. A. Ragab and Dr. U. Vandsburger for serving on my advisory committee. Special thanks also go to Shiling Huang for the outstanding and thorough explanation of circular jet stability analysis in his Ph.D. Dissertation, and for his insights and recommendations to overcome some of the difficulties experienced in this effort.

Thanks are also due to the staff of the computer laboratories at Virginia Tech, both the MECA Lab and the Laboratory for Scientific Visualization. I would like to thank Dr. R. Kriz and M. Butsch for their upkeep of the visualization lab, and M. Kafura and B. Poe for their efforts in maintaining the MECA Lab.

Sincere thanks also go to my families, for their love and support (emotional and financial) throughout the extent of my work.

Finally, and most importantly, I thank my fiancée, Sherri, for her love, support, patience, and understanding throughout, without whom, this work would not have been possible.

TABLE OF CONTENTS

Chapter 1: Introduction

1.1	Free Jet Flows	1
1.2	Applications of Free Jets	3
1.3	Historical Background	4
1.4	Circular Jet Stability and Relevant Discoveries	8
1.5	Goals and Methodology	13

Chapter 2: Circular Jet Stability Analysis

2.1	Linear Stability Analysis	16
2.2	Developing the Eigenvalue Problem	18
2.3	Solving the Eigenvalue Problem	28

Chapter 3: Integer, Fractional, and Multiple Modes

3.1	Experimental and Theoretical Excitation	37
3.2	Integer Modes of Excitation	39
3.3	Multi-Mode Excitation	42
3.4	Results -- Streakline Visualizations	46
3.4.1	Integer Modes of Excitation	46
3.4.2	Multi-Mode Excitation	50

Chapter 4: Entrainment

4.1	Description	67
4.2	Vorticity	68
4.2.1	The nature of Vorticity	68
4.2.2	Singly Excited Modes	71
4.2.3	Multiple-Mode Excitation	81
4.3	Results -- Vorticity Visualizations	85
4.3.1	Average Vorticity	85
4.3.2	Instantaneous Vorticity	87
Chapter 5: Conclusions and Final Remarks		
5.1	Conclusions	98
5.2	Possible Future Work	99
References		101
Appendix	Fractional Mode Excitation	105
Vita		131

LIST OF FIGURES

Chapter 2: Circular Jet Stability Analysis

Figure 2.1	Modified Bessel Functions of the First and Second Kind	35
Figure 2.2	Michalke's 2nd Basic Streamwise Velocity Profile	36

Chapter 3: Integer, Fractional, and Multiple Modes

Figure 3.1	Experimental Forced Jet Set-Up	53
Figure 3.2	Helix	54
Figure 3.3	Radial Direction Disturbance Eigenfunctions	55
Figure 3.4	Azimuthal Direction Disturbance Eigenfunctions	56
Figure 3.5	Axial Direction Disturbance Eigenfunctions	57
Figure 3.6	Real Axial Direction Disturbance Eigenfunctions	58
Figure 3.7	Streakline Evolution ($m=0$, $\omega=1.4$, $\epsilon=0.05$)	59
Figure 3.8	Streakline Evolution ($m=0$, $\omega=1.4$, $\epsilon=0.05$, $t=1.3T$)	60
Figure 3.9	Evolution of Streakline ($m=0$, $\omega=1.4$, $\epsilon=0.05$)	61
Figure 3.10	Streakline Evolution ($m=1$, $\omega=1.4$, $\epsilon=0.05$)	62
Figure 3.11	Streaklines ($m=1$, $\omega=1.4$, $\epsilon=0.05$, $t=1.1T$)	63

Figure 3.12	Streakline Evolution ($m=2$, $\omega=1.2$, $\epsilon=0.05$)	64
Figure 3.13	Streakline Evolution ($m=0&1$, $\omega=1.4$, $\epsilon=0.05$)	65
Figure 3.14	Streaklines ($m=2$, $\omega=1.2$, $\epsilon=0.05$, $t=1.5T$)	66

Chapter 4: **Entrainment**

Figure 4.1	Average Vorticity	$m=0$	91
Figure 4.2	Average Vorticity	$m=1$	92
Figure 4.3	Average Vorticity	$m=2$	93
Figure 4.4	Average Vorticity	$m=0&1$	94
Figure 4.5	Surfaces of Constant Vorticity	$m=0$ Time= $1.3T$	95
Figure 4.6	Surfaces of Constant Vorticity	$m=1$ Time= $1.3T$	96
Figure 4.7	Surfaces of Constant Vorticity	$m=0&1$ Time= $1.3T$	97

Appendix A: **Fractional Mode Excitation**

Figure A1	Modified Bessel Functions of Increasing Order	116
Figure A2	Growth Rates	117
Figure A3	Radial Direction Disturbance Eigenfunctions	118
Figure A4	Azimuthal Direction Disturbance Eigenfunctions	119
Figure A5	Axial Direction Disturbance Eigenfunctions	120
Figure A6	Real Axial Direction Disturbance Eigenfunctions	121

Figure A7	Streakline Evolution ($m=1/2$, $\omega=1.4$, $\epsilon=0.05$)	122
Figure A8	Streakline Evolution ($m=3/2$, $\omega=1.3$, $\epsilon=0.05$)	123
Figure A9	Streakline Evolution ($m=0,1/2,&1$, $\omega=1.4$, $\epsilon=0.05$)	124
Figure A10	Streaklines ($m=0,1/2,&1$, $\omega=1.4$, $\epsilon=0.05$, $t=1.5T$)	125
Figure A11	Average Vorticity $m=1/2$	126
Figure A12	Average Vorticity $m=3/2$	127
Figure A13	Surfaces of Constant Vorticity $m=3/2$ Time= $1.1T$	128
Figure A14	Surfaces of Constant Vorticity $m=0&1/2$ Time= $1.3T$	129
Figure A15	Surfaces of Constant Vorticity $m=0,1/2,&1$ Time= $1.3T$	130

NOMENCLATURE:

c_{ph}	Phase speed
C	Constant
D	Constant
G	Constant
i	Sqrt(-1)
\hat{i}	Unit vector
I_m	Modified Bessel func. of first kind
K_m	Modified Bessel func. of second kind
$L(r)$	Function of $W(r)$
m, M	(Azimuthal) mode number
p	Pressure
\bar{p}	Mean pressure
p'	Fluctuating pressure
v	Velocity component (Euler equations)
r	Radial direction coordinate
R	Jet radius (equal to nozzle exit radius)
t	Time

T	Forcing period ($=2\pi/\omega$)
u	Non-dimensional velocity
u'	Fluctuating velocity
U_0	Half centerline basic velocity
U_z	Basic axial velocity profile
$W(r)$	Function of m , r , ω , α , and U_z
z	Axial direction coordinate
α	Wave number (complex)
ε	Level of disturbance (% of basic centerline vel.)
θ	Azimuthal direction coordinate
	(Momentum thickness)
Γ	Vorticity
	(Gamma Function)
ξ	Function of α , W , L , and r
η	Function of α , W , L , and r
ω	Non-dimensional frequency

CHAPTER 1:

INTRODUCTION

1.1 Free Jet Flows

A jet by definition, is an unbounded fluid stream moving at higher velocities than its surroundings. In turn, a fluid is defined as a substance that will yield to any system of external forces that tends to deform it without changing the volume of the fluid element. Free jets are a classification of jet flows where the fluid stream evolves in such a way that it is undisturbed or unaffected by any surrounding surfaces or boundaries. Thus, a free jet is considered to be any jet where the so-called free jet assumption -- that any confining walls are far from the jet -- is satisfied.

Free jet flow can be broken down into three regions where the flow differs significantly from one region to the next. They are the laminar, transitional and turbulent regions. The laminar region of the jet is inherently unstable and is subject to Kelvin-Helmholtz instabilities. This instability is a result of a fatal weakness common to any shear flow: poor resistance to high Reynolds numbers. For any given type of laminar flow, there is a critical Reynolds number that jeopardizes the very nature of the flow.

As the jet evolves downstream of the nozzle or exit, small disturbances grow exponentially in the shear layer of the laminar region until they are no longer small. Generally, these disturbances need not be infinitesimal -- the concept of amplification is implicit to the instability of the jet. The fluid then undergoes a transitional period where these disturbances amplify until the entire jet erupts into turbulent flow.

The primary instability in jets is wavelike in nature and leads to a rolling-up phenomenon in the shear layer. Secondary instabilities encourage the growth of streamwise vorticity and ultimately increase the entrainment of the surrounding fluid by the jet. (Entrainment being the process by which ambient fluid is engulfed into the jet and is subsequently carried off downstream where mixing on finer and finer levels occurs.) It is only after secondary instabilities become significant that the jet takes on a less orderly nature and small scale structures dominate the flow.

Stability, by definition, is the property that causes a specific physical characteristic to be resistant to sudden change or inflection. Fluid dynamic (hydrodynamic) stability is concerned with how and when laminar flow breaks down and undergoes transition to turbulent flow. The stability of free jets is but one classification of the many types of flow where stability may be analyzed.

In the case of the free jet, stability is interpreted as the quality of being immune to small disturbances. As a phenomenon that has been established time and again by experiment; free jets

are inherently unstable. The question of stability that arises in free jet applications is whether a given physical state can withstand a disturbance and still return to its original state. If so, it is stable, and if not, it is obviously unstable.

1.2 Applications of Free Jets

Hydrodynamic stability has many physical applications: engineering, meteorology, oceanography, astrophysics, geophysics, and applied mathematics to name a few. Several areas of industrial interest in which free jets have physical applications are in fiber fabrication, transmission systems, propulsion systems and in combustors.

Thorough understanding of the temporal and spatial development of free jets is critical to improving any current physical application of free jets. The practicality of these unstable conditions present in the jet can have both positive and negative effects. On the positive side, the unstable jet allows for large desirable effects to occur by applying a minimal force to the fluid jet. On the negative side, the unstable nature of the free jet makes possible the rapid and drastic changes in flow characteristics with little or no advance warning.

One such application involving free jets that could be significantly improved upon, through better understanding of the principles of jet instability, is the combustor of a gas turbine engine. This example will be called upon regularly throughout this thesis to give a physical

illustration of how specific aspects of the early transitional properties of the jet may effect the efficiency of the combustor. Desirable effects that could be produced by forcing the free jet would be to cause the mixing process to occur thoroughly, quickly, and in the shortest distance possible. Also, better mixing on a molecular level leads directly to more efficient combustion -- another desirable effect. This molecular level mixing has to start with entrainment of the oxidizer into the fuel jet. Thus, if increasing combustor performance is desired, it could be achieved by a combination of large-scale engulfment of the surrounding oxidizing fluid into the fuel jet by large-scale coherent vortices and small scale mixing of the fuel and oxidizer.

1.3 Historical Background

The first documentation of free jets dates back to 300 B.C. with recorded accounts of Ctesibius inventing a two piston water-pump used in fire-fighting in the Greek era. There are also accounts of a steam-driven rotating device forced into motion by jet propulsion, but it was considered to be nothing more than a toy by Hero, its creator. In the early 15th century, the first documented accounts of actual attempts to understand the complex nature of transitional flow were written by Leonardo da Vinci, the famous artist, sculptor, engineer, and proud owner of a great many other occupational titles. Da Vinci was the first to derive an equation for conservation of mass for incompressible, one-dimensional, viscous flow. He also gave accurate accounts of eddy formation behind bluff bodies and the velocity distribution in a vortex.

Not much documented interest in the nature of transitional flow exists between the time of da Vinci and the mid 18th century. It wasn't until 1755 that Leonhard Euler derived the frictionless equation now credited to Bernoulli. Daniel Bernoulli (1700-1782) and Leonhard Euler (1707-1783) together described inviscid fluid flow and presented the Euler equations that same year. Euler admitted that the equations were flawed as they didn't account for the intermolecular forces he knew to exist, but failed to offer a means by which to quantify their effects.

The next historical event worth noting was the discovery, by Isaac Newton, of the contraction of jet flows immediately after exiting an orifice. This discovery however is not what Newton became famous for. In fact, the discovery of this contraction paled in comparison to his contribution of differential calculus to the field of mathematics.

In the Nineteenth Century, Hermann Ludwig von Helmholtz (1821-1894) became the first to use the equation that Louis Navier and George Stokes derived from Euler's equations, including the terms for viscous forces, to investigate the instability between two fluids of different densities. This investigation by Helmholtz became the first major contribution to the study of hydrodynamical stability as an attempt was made to take the study beyond the point of verbal description and into mathematical analysis.

The other main nineteenth century contributors identifying and studying the problems of hydrodynamic stability were Kelvin, Rayleigh, and Reynolds. Lord Rayleigh (1878-1917), the

founder of hydrodynamic stability, conducted analyses that eventually lead to predictions of how the wavelength of a disturbance affected the amplification of normal mode disturbances. He was the first to introduce to concepts of “cutoff” and “most dangerous disturbance”. Rayleigh is also credited with the discovery of instabilities in flow between rotating cylinders. Perhaps his most notable contribution to the field of hydrodynamic stability was his Inflection Point Theorem which identified the necessary condition for instability as the existence of an inflection point in the basic velocity profile of the flow.

Reynolds is widely recognized as having been the first to discover experimental evidence of “sinuous” motion and for providing the first description of random flow using the term “turbulent”. His most notable contribution to the field of fluid dynamics was his use of dimensional analysis to quantify a critical value, above which, flow experiences transition to turbulence: this quantity now bears his name: the Reynolds number.

It was not until the years 1907 and 1908 that Orr and Sommerfeld independently derived the key equation relating hydrodynamic stability to viscous forces. This equation remained unsolved for 22 years until Tollmien found the solution in 1929. Tollmien solved the Orr-Sommerfeld equation and arrived at the first neutral eigenvalues determining the critical Reynolds number at which a flow would begin transition from laminar to turbulent flow.

Several years prior to the accomplishments of Tollmien (1923), G.I. Taylor experimentally confirmed linear theory for the first time while working with vortices forming

between concentric rotating cylinders. During the span from 1932 to 1935, Schlichting built upon the initial success of Tollmien to further evaluate the critical Reynolds numbers and amplification rates.

The invention of the jet engine in 1939 sparked renewed interest in jet phenomena. The two major questions that were asked at that time and are still not completely answered today were the questions on the mechanisms responsible for jet mixing and noise production. Today these phenomena are still being researched with the goals to increase combustor efficiency, improve jet mixing, and determine methods to decrease noise production levels.

In the mid 1940's, Heisenberg and Lin proved Lin's general expansion to stability analysis by considering Poiseuille flows. Before this proof, Lin's work was viewed with a degree of skepticism. In 1950, Fjortoft published his theorem as an additional requirement to Rayleigh's Inflection Point Theorem for unstable flow. It consisted of the fact that if a flow is subject to instabilities, the quantity $U''(U-U_s) < 0$ somewhere in the flow field where z_s is a point at which $U''=0$ and $U_s=U(z_s)$. Like Rayleigh's Theorem, Fjortoft's Theorem did not prove conditions resulting in the presence of instabilities, it only disproved some situations where Rayleigh's Theorem allowed for the possibility of an unstable situation.

Schubauer and Scramstad [1947] took measurements of transition occurring over a flat plate. They were one of the first to take dynamic measurements of a transitional flow using a hot wire. Among their discoveries was the selective amplification of the random fluctuations during

transition.

The major achievements in hydrodynamic stability studies prior to 1960, were closed out with the 1955 publication of a comprehensive monograph by Lin, covering the field of hydrodynamic stability. Essentially, Lin used asymptotic power series that have since been improved, but the work laid the foundation for future endeavors in stability studies.

1.4 Circular Jet Stability and Relevant Discoveries

In the early sixties, Batchelor and Gill [1962] analyzed the temporal stability of axisymmetric jets with streamwise velocity profiles obtained from solving the Navier-Stokes equation. Their studies assumed that the jet emanated from a forced point source making the results valid only in the far field. They managed to extend the necessary conditions for unstable physical situations in axisymmetric jet flows and found a similar relationship to Howard's Theorem existed for a range of complex phase speeds. Finally, they succeeded in demonstrating that one and only one neutral disturbance with a non-zero wave number existed for this jet flow.

Prior to the sixties, flow instability was treated as a wave property only. Michalke [1965] was the first to predict the rolling-up phenomenon of traveling instability waves into periodic vortices, taking the treatment of hydrodynamic instabilities to a new level. This was demonstrated experimentally and verified by Freymuth [1966] one year later. Michalke had also

studied spatial and temporal characteristics of planar shear layers. He used asymptotic solutions for the boundary conditions in order to integrate the Rayleigh equation. A fourth order Runge-Kutta method was used in his integration scheme. This integration was performed twice, from a distance far from the shear layer (considered to be infinity), inward, approaching the shear layer from either side. Michalke required that when the correct solution was obtained, the solution and its derivative determined from each integration matched where the two integration steps met in the shear layer, the so-called shooting method. Through his study of inviscid shear layers, Michalke was able to show that the shear layer was temporally unstable over a range of spatial wave frequencies and that two neutral frequencies existed where disturbances neither grew nor dissipated. This work disproved the notion that one and only one neutral disturbance was possible as Batchelor and Gill [1962] had claimed several years earlier. Michalke [1966] also completed a spatial linear stability analysis for a planar shear layer to obtain similar results to those of his temporal linear stability analysis.

It was in the studies of jet noise production by Crow and Champagne [1971] that the existence of a preferred mode of instability was demonstrated. Crow and Champagne showed that modestly forcing the jet at its preferred frequency resulted in increasing the size of large-scale structures and increased entrainment. This most amplified frequency is a very important concept in planar mixing layers and jet shear layer control as both mixing layers have a thin shear layer in the near field. Crow and Champagne also proved that coherent structures could be strengthened and stabilized by periodic stimulation. The following year, Crow and Champagne [1972] observed the preferred mode of jet column instability to scale approximately with the jet

diameter and velocity. This characterized a single scale that dominated the turbulent region.

Lessen and Singh [1973] found that axisymmetric shear layers are more stable than corresponding planar shear layers. Browand and Laufer [1975] confirmed the existence of the preferred frequency resulting in the greatest growth rate as proposed by Crow and Champagne. They also observed the development of large scale vortical structures in the near field of circular jets in demonstrating the preferred frequency phenomenon. Entrainment was attributed to the pairing of vortex rings and Browand and Laufer postulated that entrainment and noise production were governed by vortex dynamics in the near field.

Ho and Huang [1982] and Ho and Huerre [1984] investigated the basic mechanisms of the instabilities of the vortex sheet leaving a trailing edge. They found the existence of a most amplified frequency in the flow that scaled with the local momentum thickness. Strange [1983], studied high Reynolds number axisymmetric jets excited at modes $m = 0, 1$, and 2 . He showed that the growth rates for $m = 0$ and $m = 1$ were comparable.

Michalke [1981, 1984] performed another spatial linear stability analysis of a circular jet using the shooting method. Using modified Bessel functions of the first and second kind as approximations at small and large radii in the integrations to find the pressure eigenfunction, he found that the growth rate increased for larger values of R/θ , where R is the jet radius and θ is the momentum thickness. He also demonstrated that the phase speed increases with decreasing R/θ and that increasing the Mach number decreased the growth rates at higher frequencies while

the growth rates at lower frequencies were unchanged by Mach number variations. The compressibility of the fluid at high Mach numbers absorbing energy and thus, causing a decrease in growth rate, was postulated as the reason for this natural event.

Axisymmetric air jets of moderate Reynolds numbers were studied by Petersen and Samet [1987]. They found that the natural instabilities scaled with the local shear layer thickness. The preferred mode of instability was found to be a shear layer instability. Over a range of low to high levels of excitation, linear stability analysis of the Orr-Sommerfeld equation proved to accurately predict the results of experiment.

Lin and Corcos [1984] suggested that streamwise vorticity was produced in the braid region between large scale structures. Their claim was that streamwise structures were responsible for the onset of mixing transition in axisymmetric jets. Cohen and Wygnanski [1987], Peterson [1990] and Corke [1993] showed that in the near field of circular jets, where the shear layer is usually thin, many azimuthal modes are equally unstable, not just for the modes $m=0$ and $m=1$ as Strange and Crighton [1983] had found. There are many similarities between mixing layers and jets. First, the momentum thickness used in mixing layers as a length scale is also an appropriate length scale for near-field jet dynamics. Further downstream, at axial distances greater than three jet diameters, according to Corke [1993], the jet diameter generally governs the evolution of the flow.

Bayly, Orzag, and Herbert [1988] studied instability mechanisms in shear flows and

found that the primary periodic instability imposed on the basic flow causes roll-up of the Kelvin-Helmholtz instability waves into large scale vortical structures. Monkewitz and Pfizenmaier [1991] claimed that the development of streamwise vorticity initiates the breakdown of the laminar jet. Grosch and Jackson [1991] studied inviscid spatial stability characteristics of three-dimensional mixing layers. They proved that the three-dimensional problem could be reduced to a two-dimensional problem and found a universal dispersion relationship curve that could be used to find the growth rate of the shear layer with any other parameter.

The extent of study on multi-mode excitation has been limited to what Strange [1983] refers to as spinning modes. Spinning modes consist of counter-propagating modes of equivalent azimuthal mode number. Cohen and Wygnanski [1987] extended the work of Strange to show that the standing wave excitation produced by spinning modes allows for control of the directional jet expansion. Iso-velocity contours predict elliptic evolution of the jet for $m = \pm 1$ excitation, triangular evolution for $m = \pm 1.5$ excitation, and square evolution for $m = \pm 2$ excitation.

Flow visualization by Leipman and Gharib [1992] showed the existence of streamwise vorticity in round jets. These structures were found to drastically alter the entrainment process in the near-field and were identified as a major mechanism contributing to the entrainment. Leipman and Gharib claimed that as the flow evolved downstream, the efficiency of streamwise vorticity in entraining fluid increased relative to entrainment due to azimuthal vorticity. (It is

important to note that when identifying vorticity components, Liepman and Gharib refer to the plane that the rotational motion lies in, not what mathematical component the vortical structures represent.)

Huang [1994] performed a spatial linear stability analysis of a non-reacting, circular, free jet that allowed for the presence of a swirling basic flow. Huang followed the shooting method as prescribed by Michalke [1981] to find the solution to a linearized form of the perturbed Euler equations. His results for the non-swirling jet agreed with those of Michalke's earlier work, demonstrating the strong influence of momentum thickness on the stability of the jet.

Studies of active control of free shear flows were conducted by Ding [1995]. These studies focused on control of the far field. Ding found that by exciting the jet at non-integer and counter-propagating azimuthal modes, marked changes in the streamwise evolution of the jet could be achieved. Increased entrainment of the surrounding air by somewhat more than two-fold was demonstrated for the non-integer and counter-propagating azimuthal modes when compared with the unexcited jet.

1.5 Goals and Methodology

The objectives of the research described in this thesis are two distinct, but connected efforts leading toward similar goals. With the linear stability analysis tool developed by Huang

[1994] available as a foundation for the current work, this tool will be modified to ignore the effects of swirl and to allow for the solution of the eigenvalue problem for the spatial linear stability analyses at fractional modes of excitation. The effects of exciting a circular jet at several modes simultaneously will also be explored.

The investigation of integer, fractional, and multi-mode excitation will focus on identifying mechanisms responsible for the instabilities that develop in non-reacting, circular, free jets that cause the jet to experience transition from laminar to turbulent flow. The results of the fractional mode analysis will be presented in the Appendix due to unresolved questions regarding proper mathematical analysis. If possible, these mechanisms responsible for the entrainment of ambient fluid into the jet will be identified and possible methods (if any) of increasing the entrainment will be addressed.

This investigation is intended to be exploratory. The limitations of linear stability analysis in accurately predicting flow characteristics is well known. The emphasis of the effort is on gaining the most insight possible given the tools available. The current work is intended to provide a starting point for a more in-depth look at the concepts of mathematical analysis of fractional and multi-mode excitation.

These tasks will be accomplished by first performing the linear stability analyses necessary to determine the linear effects on the evolution of the flow field for all modes to be considered, and streakline visualizations will be analyzed to gather information that could

possibly lead to better understanding of structure formation and evolution in the streamwise direction of the jet. Then a means of measuring the entrainment for a given mode or modes of excitation will be developed in order to form a basis upon which entrainment resulting from different modes of excitation may be evaluated and compared.

Finally, visualizations of instantaneous plots of vorticity will be produced and examined in the hope of gaining insight to the development of near-field structure formation and evolution. These visualizations should provide some perspective as to what structures develop as a result of the interaction of differing modes of excitation. In addition, the possibility of future work building upon the foundation of the present effort will be addressed.

CHAPTER 2:

CIRCULAR JET STABILITY ANALYSIS

2.1 Linear Stability Analysis

Many scientific fields of study offer physical situations in which the stability of the system is questionable. Mechanical, astronomical and electrical systems are all such examples. In addition to being potentially unstable, they all have in common a finite (generally few) number of degrees of freedom. It has already been stated that many hydrodynamic systems are inherently unstable. However, the analysis of hydrodynamic systems are quite different from the examples cited above in the respect that hydrodynamics deal with continuums. In a continuum, there exist an infinite number of degrees of freedom. When studying infinite degree of freedom systems, the mathematical analysis generally leads to an expression in some form of a partial differential equation.

The solution to many of these problems requires solving a linearized form of the partial differential equation formed into an initial value problem. While linearizing the equations causes the problem to lose a degree of physical reality, linear stability analysis has proven itself to provide accurate models of the early stages of the mixing process in jets (Petersen and Samet

[1988]). According to Brown and Roshko [1974], depending upon the initial shear layer thickness, features of the flow field many diameters downstream may bear a remarkable resemblance to features predicted by linear stability analysis. The stability analysis on circular and elliptical jets by Huang [1994] proved effective in obtaining insight into the entrainment process and possible methods of enhancing the entrainment of elliptical jets was offered.

Linear stability analysis provides an efficient method of investigating the influence of geometrical parameters on the stability properties of jet flows. The results are generally limited in accuracy to the near field, however, linear stability analysis can be used to propose mechanisms responsible for the appearance of large scale structure in transitional regions. The procedure for the stability analysis can be outlined as follows (Sherman [1990]):

- 1.) Select a basic solution flow.
- 2.) Add a disturbance.
- 3.) Find the disturbance equations.
- 4.) Linearize the equations.
- 5.) Simplify (if possible and if necessary).
- 6.) Solve for the eigenvalues.
- 7.) Interpret the stability conditions. (Find ranges of stability, growth rates, decay rates, etc.)

The analysis is generally approached in one of two ways: temporal or spatial analysis.

First, for either temporal or spatial analysis, a streamwise invariant but radially varying basic flow must be assumed. The temporal analysis involves tracking the temporal evolution of spatially periodic perturbations. The spatial analysis consists of tracking the spatial evolution of temporally periodic perturbations. In both cases, the perturbation terms are assumed to vary exponentially; either in time for the temporal analysis, or in streamwise direction for the spatial analysis. The linear stability analysis for the circular jet is a linear combination of an infinite number of solutions; each with a periodic, azimuthally dependant eigenfunction (Drazin and Reid [1982]). Defining these dependancies is called mode classification.

In solving the eigenvalue problem, the real and imaginary parts of the eigenvalue relationship and the temporal or spatial frequency is the dispersion relation. The dispersion relation gives information on the growth rate and phase speed of the disturbance. The resulting eigenfunction provides the spatial distribution of the disturbance.

2.2 Developing the Eigenvalue Problem

In order to study the evolution of circular jets excited simultaneously at several modes, linear stability analysis was used to predict the distribution of the velocity disturbance fields resulting from excitation of azimuthal (helical) and axisymmetric modes. The spatial linear stability analysis developed by Huang [1994] featured spatial instabilities resulting from an excited, swirling, continuous basic velocity. It is Huang's approach that will be followed here

except that the effects of swirl will not be considered. Thus, it will be assumed that no basic azimuthal variation will be present in the velocity field and all terms including this basic azimuthal velocity according to Huang's [1994] development will be ignored. The analysis will be further adapted to allow for fractional mode excitation and extended to analyze the effects of multiple mode excitation. These two topics will be discussed in further detail in subsequent chapters and in the appendix after the development and solution of this problem have been addressed.

Following Huang's [1994] approach of linearizing Euler's equations, the fluid comprising the jet is assumed to be inviscid and incompressible. Another dissipative property, the thermal diffusivity, will also be assumed to be negligible. When the effects of viscous forces are ignored, the fluid moves according to the equilibrium between its inertia and the pressure forces. A small disturbance may upset this balance. In fact, in the absence of viscous forces, the free jet presents an even more unstable situation in comparison to its viscous counterpart.

The coordinate system chosen for this problem will be the circular cylindrical coordinate system (r, θ, z) , where every point in a three dimensional space is defined by a radius (r), an azimuthal location, designated by an angle (θ), and an axial coordinate (z), measuring distance from the origin. In circular cylindrical coordinates, Euler's equations are:

$$\frac{\partial v_r}{\partial t} + v_r \frac{\partial v_r}{\partial r} + v_z \frac{\partial v_r}{r \partial \theta} + v_z \frac{\partial v_r}{\partial z} - \frac{v_\theta^2}{r} = - \frac{\partial p}{\partial r} \quad (2.1)$$

$$\frac{\partial v_\theta}{\partial t} + v_r \frac{\partial v_\theta}{\partial r} + v_\theta \frac{\partial v_\theta}{r \partial \theta} + v_z \frac{\partial v_\theta}{\partial z} + \frac{v_\theta v_r}{r} = - \frac{\partial p}{r \partial \theta} \quad (2.2)$$

$$\frac{\partial v_z}{\partial t} + v_r \frac{\partial v_z}{\partial r} + v_\theta \frac{\partial v_z}{r \partial \theta} + v_z \frac{\partial v_z}{\partial z} = - \frac{\partial p}{\partial z} \quad (2.3)$$

$$\frac{1}{r} \frac{\partial(r v_r)}{\partial r} + \frac{1}{r} \frac{\partial v_\theta}{\partial \theta} + \frac{\partial v_z}{\partial z} = 0 \quad (2.4)$$

where v_r , v_θ , and v_z are the three velocity components in the radial, azimuthal, and axial directions, respectively. Note that these equations are intended to be interpreted in non-dimensional form where all lengths are non-dimensionalized by the jet radius, R (simply taken as the radius of the nozzle at the jet exit), all velocities are non-dimensionalized by the half centerline basic streamwise velocity U_0 , and all pressures are non-dimensionalized by the quantity ρU_0^2 . It should be noted here that the flow in question will be assumed to be parallel.

The three components of velocity can be expressed as a mean value, and a fluctuating disturbance value. The only mean value of velocity which is non-zero is the axial velocity

component where the mean velocity is the axial velocity of the basic flow, U_z , thus

$$v_r = u_r' \quad (2.5)$$

$$v_\theta = u_\theta' \quad (2.6)$$

$$v_z = U_z + u_z' . \quad (2.7)$$

The pressure is again expressed as a mean and a fluctuating value:

$$p = \bar{p} + p' \quad (2.8)$$

where \bar{p} is the mean pressure and p' is the fluctuating pressure. There is no basic radial or azimuthal velocity component. Notice that this is consistent with the basic parallel flow assumption. The consequences of the above assumptions are that the basic flow is independent of streamwise location and azimuthal coordinate. Azimuthal dependency only results from a swirling flow which is not considered in the present work. The basic streamwise velocity U_z will be described as a function of radial location (r) only. Later, when the form of the basic streamwise velocity becomes important, it will be addressed; for now however, it is only important to note that U_z is dependant upon radius (r), or that:

$$U_z = U_z(r) . \quad (2.9)$$

The primed (') quantities in equations (2.5) - (2.8) are the fluctuating disturbance quantities which, when averaged over time are zero.

Substituting the basic velocity components into equations (2.1) - (2.4) yields the equations for the basic velocity and the mean pressure:

$$0 = \frac{\partial \bar{p}}{\partial r} \quad (2.10)$$

$$0 = - \frac{\partial \bar{p}}{r \partial \theta} \quad (2.11)$$

$$0 = - \frac{\partial \bar{p}}{\partial z} . \quad (2.12)$$

Thus, the average (basic) pressure is constant and does not change throughout the flow field. (Note that a temporal variation of the pressure, p , still exists due to the fluctuating component.)

The Euler equations can now be linearized by taking the following steps:

- 1.) Substitute equations (2.5) - (2.8) into equations (2.1) - (2.4);
- 2.) Subtract the equations for the basic flow quantities;
- 3.) Neglect quadratic and higher order terms.

Thus, the linearized form of the Euler equations become:

$$\frac{\partial u_r'}{\partial t} + U_z \frac{\partial u_r'}{\partial z} = -\frac{\partial p'}{\partial r} \quad (2.13)$$

$$\frac{\partial u_\theta'}{\partial t} + U_z(r) \frac{\partial u_\theta'}{\partial z} = -\frac{1}{r} \frac{\partial p'}{\partial \theta} \quad (2.14)$$

$$\frac{\partial u_z'}{\partial t} + u_r' \frac{\partial U_z(r)}{\partial r} + U_z(r) \frac{\partial u_z'}{\partial z} = -\frac{\partial p'}{\partial z} \quad (2.15)$$

$$\frac{u_r'}{r} + \frac{\partial u_r'}{\partial r} + \frac{1}{r} \frac{\partial u_\theta'}{\partial \theta} + \frac{\partial u_z'}{\partial z} = 0 . \quad (2.16)$$

If the normal mode assumption is made, the velocity and pressure disturbance terms can be represented as:

$$u_r' = u_r(r) e^{i(\alpha z + m\theta - \omega t)} \quad (2.17)$$

$$u_\theta' = u_\theta(r) e^{i(\alpha z + m\theta - \omega t)} \quad (2.18)$$

$$u_z' = u_z(r) e^{i(\alpha z + m\theta - \omega t)} \quad (2.19)$$

$$p' = p(r) e^{i(\alpha z + m\theta - \omega t)} \quad (2.20)$$

where $u_r(r)$, $u_\theta(r)$, $u_z(r)$, and $p(r)$ represent the velocity and pressure disturbance eigenfunctions. In the exponent, α is called the wave number. The specific mode of excitation is determined by the mode number m . When $m=0$, the disturbance is called the axisymmetric disturbance. The reasoning behind this name should be clear as when $m=0$, there can be no azimuthal variation in the disturbance since dependence upon azimuthal coordinate θ disappears. For any mode: $m>0$, the disturbance is said to result from a helical disturbance of mode m . These modes are also typically called azimuthal modes in which case m is referred to as the azimuthal wave number. The argument ω , is the temporal (non-dimensional) frequency of the disturbance at a particular mode, m . For a given mode m , there are a range of frequencies where the disturbance will grow exponentially, as well as a range of frequencies for which the disturbances will have a negative

growth rate and will be damped out, disappearing with increasing streamwise coordinate z . It can also be shown (and was proven by Michalke [1975]) that there exist two neutral eigenvalues for which the disturbances neither grow, nor dissipate.

In spatial stability analysis, the approach used here, has both m and ω as real numbers. The wave number α however, is a complex value where both the real and imaginary parts have significance in spatial linear stability analyses. The real part is used to determine the phase speed, a measure of how fast the disturbances travels axially (in the streamwise direction). The phase speed is given by:

$$C_{ph} = \frac{\omega}{\alpha_r} . \quad (2.21)$$

The negative of the imaginary part of the complex wave number is called the growth rate. Since $-\alpha_i z$ is the only real part of the exponential term, it should be obvious that it is the only quantity that will cause the disturbance to grow exponentially. The greater the quantity α_i becomes, the faster the disturbances will grow with increasing axial distance z . The relationship of the complex wave number with the frequency is called the dispersion relationship and this, along with the disturbance eigenfunctions, determine the stability characteristics of the jet. Thus, in the normal mode representation, the physically meaningful portion of the complex disturbances corresponds to the real part of the eigenfunctions (Drazin and Reid [1981]).

Substituting the expressions for the velocity and pressure disturbance eigenfunctions into the linearized forms of Euler's Equations, yields the equations for the disturbance eigenfunctions:

$$u_r W(r) i = - \frac{dp}{dr} \quad (2.22)$$

$$u_\theta W(r) = - \frac{m}{r} p(r) \quad (2.23)$$

$$u_z W(r) i + u_r \frac{dU_z(r)}{dr} = -i \alpha p(r) \quad (2.24)$$

$$\frac{u_r}{r} + \frac{du_r}{dr} + \frac{1}{r} i m u_\theta + i \alpha u_z = 0 \quad (2.25)$$

where W , a function of radius r , only, is introduced to simplify the equations and takes on the following form:

$$W(r) = -\omega + \frac{m}{r} + U_z \alpha. \quad (2.26)$$

Expressing the velocity disturbance eigenfunctions u_r , u_θ , and u_z in terms of the pressure disturbance eigenfunction $p(r)$, yields:

$$u_r = i \frac{1}{W(r)} \frac{dp}{dr} \quad (2.27)$$

$$u_\theta = -\frac{m}{r W(r)} p \quad (2.28)$$

$$u_z = -\frac{\alpha}{W(r)} p - \frac{1}{W(r)^2} \frac{dU_z(r)}{dr} \frac{dp}{dr} . \quad (2.29)$$

Substituting the expressions for u_r , u_θ , and u_z in terms of the pressure disturbance p , into equations (2.22) - (2.25) and solving the system of equations for pressure p , yields a second order ordinary differential equation for the pressure disturbance eigenfunction:

$$\frac{d^2 p}{dr^2} = C_1 \frac{dp}{dr} + C_2 p = 0 \quad (2.30)$$

where

$$C_1 = \frac{1}{r} + \frac{1}{W(r)} \frac{dW(r)}{dr} - \frac{1}{L(r)} \frac{dL(r)}{dr} - \frac{\alpha}{W(r)} \frac{dU_z(r)}{dr} \quad (2.31)$$

$$C_2 = -\frac{m^2}{r^2} - \alpha^2 \quad (2.32)$$

$$L(r) = -W(r)^2 . \quad (2.33)$$

2.3 Solving the Eigenvalue Problem

At this point it will be repeated that the point of linear stability analysis is to find the complex wave number (growth rate and phase speed), the velocity disturbance eigenfunctions, and the pressure disturbance eigenfunction for a specific mode m , at a specific frequency ω . In order to solve the above differential equation, two boundary conditions need to be specified. The requirements that equation (2.30) must satisfy are that the pressure disturbance must be finite as the centerline of the jet is approached, and that the pressure disturbance must tend to zero as the radius becomes infinite. Thus the boundary conditions become:

$$r \rightarrow 0: \quad p = \text{finite} \quad (2.34)$$

$$r \rightarrow \infty: \quad p = 0. \quad (2.35)$$

The solution to the differential equation (2.30) is not immediately recognizable as the

boundary conditions make the problem difficult. However, as the radius tends to zero, it should be noted that the solution takes on the form of a modified Bessel function of the first kind. Likewise, when the radius in equation (2.30) increases to infinity, the solution takes on the form of a modified Bessel function of the second kind. This can be shown to be true by applying the following transformation to equation (2.30):

let

$$\xi = \frac{\alpha}{W(0)} \sqrt{-L(0)} r \quad (2.36)$$

as $r \rightarrow 0$,

$$\xi^2 \frac{d^2 p}{d\xi^2} + \xi \frac{dp}{d\xi} + (-\xi^2 - m^2)p = 0 \quad (2.37)$$

and let

$$\eta = \frac{\alpha}{W(\infty)} \sqrt{-L(\infty)} r \quad (2.38)$$

as $r \rightarrow 0$,

$$\eta^2 \frac{d^2 p}{d\eta^2} + \eta \frac{dp}{d\eta} + (-\eta^2 - m^2)p = 0 . \quad (2.39)$$

Inspecting the above transformed differential equation and looking at the plots of the first two orders of the modified Bessel functions of the first and second kind (Fig. 2.1), it should be evident that the solutions for the modified Bessel functions satisfy the boundary conditions. Particular solutions of the modified Bessel functions of the first kind are denoted as $I_m(x)$ and match the requirement that the disturbances remain finite at the jet centerline. Particular solutions to the modified Bessel functions of the second kind are designated $K_m(x)$ and match the requirement that the disturbances tend to zero as the radius tends to infinity. The general solution to equation (2.30) is a linear combination of the particular solutions I_m and K_m , where the order of the Bessel function m corresponds to the azimuthal mode number m .

From the above explanation, it is clear that the boundary conditions satisfying equation (2.30) are:

as $r \rightarrow 0$

$$p = I_m(\xi) = I_m\left(\frac{\alpha}{W(0)} \sqrt{-L(0)} r\right) \quad (2.40)$$

and as $r \rightarrow \infty$,

$$p = K_m(\eta) = K_m\left(\frac{\alpha}{W(\infty)} \sqrt{-L(\infty)} r\right) . \quad (2.41)$$

To solve the eigenvalue problem for equation (2.30), the adaptive step size Runge-Kutta method is used to integrate the equation in two regions. In the first region, for radial locations R_1 , between some point close to the jet centerline and the jet radius R , the I_m modified Bessel solutions are used as approximate boundary conditions in the integration. In the second region, for radial locations R_2 , starting at some location (infinity) far from the jet centerline and moving inward to the jet radius R , approximations for the boundary conditions are made using the K_m modified Bessel solutions in the integration. The third and final condition that must be satisfied is that the disturbance eigenfunctions must be smooth and continuous everywhere, particularly at the location of the jet radius R , or in mathematical terms:

$$F(\alpha) = p_2(R) \frac{dp_1(R)}{dr} - p_1(R) \frac{dp_2(R)}{dr} = 0 \quad (2.42)$$

where p_1 and p_2 are the pressure disturbance eigenfunctions at the jet radius obtained from the two integrations. $F(\alpha)$ in equation (2.42) is a non-linear function of complex eigenvalue α . Now equation (2.42) can be solved using the Newton method, where a simple algorithm to find the solution is as follows:

- a.) For a specific mode m and frequency ω , make an initial guess at the eigenvalue (the complex wave number) α ;

- b.) Integrate equation (2.30) outward from R_1 to the jet radius R to get $p_1(R)$ and its derivative $dp_1(r)/dr$;
- c.) Integrate equation (2.30) inward from R_2 to the jet radius R to get $p_2(R)$ and its derivative $dp_2(R)/dr$;
- d.) Calculate $F(\alpha)$ from equation (2.42);
- e.) If $F(\alpha)$ is less than a specified tolerance ($<10^{-6}$), then the guess at α is correct; the eigenfunction may be computed and the algorithm ended;
- f.) If $F(\alpha)$ is greater than a specified tolerance, then repeat the solution process using a new value for α where:

$$\alpha_{new} = \alpha_{old} - \frac{F(\alpha_{old})}{F'(\alpha_{old})} . \quad (2.43)$$

After executing the Newton method algorithm and finding the eigenvalue (complex wave number) α , the pressure disturbance eigenfunction ($p(r)$), and its derivative ($dp(r)/dr$), the velocity disturbance eigenfunctions may be solved for by substituting the pressure disturbance eigenfunction $p(r)$, back into equations (2.27) - (2.29).

At this point, the only other piece of information needed to perform the linear stability analysis for a given mode m and a given frequency ω , is the basic streamwise velocity. Again, following the process outlined by Huang [1994], Michalke's second basic streamwise velocity profile is used (Fig. 2.2.):

$$U_z(r) = \frac{1}{2} \left\{ 1 + \tanh \left[\frac{R}{4\theta} \left(\frac{R}{r} - \frac{r}{R} \right) \right] \right\} \quad (2.44)$$

where R is the jet radius and θ is the momentum thickness (not to be confused with θ , the azimuthal coordinate).

When linearizing the perturbation equations, losing the non-linear effects of the flow evolution takes away a great deal of the physical reality of the flow and makes the solution valid only in the region where the linear effects outweigh the non-linear effects. This region is limited to as little as one jet radius downstream. However, when adding Michalke's second basic streamwise velocity profile, a profile found to closely fit true jet behavior near the nozzle exit in experiment, a new degree of physical validity is introduced back into the analysis causing not only better results than expected, but also extending the region of validity of the solution of the linearized equations.

Now, for a given mode m , frequency ω , momentum thickness θ , and two guesses at the eigenvalue (complex wave number) α , the disturbance eigenfunctions may be solved for along

with the correct eigenvalue α .

Figure 2.1
Modified Bessel Functions of the First and Second Kind

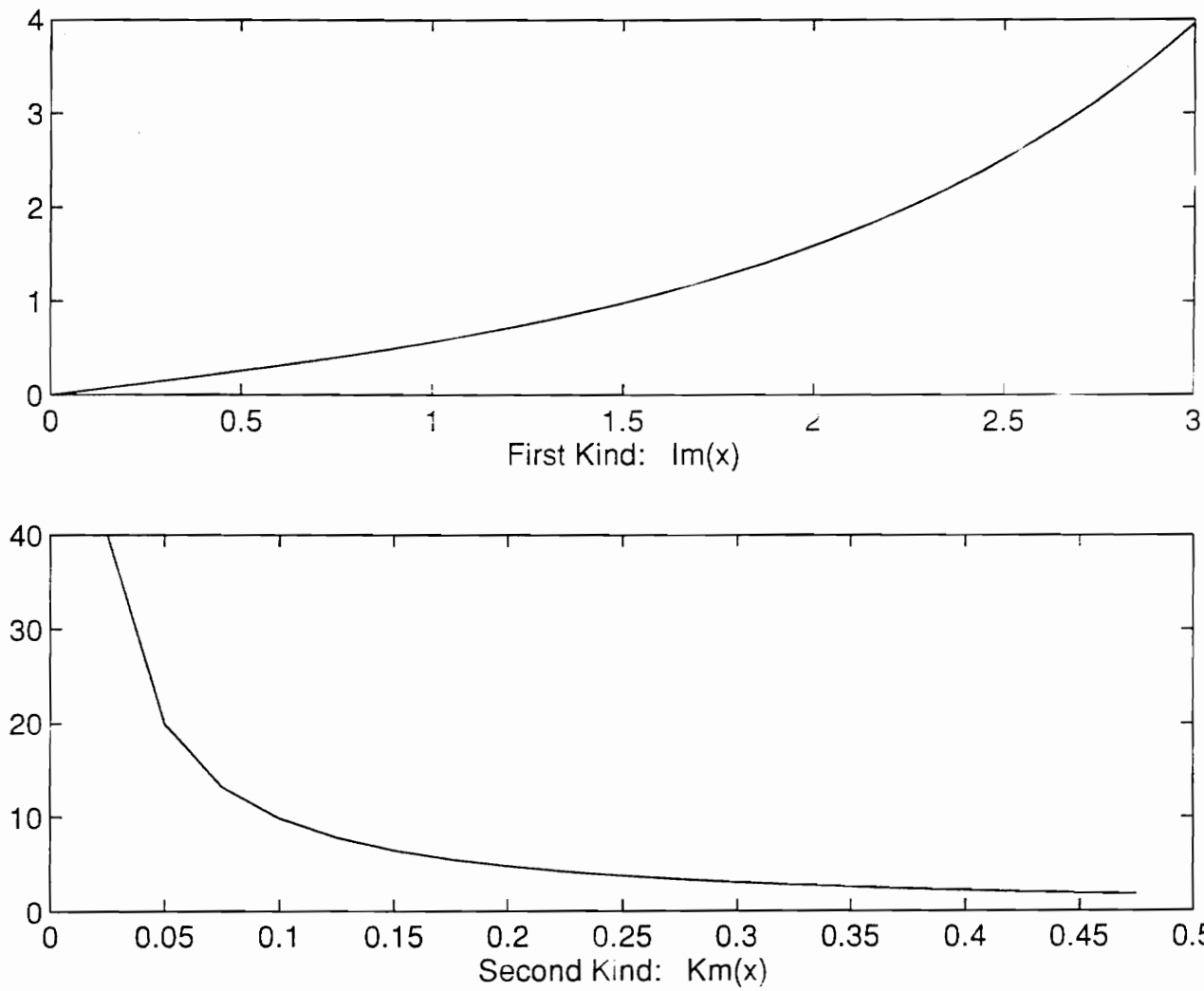
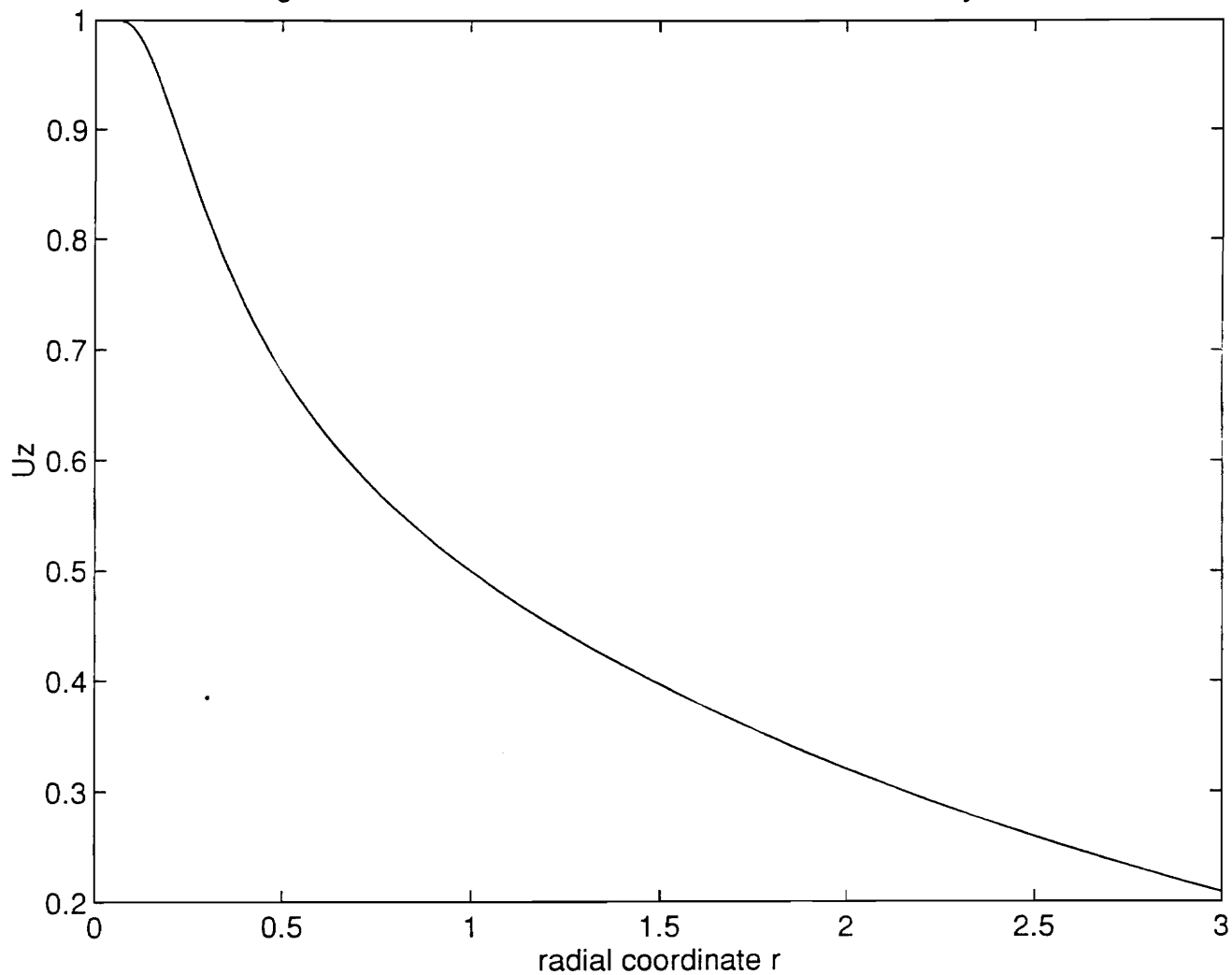


Figure 2.2 Michalkes 2nd Basic Streamwise Velocity Profile



CHAPTER 3:

INTEGER, FRACTIONAL AND MULTIPLE MODES

3.1 Experimental and Theoretical Excitation

In the previous chapter, the linear stability analysis of Huang [1994] was adapted and developed for the non-swirling circular jet according to Michalke's shooting method using Michalke's second basic streamwise velocity profile. In this chapter, the significance of azimuthal mode excitation will be addressed and the excited jet will be studied through the use of streakline visualizations. The concept of multiple mode excitation will also be investigated.

The linear stability analysis tool provides the eigenvalue (complex wave number α) and the shapes of the velocity and pressure disturbance eigenfunctions. These eigenfunctions must be normalized before they can be used to determine the physical disturbance fields. The code by Huang [1994] normalizes the eigenfunctions by requiring that the matching conditions in the solving routine meets a specific tolerance, thus, forcing the absolute maximum and minimum to be on the order of one. It was felt that for the quantitative comparisons used here that the degree of normalization was sufficient. No additional normalization was carried out. These eigenfunctions are in non-dimensional form as are all of the other arguments in the analysis. The

eigenfunctions therefore have the same units as the basic velocity and are measured on the same scale. In order to more accurately model the jet instability phenomenon, the jet is excited at some percentage of the basic centerline velocity ϵ ; generally a value less than five percent (0.05). Thus, the actual velocity fluctuations are given by equations 2.27 - 2.29, where each disturbance quantity is pre-multiplied by the level of disturbance ϵ :

$$v_r = \epsilon u_r(r) e^{i(\alpha z + m \theta - \omega t)} \quad (3.1)$$

$$v_\theta = \epsilon u_\theta(r) e^{i(\alpha z + m \theta - \omega t)} \quad (3.2)$$

$$v_z = U_z(r) + \epsilon u_z(r) e^{i(\alpha z + m \theta - \omega t)} . \quad (3.3)$$

The mode m , of excitation affects the perturbation terms by acting as a frequency modulator of sorts. This is more easily seen by decomposing the complex exponential into its real and imaginary parts and expressing the exponential with the imaginary argument trigonometrically as follows:

$$\begin{aligned} e^{i(\alpha z + m \theta - \omega t)} &= e^{-\alpha_r z} e^{i(\alpha_r z + m \theta - \omega t)} \\ &= e^{-\alpha_r z} [\cos(\alpha_r z + m \theta - \omega t) + i \sin(\alpha_r z + m \theta - \omega t)] . \end{aligned} \quad (3.4)$$

With the exponential in this form, several things become apparent. First, for any complex wave number α , when the imaginary part is negative, the disturbance will grow exponentially with axial distance z . Second, at any axial location z , and time t , the mode of excitation m , serves to change the phase of the sine and cosine terms with azimuthal location θ , thus modulating the disturbance as mentioned above. It is this analytical phase modulation that is physically reproduced when experimentally exciting jets at modes other than the axisymmetric ($m=0$) mode.

In physical experimentation, different azimuthal modes are excited by an arrangement of electrically driven actuators located around the periphery of the jet exit. Figure 3.1 shows the experimental set-up of Ding [1995] illustrating the experimental set-up described above. The generators send sinusoidal electrical signals to the actuators such that the phase of the signal from one actuator to the next is offset by the value $2\pi m / N$, where m is the azimuthal mode number, and N is the number of actuators around the periphery of the jet. This phase difference occurs between one actuator and the next in a clockwise direction for a positive mode number m , and the same difference occurs between one actuator and the next counter-clockwise actuator for a negative mode number m .

3.2 Integer Modes of Excitation

In integer mode excitation the phase difference between any one actuator and either the previous actuator or the next is the same. This result from the geometry ends up creating a

continuous disturbance at any streamwise cut through the jet. A continuous azimuthal disturbance also results. (The same cannot be said to result from fractional mode excitation.)

The commonly referred to helical mode for any mode $m > 0$, should now make some physical sense. If one were to track a constant phase of the disturbance beginning at time $t=0$, at some radius r , starting at the jet exit, the trajectory of this constant phase evolving with time would in fact produce a helix (Fig 3.2), and thus, the term helical mode.

As Huang [1994] only dealt with integer modes of excitation, a general algorithm could be used to calculate the modified Bessel functions of the first and second kind. When calculating the modified Bessel functions of the first kind, for a given azimuthal mode, the $(n+1)$ th order function could be calculated using the recursion relations:

$$I_{n+1} = I_{n-1}(x) - \frac{2n}{x} I_n(x)$$

for (3.5)

$$I_n(x) = \sum_{k=0}^{\infty} \frac{\left(\frac{x}{2}\right)^{n+2+k}}{k! \Gamma(n+k+1)}$$

where Γ , the Gamma function is given as:

$$\Gamma(n+1) = n! \quad \text{for } n = 0,1,2,\dots \quad \text{where } 0! = 1. \quad (3.6)$$

When calculating the zeroth order (axisymmetric mode: $m=0$) modified Bessel function of the first kind, only the ascending series shown in Eq. 3.5 was used. The modified Bessel functions of the second kind were calculated from the modified Bessel functions of the first kind again using the ascending series for the zeroth order function as follows:

$$K_0(x) = -\left\{\ln\left(\frac{x}{2}\right) + \gamma\right\} I_0(x) + \frac{x^2}{2^2} + \frac{x^4}{2^2 4^2} \left(1 + \frac{1}{2}\right) + \frac{x^6}{2^2 4^2 6^2} \left(1 + \frac{1}{2} + \frac{1}{3}\right) + \dots, \quad (3.7)$$

where $\gamma = 0.5772156649$, and for modified Bessel functions of the second kind of integer order greater than zero:

$$K_1(x) = \frac{1}{I_0(x)} \left[\frac{1}{x} - I_1(x) K_0(x) \right] \quad (3.8)$$

$$K_i(x) = -\frac{2(i+1)}{x} K_{i+1}(x) + K_{i+2}(x). \quad (3.9)$$

As stated earlier, the above equations only hold when calculating modified Bessel functions of integer order. An interesting trend can be identified in the real part of the axial direction velocity disturbance eigenfunction. Figures 3.3 - 3.6 show the eigenfunctions for

modes 0, 1, and 2. In Fig 3.6, the real part of the axial direction velocity disturbance eigenfunction, a clear trend exists regarding the location of the relative minima and maxima with respect to one another for a given eigenfunction. The intermediate minima and maxima for the real part of the velocity disturbance eigenfunction for the mode $m = 0$ grow in their relative positions to the absolute minimum and maximum, as the mode of excitation increases until finally, at mode $m = 2$, the absolute minimum and maximum occur between a local minimum and a local maximum.

It is also of interest to note that while it has been proven that the growth rates decrease as azimuthal mode number of excitation increases (Huang [1994]), the velocity disturbance eigenfunctions become more inclined, (steeper), suggestive of larger velocity gradients in the shear layer of the jet. While this phenomena is more pronounced in the axial (z) direction velocity disturbance eigenfunctions (particularly in the real component of velocity), the trend is still evident in the azimuthal and radial direction disturbance eigenfunctions. This effect may be better measured, as will be seen shortly, by means of an average total vorticity level measurement.

3.3 Multi-Mode Excitation

As a free jet undergoes transition from laminar to turbulent flow, it is safe to say that as the turbulence evolves, the fluid motion (on a fine scale) becomes random. Thus, it could be

argued, to a greater or lesser extent, that the frequency content for an infinite number of independent frequencies with which velocity fluctuations occur, would be found in this turbulence. This finite amount of frequency content over all frequencies within a specified range, could be looked at as a sort of excitation of an infinite number of modes at levels corresponding to the relative amount of content at a particular frequency. In such a case, the total excitation energy would be analogous to the mean turbulence kinetic energy. This phenomena could be looked at as being a problem of multiple mode excitation and leads to an interesting question: what effect would simultaneously forcing a jet at several modes of excitation have on the stability of the jet and ultimately upon the entrainment resulting from this unstable physical situation.

Now it would seem that in order to experimentally excite a jet simultaneously at multiple modes, a separate series of actuators would be required to operate under a specific phase offset from one actuator in its group to the next actuator in its group at a frequency also specific to its series of actuators, for each mode of excitation. That is, for each mode that is to be excited, a separate series of actuators would be required to disturb the flow. It is much easier to accomplish this from a linear stability analysis point of view than to produce this effect experimentally.

At first, one might question whether or not additional speakers would be necessary.

When looking at the exponential part of the normal mode assumption:

$$e^{i(\alpha z + m\theta - \omega t)} \quad (3.10)$$

and breaking the exponential down into sines and cosines and adding them to the resulting sines and cosines of another mode of excitation with a different azimuthal mode number and a different frequency, a product of sines and cosines of the combined argument would result. This result could then be interpreted as a resulting mode, m , made up of some expression of the arguments of the exponents of the two original modes of excitation. This representation of multiple modes as a single combined mode, in fact, would not work, because of the effects of multiplying the exponential by the disturbance eigenfunction corresponding to a specific mode. It would be similar to performing the addition of: $Ae^{x^1} + Be^{x^2}$ and coming up with something of the form: Ce^{x^3} . For example, breaking the complex exponential into sines and cosines, it is clear that $A\sin(x_1) + B\sin(x_2)$ cannot be represented as $C\sin(x_3)$. Therefore, it should also be clear that the complex arguments cannot be combined into a single complex term of the form previously mentioned.

To excite the circular jet at two different modes, the linear stability analysis needs only to be performed separately for each mode of excitation, then the velocity disturbance components in the radial, azimuthal, and axial directions resulting from one mode of excitation would simply be added to the velocity disturbance eigenfunction components of the same direction resulting from the second mode of excitation. This superposition of velocity disturbance fields applies for any number of modes that one wishes to consider.

Thus for any two modes m_1 and m_2 , excited at frequencies ω_1 and ω_2 respectively, the velocity disturbances in some arbitrary direction x are:

$$v_{x1} = \varepsilon_1 u_{x1}(r) e^{i(\alpha_1 z + m_1 \theta - \omega_1 t)} \quad (3.11)$$

and

$$v_{x2} = \varepsilon_2 u_{x2}(r) e^{i(\alpha_2 z + m_2 \theta - \omega_2 t)} \quad (3.12)$$

where ε_1 and ε_2 are the levels of disturbance (percent of jet centerline basic velocity) for excitation at modes m_1 and m_2 respectively. The quantities $u_{x1}(r)$ and $u_{x2}(r)$ are the velocity disturbance eigenfunctions in the x-direction which are given as a function of radius, r . Thus the velocity disturbance (in the x-direction) for a circular jet simultaneously excited at modes m_1 and m_2 becomes:

$$\begin{aligned} v_x &= v_{x1} + v_{x2} \\ &= \varepsilon_1 u_{x1}(r) e^{i(\alpha_1 z + m_1 \theta - \omega_1 t)} + \varepsilon_2 u_{x2}(r) e^{i(\alpha_2 z + m_2 \theta - \omega_2 t)} \end{aligned} \quad (3.13)$$

and the velocity disturbance (in the x-direction) for a circular jet excited at some arbitrary number (k), of modes is given by the following expression:

$$\begin{aligned}
v_x &= \sum_{i=1}^k u_{xi} \\
&= \sum_{i=1}^k \varepsilon_i u_{xi}(r) e^{i(\alpha_i z + m_i \theta - \omega_i t)} .
\end{aligned}
\tag{3.14}$$

Given this expression (Eq. 3.14), any application which involves the effects of excitation at one mode can be easily adapted to account for multi-mode excitation.

When superimposing the resulting disturbance fields from different modes of excitation upon one another, there is the inherent question of the phase relationship between the different modes excited. Because of the lack of an imposed normalization of the eigenfunctions in addition to the approximate normalization preserved by the matching process, the phase relationship between multiply excited modes will be to some extent arbitrary and uncontrolled. This will not affect the conclusions that will be drawn from the visualizations.

3.4 Results -- Streakline Visualizations

3.4.1 Integer Modes of Excitation

One method of visualizing the results of linear stability analysis is to look at visualizations of streakline evolution using the velocity disturbance fields resulting from the stability analysis. The spatial linear stability analysis tool created by Huang [1994] and adapted by the author provides the eigenfunctions necessary to calculate the velocity at any point in the flow. With this knowledge, a particle released at some specific time t , at some location (r, θ, z) , in the flow field, can be tracked as it travels downstream. The path that it follows can reveal a great deal about how structures in the near field evolve. The limit to the usefulness of the streakline method of flow visualization for linear stability analysis corresponds to the limit of the prevailing linear effects of the perturbed the Euler equations over the non-linear effects.

The original code used to calculate the streaklines was written by Huang [1994], however, it was only intended to calculate the streaklines for the axisymmetric ($m=0$) mode. This code was altered by the author to allow for azimuthal variation of the streaklines (as well as for fractional mode excitation). For each mode investigated (0, 1, and 2), six streakline plots were calculated over a range of times, measured in forcing periods, from 0.5 forcing periods, up to 1.5 forcing periods. The plots show the streaklines at times $0.5T$, $0.7T$, $0.9T$, $1.1T$, $1.3T$, and $1.5T$, where $T = 2\pi/\omega$ is the forcing period for a particular mode of excitation. Thus, the developing streaklines were calculated over one forcing period and should provide all the information that could be gathered from any streakline study of the flow.

In addition to the single-mode excitation streakline calculations, visualizations were also calculated for jets excited at multiple modes. The modes excited for this case were modes zero

one (0 and 1).

In each case, the streaklines were only calculated out to a maximum of four jet radii downstream, and only for one half (one side) of the jet. Looking at Figs. 3.10 - 3.15, it can be seen that if the streaklines were to be calculated around the full periphery of the jet, it would be difficult to determine any definite structures present in the flow field. Again, in all cases the total level of disturbance at the jet exit was 5 percent of the centerline basic axial velocity. In cases where multiple modes were excited, each mode was excited with a fraction of the disturbance energy proportional to the number of modes excited for that case. That is, for the calculations performed for two modes of excitation, each mode was excited with 2.5 percent of the centerline basic axial velocity. The constant disturbance level for all cases was chosen to ensure that an equivalent amount of energy went into forcing the flow, and so that any comparison of the results of different modes of excitation would be on an equal basis.

The axisymmetric mode ($m=0$) streaklines will be investigated first since they are the least complex. It should be obvious in Fig. 3.7 that exciting the jet at mode $m=0$ results in a pulsating, axisymmetric disturbance. A particle released in the shear layer of the jet, very close to the exit would travel along one of the trajectories shown in Fig. 3.7. Roll-up of the flow into vortices occurs at the same axial distance from the jet exit independent of azimuthal location. This can be seen in Fig. 3.8 where the streaklines are displayed from a side, top (looking down the streamwise axis), and arbitrary view. The top view will subsequently be referred to as a view looking down the streamwise axis (the axial direction). Although not to scale, the top view of

the streaklines clearly shows that no azimuthal disturbance exists in the jet. Thus, for the axisymmetric case, a single streakline is indicative of the entire flow field and may reveal more insight to the development of vortical structures when viewed alone as it is in Fig. 3.9.

The periodic nature of the jet is also evident at time $1.5T$, as the vortical structure at three jet radii from the exit is well developed, while another vortical structure can be seen forming just after exiting the jet. It is important to note that the streaklines shown for time $0.5T$ are exactly the same as those at time $1.5T$ with the exception that at time $1.5T$, the flow field has been allowed to evolve further downstream.

Looking at Fig. 3.10 gives a good indication of the evolution of the flow field resulting from excitation at the first azimuthal mode ($m=1$). It should be immediately obvious that excitation at mode $m=1$ results in an azimuthal deviation from the initial starting point for a given fluid particle. That is the flow is clearly no longer axisymmetric as it was for the $m = 0$ case. It can be seen that as the jet first begins to show signs of roll-up, one side of the jet is being sucked inward toward the jet center while the opposite side is being pushed outward, away from the jet center (Fig. 3.11). This figure also shows that roll-up occurs on one side of the jet before occurring on the opposite side in an un-even, or rather non-parallel evolution of the jet. Actually, rather than one side of the jet experiencing roll-up prior to the other side as is seen in the evolution of elliptical jets (where roll-up occurs on the minor axis before occurring on the major axis (Mutter [1994], Huang [1994] and Blair [1995])), the formation of the structure can be seen to develop in such a manner that a continuous helical vortical structure is produced as the jet

evolves downstream. Again, notice that the streaklines are the same for time $0.5T$ and time $1.5T$ except that at time $1.5T$ the flow field has evolved further (Fig. 3.10). Unfortunately, the streaklines cannot be viewed as a single streakline as in Fig. 3.9 for the axisymmetric mode case. The three dimensionality of the flow precludes a clear representation of the flow in a single meridional plane.

For excitation at the second azimuthal or helical mode $m=2$ (Fig. 3.12), effects similar to those seen to result from forcing the jet at mode $m=1$ are apparent. Again, one side of the jet is sucked in while the side experiencing roll-up first is being pushed out. The appearance of the continuous helical vortical structure can be seen again as well. However, it now appears that the vortical structure travels downstream at a faster rate than its $m=1$ counterpart. This result is expected as the effect of increasing the mode number, should be predicted from the mathematical representation of normal modes. The mode number plays a major role in the exponential term:

$$e^{i(\alpha z + m \theta - \omega t)} = \cos(\alpha z + m \theta - \omega t) + i \sin(\alpha z + m \theta - \omega t) , \quad (3.15)$$

where the expected effect of increasing the mode number m , increases the rate at which the phase of the disturbance cycles with azimuthal location θ (spatially), at some time t . Thus, for $m = 2$, the helical evolution of the disturbance would be expected to complete two spatial cycles in the time it would take for the first azimuthal mode to complete one temporal cycle.

3.4.2 Multi-Mode Excitation

The effects of multi-mode excitation can be seen in Fig. 3.13 showing streakline evolution for modes zero and one (0 and 1) excited simultaneously. Comparing the resulting streaklines from multi-mode excitation with those from single mode excitation show more or less what one might expect, that there is a definite helical tendency to the vortical structure, however, it is no longer a continuous vortical structure such as those seen in the singly excited azimuthal modes. Roll-up still occurs at approximately the same downstream distance as in the axisymmetric case, however, now roll-up occurs on one side of the jet considerably earlier than it does on the opposite side of the jet.

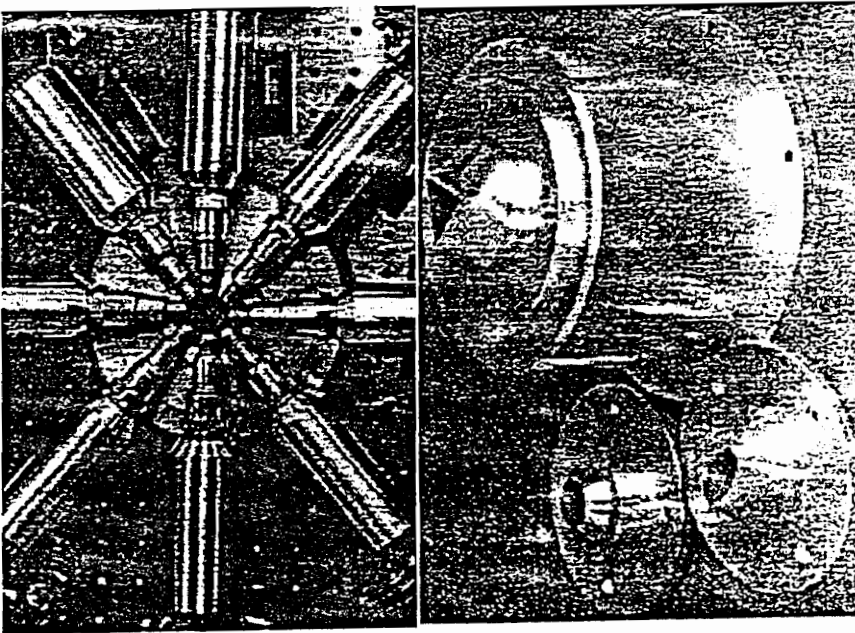
Another interesting aspect of the multi-mode excitation is the stretching of the vortices in the azimuthal direction. Close inspection of the evolution plot, Figs. 3.13, shows the centers of the vortex like structures being drawn out in the azimuthal direction. It is also of interest to note that the formation of the vortices appear to be much more coherent (orderly) than those due solely to azimuthal excitation. Again, this can be explained by the resulting roll-up of the flow in the axisymmetric jet combined with the appearingly less structured vortical elements in azimuthally excited jet resulting in vortical structures of decreasing levels of order.

With one of the goals of this effort being to identify causes of jet instabilities leading to increased levels of entrainment, one would assume that for higher levels of disorder in the flow, correspondingly higher levels of entrainment would result. Thus, one might expect that with greater levels of disorder in the vortical structures, such as those seen in Fig. 3.14 from a view looking directly at the jet exit, there would be higher levels of entrainment. However, it is well

documented that in experiment (Michalke [1964] and many others), that the axisymmetric and first azimuthal modes, the modes with the highest growth rates, cause the highest levels of entrainment. It is clear from Figs. 3.7 and 3.13 that as the vortical structure forms and is carried off down stream, the fluid below it wells up (appearing similar to the mushroom cloud resulting from a large explosion) and the potential core is sucked inward. This is a clear indicator of how the surrounding ambient fluid is entrained into the jet and carried off downstream where it undergoes fine scale mixing. This phenomena is perhaps better predicted by a property called vorticity which will be discussed next.

Figure 3.1

Experimental Set-Up



Courtesy of Ding [1995]

Figure 3.2

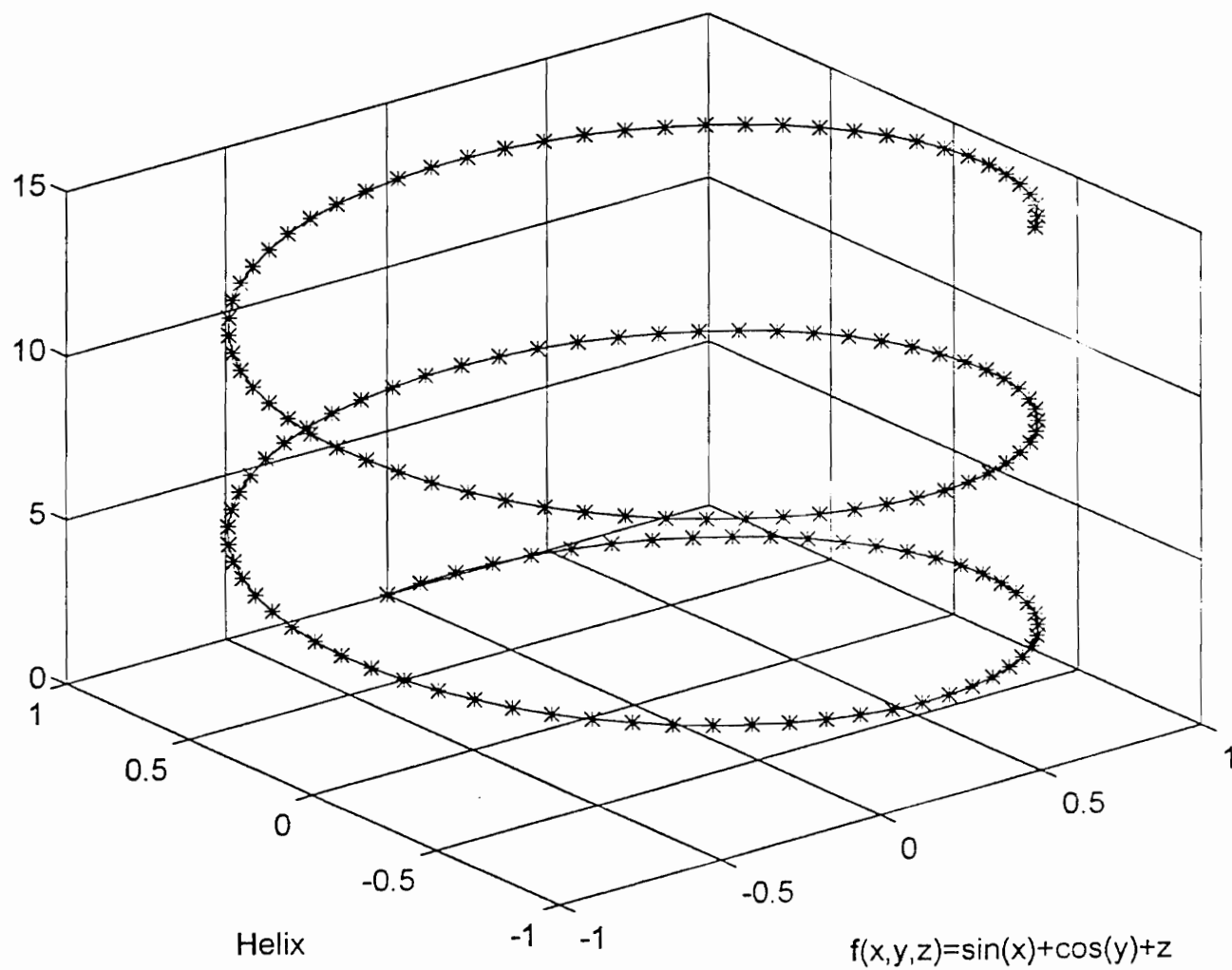
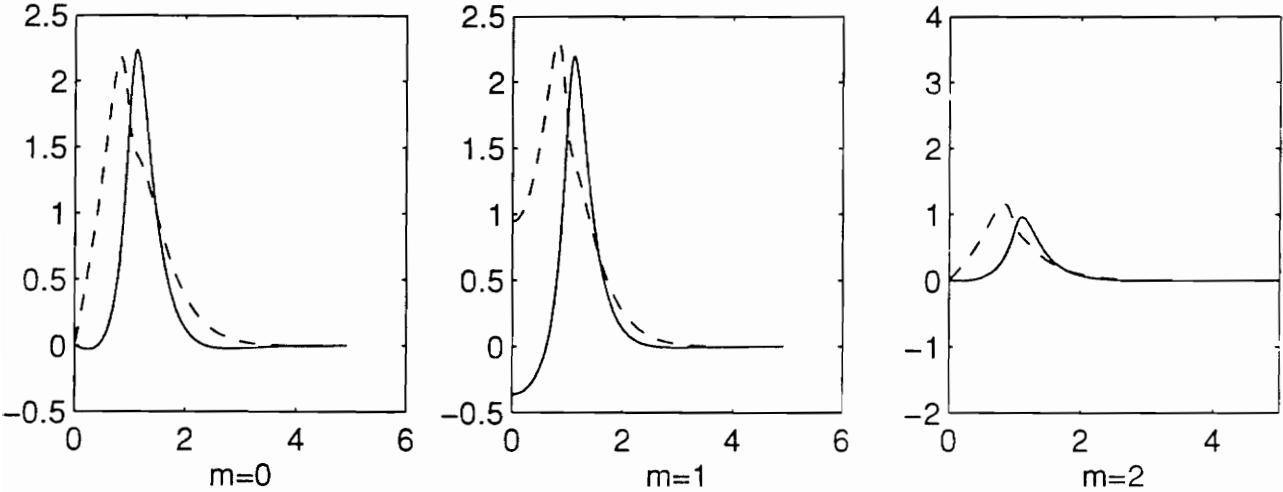
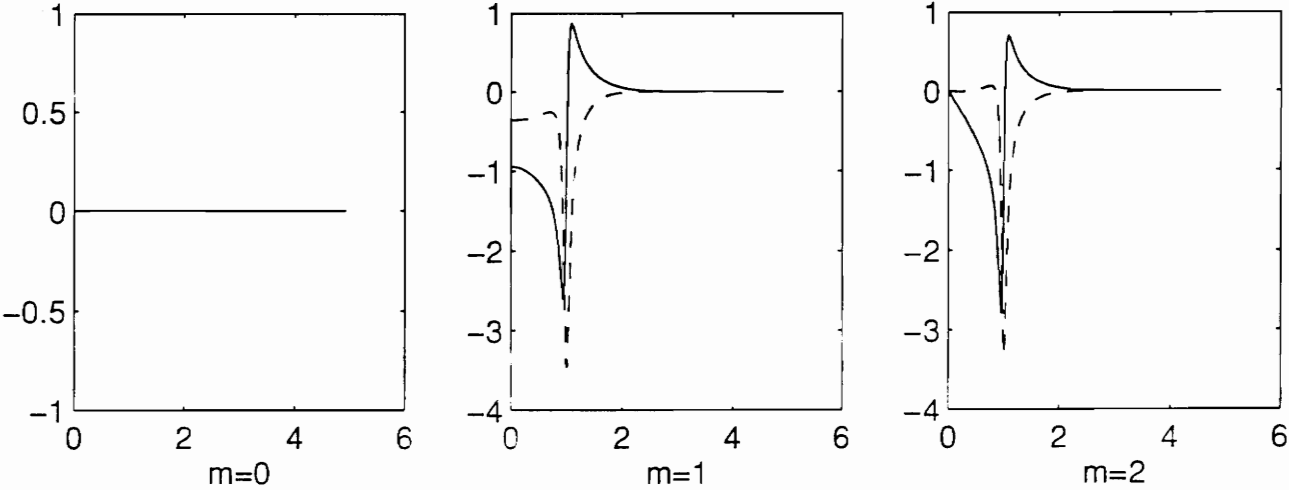


Figure 3.3 Radial Direction Velocity Disturbance Eigenfunctions



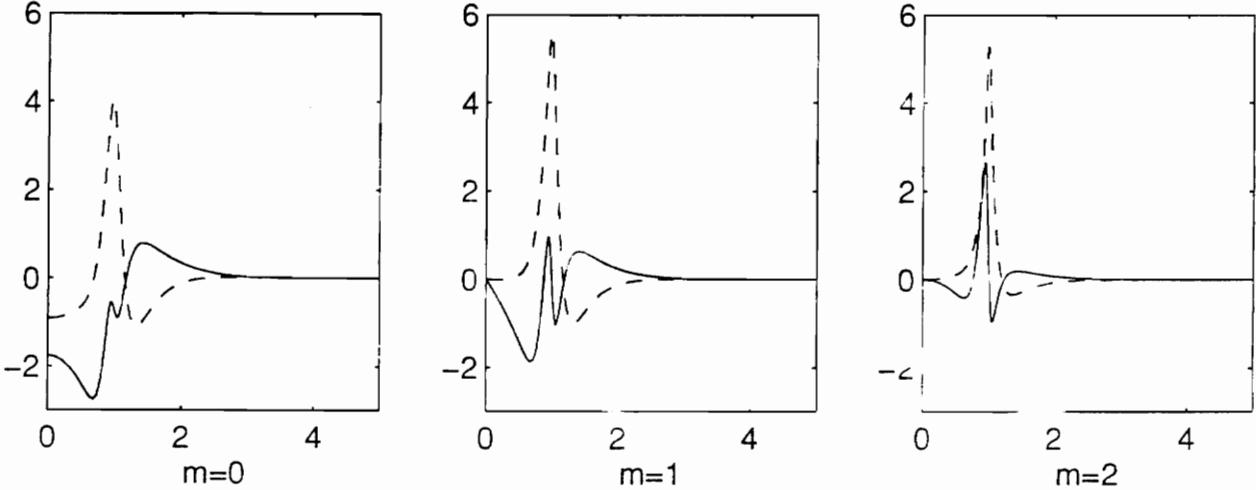
axes: radial coordinate vs. magnitude

Figure 3.4 Azimuthal Direction Velocity Disturbance Eigenfunctions



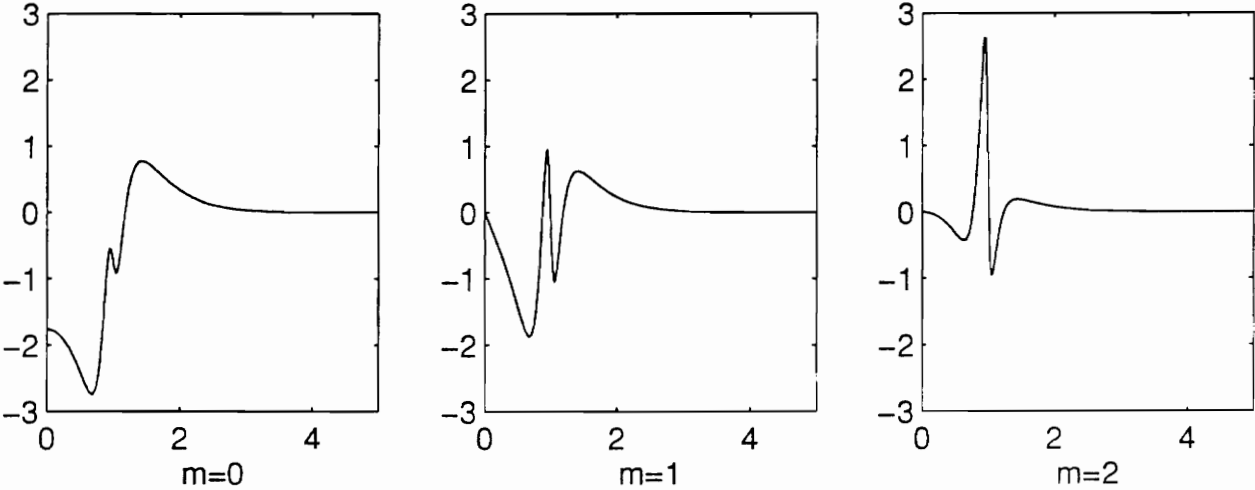
axes: radial coordinate vs. magnitude

Figure 3.5 Axial Direction Velocity Disturbance Eigenfunctions



axes: radial coordinate vs. magnitude

Figure 3.6 Real Axial Direction Disturbance Eigenfunctions



axes: radial coordinate vs. magnitude

Figure 3.7

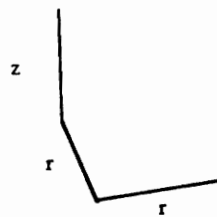
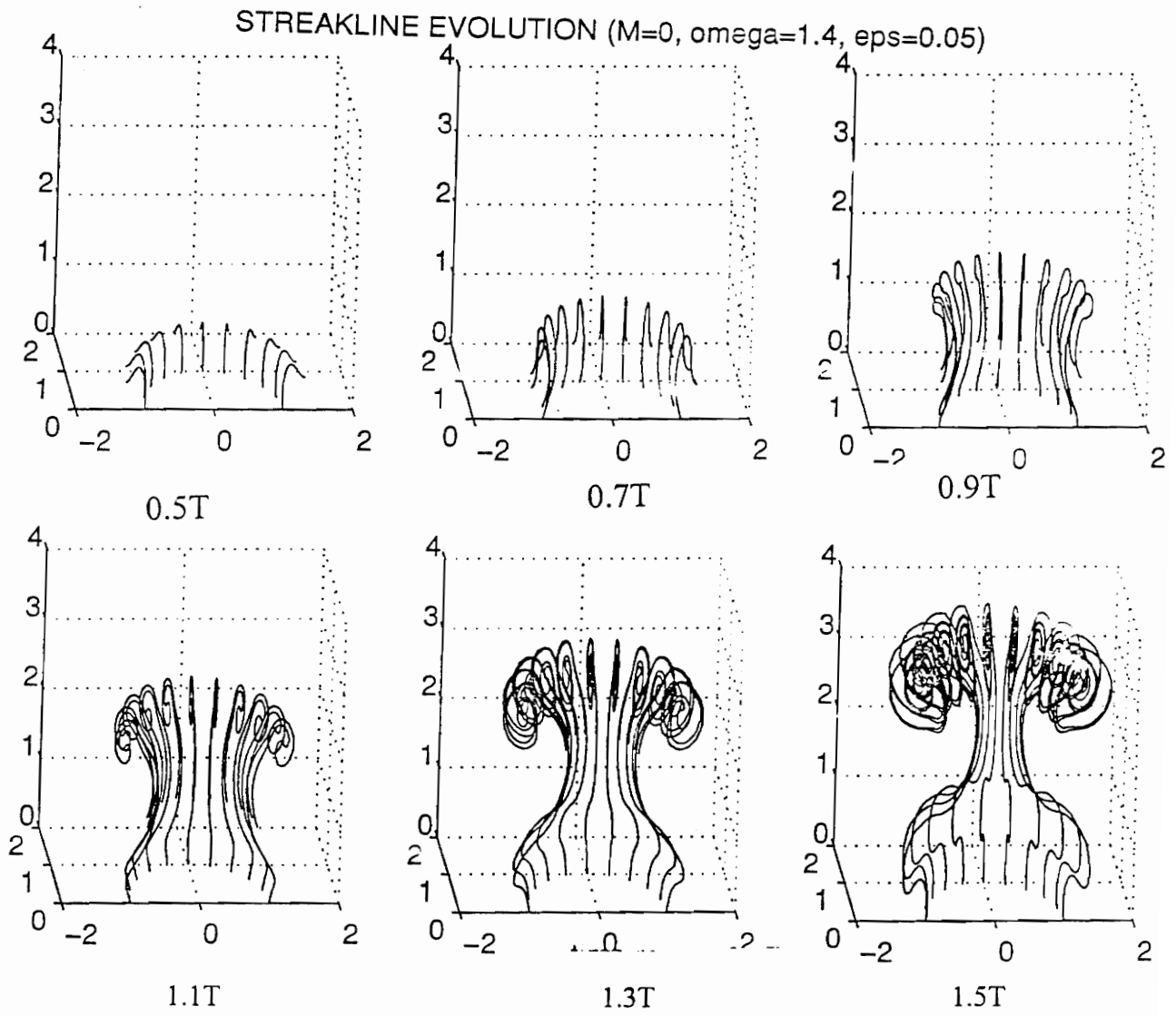


Figure 3.8

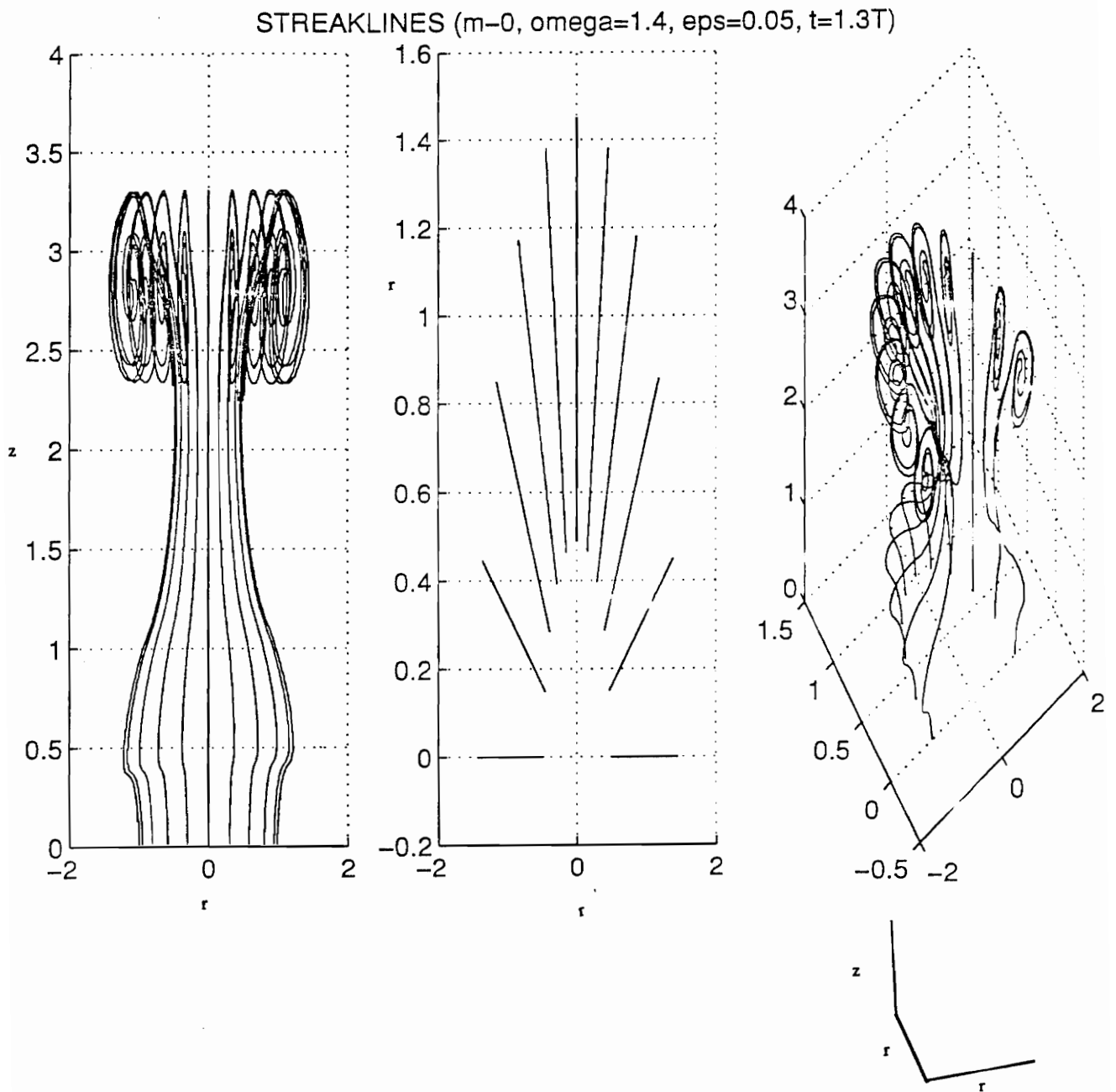


Figure 3.9

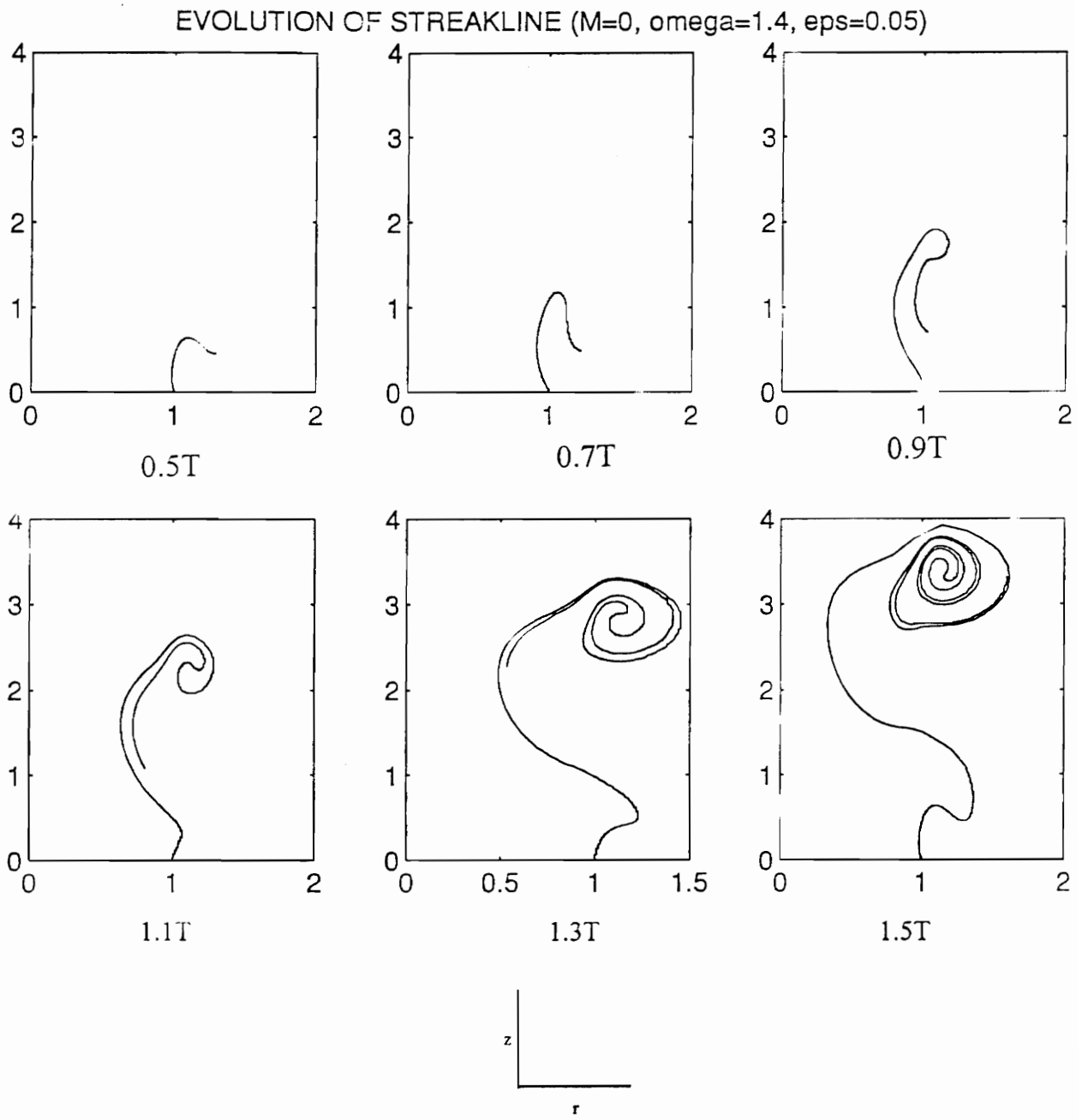


Figure 3.10

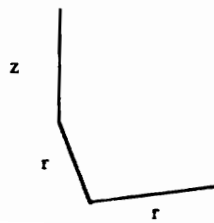
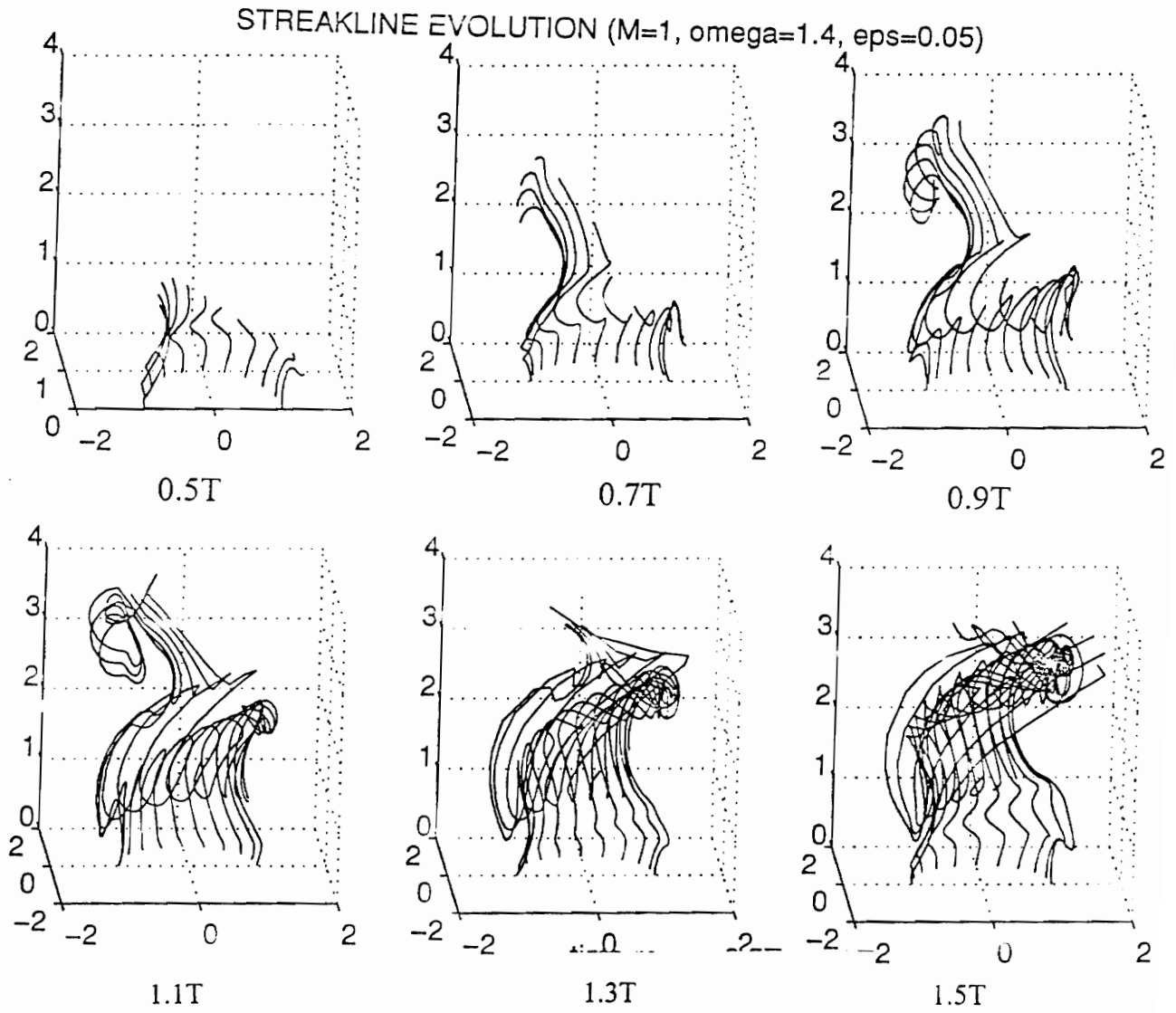


Figure 3.11

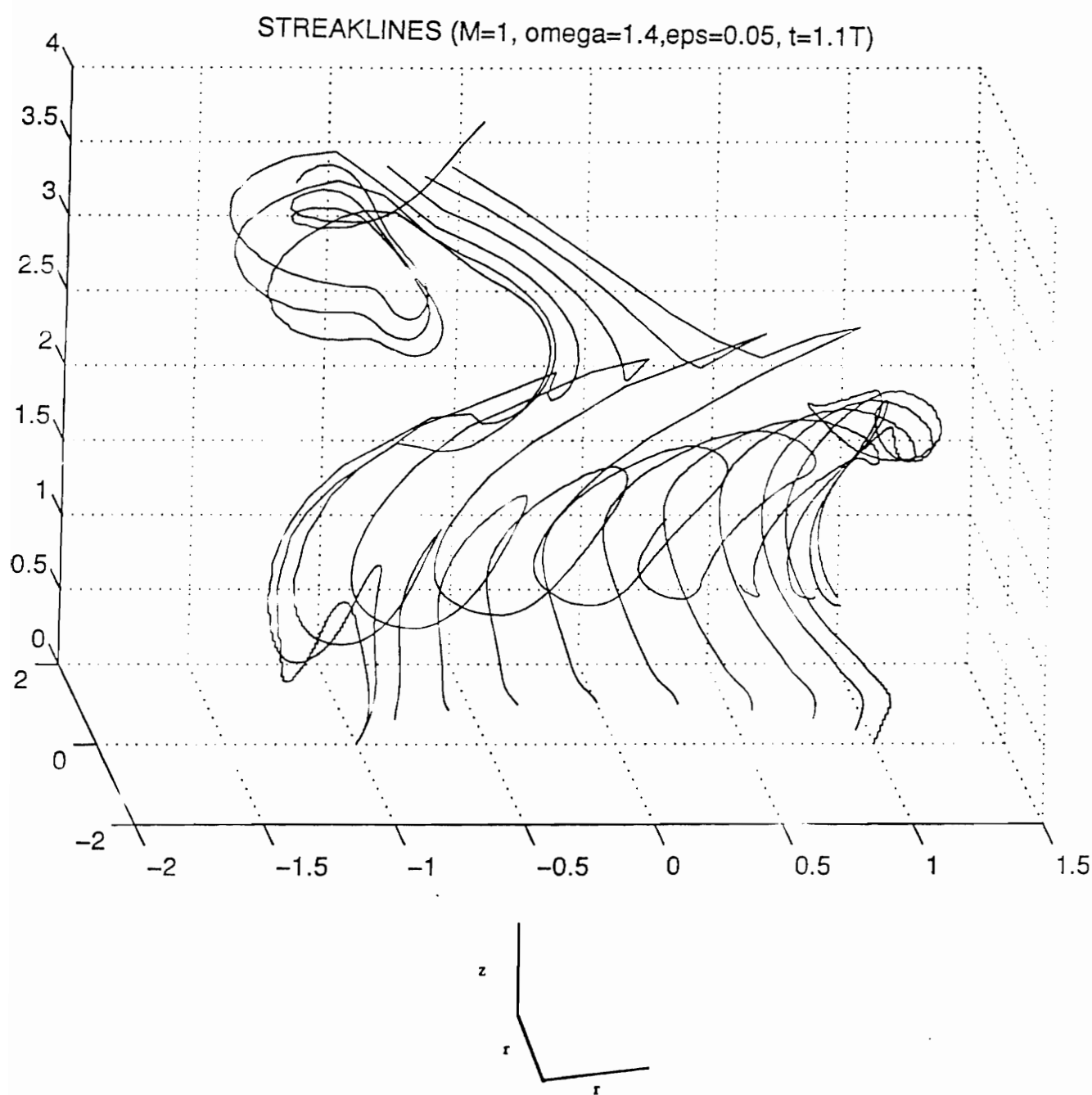


Figure 3.12

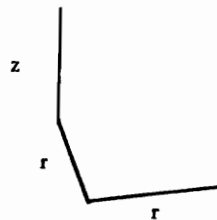
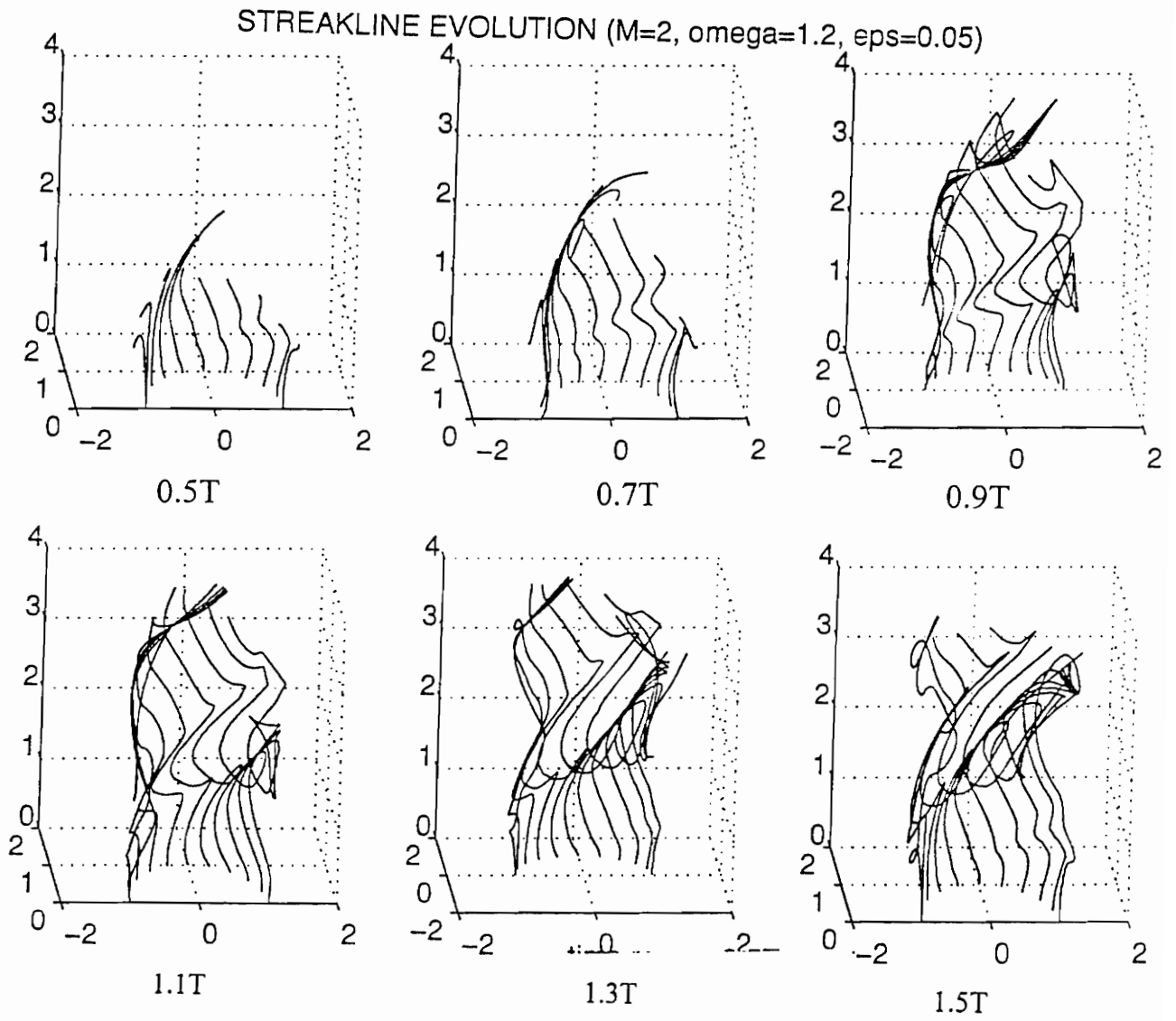


Figure 3.13

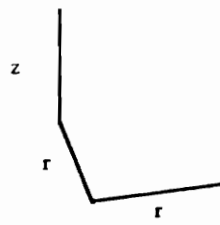
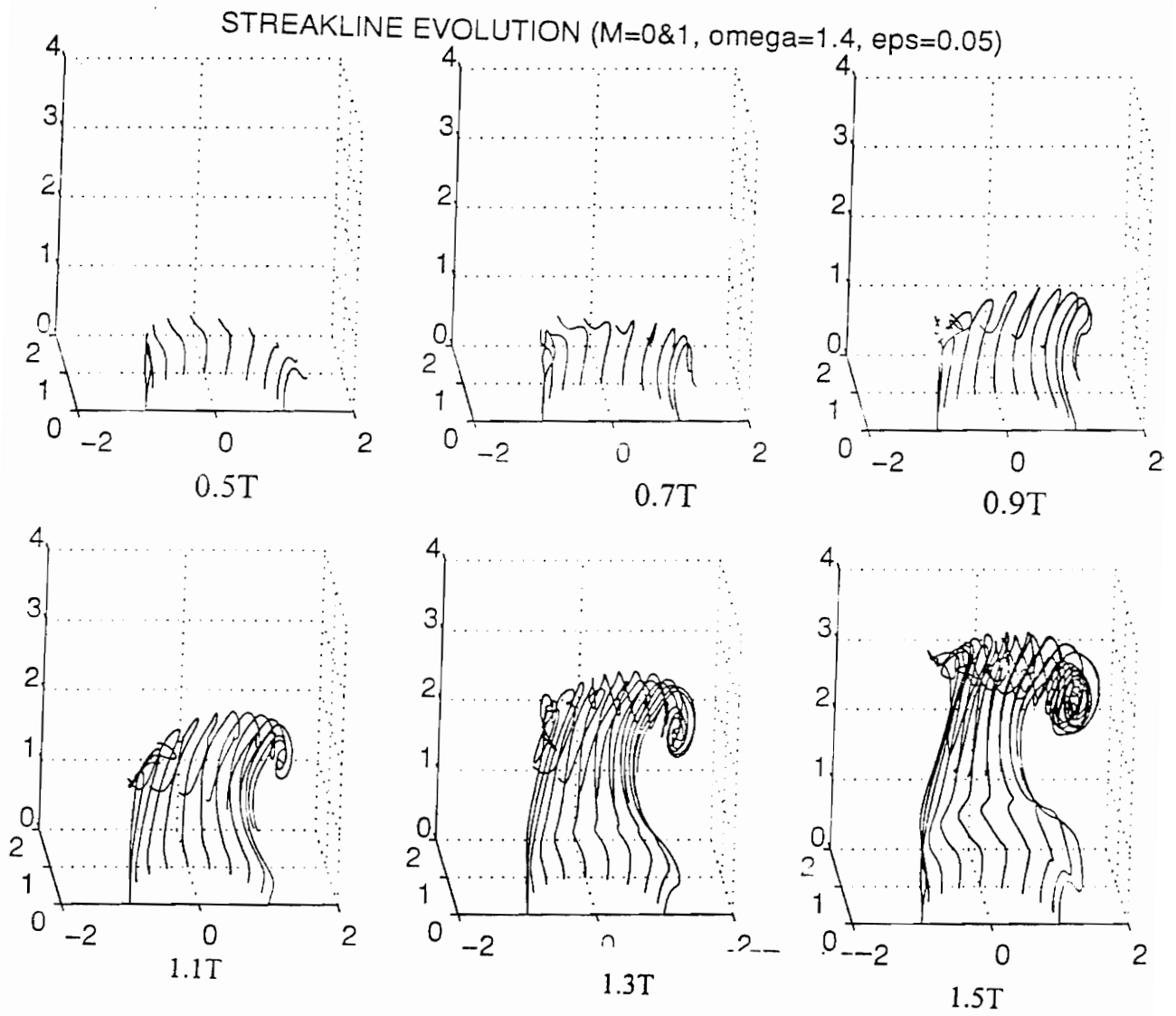
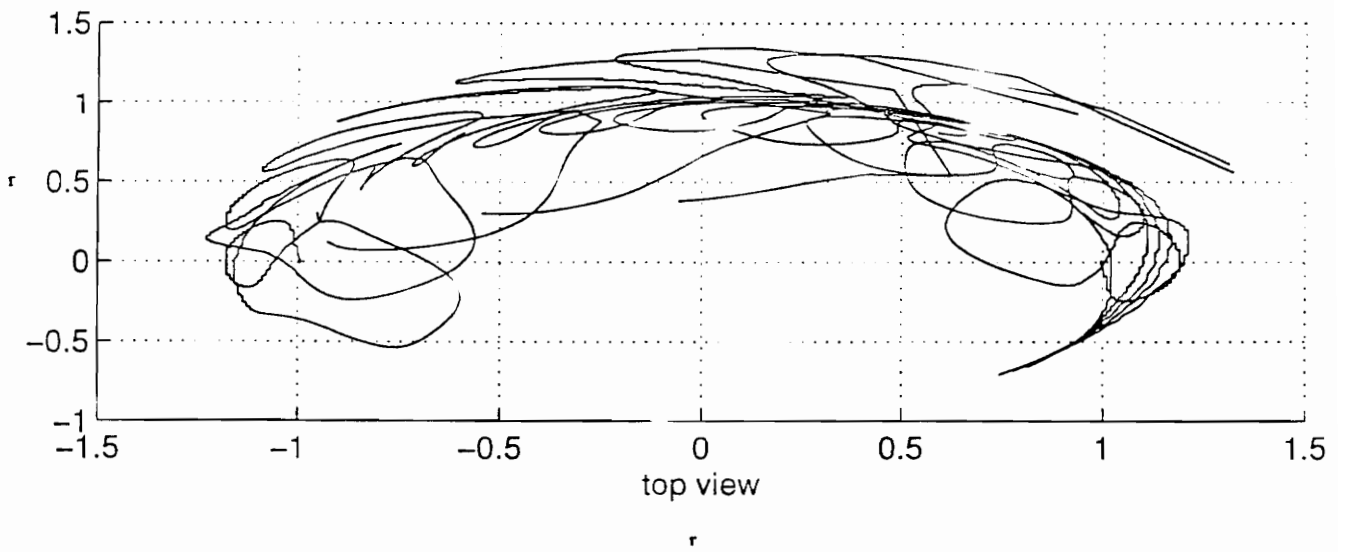
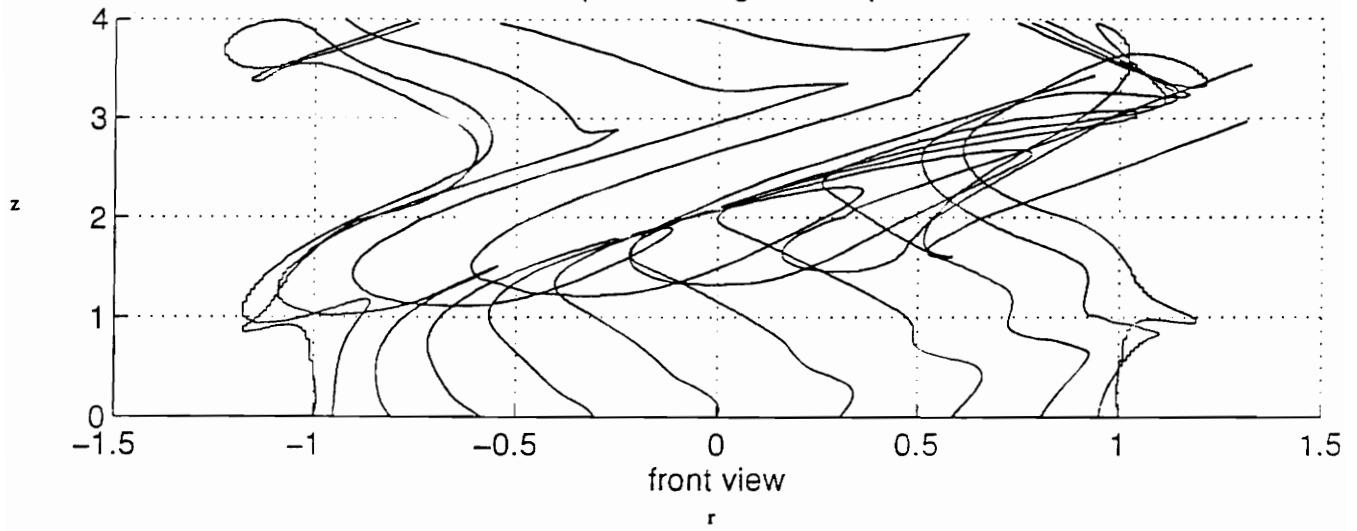


Figure 3.14

STREAKLINES ($M=2$, $\omega=1.2$, $\epsilon=0.05$, $t=1.5T$)



CHAPTER 4:

ENTRAINMENT

4.1 Description

Accompanying the vortical patterns described in the previous chapter is the induced motion of the surrounding fluid near the shear layer of the jet. As the jet evolves downstream from the exit, the surrounding fluid is engulfed into the jet, begins mixing with the jet fluid, and is carried off down stream. This induced motion of the fluid surrounding the potential core is called entrainment.

Vortical structures forming in the shear layer of the jet engulf relatively large quantities of the surrounding fluid into the jet stream. As the original jet fluid and the entrained fluid travel downstream, they continue to mix on finer and finer scales until mixing on a molecular level has occurred. For applications such as combustors, as mentioned earlier, the more rapidly the entrainment process leads to molecular level mixing, the sooner combustion can occur. Also, the more homogenous the mixing of the fuel and oxidizer, the more efficient the combustion process. Both of these effects are desirable developments in combustor design.

As one of the goals of the present work is to investigate the effects of fractional mode excitation and multiple mode excitation to suggest improvements to increase entrainment, there is a need to determine how best to measure entrainment resulting from different modes of excitation.

Huang [1994] showed a connection between high levels of vorticity and corresponding high levels of entrainment. His argument was based upon vorticity counts. Dividing the flow field up into many locations on a grid, the vorticity count was taken as the number of grid locations that represented areas of the flow field where the vorticity level was above a specific threshold. As the flow evolved downstream, the number of counts at an axial location for vorticity levels above this threshold increased, indicating a spreading of the jet. This spreading indicated the induced motion of the previously unmoving flow, thus indicating higher levels of entrainment. Thus it is postulated that high levels of vorticity are indicative of large gradients. Real fluids tend to diffuse local regions of high vorticity which lead to higher vorticity counts indicative of higher levels of entrainment. Thus, the total level of vorticity is suggested as providing a good basis of comparing the levels of entrainment resulting from excitation at different modes.

4.2 Vorticity

4.2.1 The nature of Vorticity

Vorticity is a vector indicative of the rotation of a small mass of fluid with respect to a set of chosen coordinates. In a fluid flow, tangential stresses on a viscous fluid element can induce angular velocities in the fluid element and set the particles spinning. Mathematically speaking, the vorticity $\vec{\Gamma}$, is the curl of the velocity vector:

$$\begin{aligned}\vec{\Gamma} &= \text{curl}(\vec{u}) \\ &= \nabla \times \vec{u}\end{aligned}\tag{4.1}$$

where ∇ is the ‘del’ operator given in cylindrical coordinates by:

$$\nabla = (\hat{i}_r \frac{\partial}{\partial r} + \hat{i}_\theta \frac{1}{r} \frac{\partial}{\partial \theta} + \hat{i}_z \frac{\partial}{\partial z})\tag{4.2}$$

and \hat{i}_r , \hat{i}_θ hat, and \hat{i}_z hat are unit vectors in the radial, azimuthal, and axial directions respectively.

Since the modified spatial linear stability analysis of Huang [1994], developed in Chapter 2, gives the non-dimensional velocity at every point in the flow field, we can use the expressions for the velocities to derive the expressions for the vorticity. The three components of vorticity thus become:

$$\Gamma_r = \varepsilon \left(\frac{1}{r} u_z(r) i m - u_\theta(r) i \alpha \right) e^{i(\alpha z + m \theta - \omega t)} \quad (4.3)$$

$$\Gamma_\theta = -\frac{dU_z(r)}{dr} + \varepsilon \left(u_r(r) i \alpha - \frac{du_z}{dr} \right) e^{i(\alpha z + m \theta - \omega t)} \quad (4.4)$$

$$\Gamma_z = \varepsilon \left(\frac{du_\theta}{dr} - \frac{1}{r} u_r(r) i m + \frac{u_\theta}{r} \right) e^{i(\alpha z + m \theta - \omega t)} \quad (4.5)$$

for the radial, azimuthal and axial directions. Continuing to use Michalke's second basic streamwise velocity profile, Eq. 2.44, the derivative of the basic axial velocity term in the azimuthal component of vorticity becomes:

$$U_z(r) = \frac{1}{2} \left\{ 1 + \tanh \left[\frac{1}{4} \frac{R}{\theta} \left(\frac{R}{r} - \frac{r}{R} \right) \right] \right\} \quad (2.44)$$

$$\frac{dU_z(r)}{dr} = -\frac{1}{8} \frac{R}{\theta} \left(\frac{1}{R} + \frac{R}{r^2} \right) \text{sech}^2 \left[\frac{1}{4} \frac{R}{\theta} \left(\frac{R}{r} - \frac{r}{R} \right) \right] \quad (4.6)$$

where R is the jet radius and θ is the momentum thickness (not to be confused with azimuthal coordinate θ).

Now, in order to compute the vorticity field at any time t , for a given disturbance level ε , the linear stability analysis must be carried out for a given mode m , frequency ω , and momentum thickness θ . The analysis will determine the eigenfunctions (as a function of radius), and the eigenvalue (complex wave number α). The stability analysis, level of disturbance and the specific time at which the jet is observed, provide all the information needed for computation of the vorticity field. Unfortunately, the computed vorticity field only holds at this specific time t , and is continuously changing in time. Thus, if the vorticity fields resulting from two different modes of excitation are to be compared, depending upon the time at which the two are compared and depending upon the location (r, θ, z) in the flow field, either mode of excitation may be indicative of a greater level of vorticity in either the radial, azimuthal, or axial directions. Thus, some sort of average vorticity measure is required.

4.2.2 Singly Excited Modes

The most logical method of taking an average vorticity measurement would be to average

the vorticity values over one period. This could be accomplished by integrating the expression for the vorticity over one period T , with respect to time t , and then dividing by the period; mathematically expressed by the following:

$$\Gamma_{r \text{ avg}} = \frac{1}{T} \int_0^T \Gamma_r dt \quad (4.7)$$

$$\Gamma_{\theta \text{ avg}} = \frac{1}{T} \int_0^T \Gamma_{\theta} dt \quad (4.8)$$

$$\Gamma_{z \text{ avg}} = \frac{1}{T} \int_0^T \Gamma_z dt \quad (4.9)$$

where the period is equal to $2\pi/\omega$. With the only term containing time (t) as a variable being the exponential, the proposed average measurements for vorticity would be:

$$\Gamma_{r \text{ avg}} = \frac{1}{T} C_r \int_0^T e^{-i\omega t} dt = 0 \quad (4.10)$$

$$\Gamma_{\theta_{avg}} = -\frac{dU_z(r)}{dr} + \frac{1}{T}C_\theta \int_0^T e^{-i\omega t} dt = -\frac{dU_z(r)}{dr} \quad (4.11)$$

$$\Gamma_{z_{avg}} = \frac{1}{T}C_z \int_0^T e^{-i\omega t} dt = 0 \quad (4.12)$$

where C_r , C_θ , and C_z are constants made up of the arguments forming the equations for the vorticity components in the radial, azimuthal, and axial directions. Unfortunately, since the only term that varies with time (t) is a complex exponential, when expressed as a sine and a cosine term and integrated over a period, they will always yield zero. Thus, the only component of vorticity that has a non-zero value when averaged in this way is the azimuthal component.

Worse still is the fact that regardless of the mode of excitation, the proposed azimuthal component of vorticity will always be the derivative of the basic streamwise velocity.

This result should be somewhat expected. After all, when looking at the velocity field, each component of velocity results from velocity perturbations except the basic axial velocity. By definition, the mean of the perturbations is zero, and thus any vorticity resulting from a perturbed velocity would also be zero. This being the case, another method of taking an average measurement of the vorticity must be devised.

The expressions for the vorticity contain both real and imaginary parts, thus, integrating the absolute value of the square of a particular component of vorticity would have to lead to a non-zero value unless both the real and imaginary parts of that component of vorticity were both 0 for all instances of time t . Therefore, it is now proposed to take an average measurement of the vorticity as follows:

$$\Gamma_{r \text{ avg}} = \frac{1}{T} \int_0^T |\Gamma_r|^2 dt = \frac{1}{T} \int_0^T |\Gamma_r \Gamma_r^*| dt \quad (4.13)$$

$$\Gamma_{\theta \text{ avg}} = \frac{1}{T} \int_0^T |\Gamma_\theta|^2 dt = \frac{1}{T} \int_0^T |\Gamma_\theta \Gamma_\theta^*| dt \quad (4.14)$$

$$\Gamma_{z \text{ avg}} = \frac{1}{T} \int_0^T |\Gamma_z|^2 dt = \frac{1}{T} \int_0^T |\Gamma_z \Gamma_z^*| dt \quad (4.15)$$

$$\Gamma_{total \text{ avg}} = \Gamma_{r \text{ avg}} + \Gamma_{\theta \text{ avg}} + \Gamma_{z \text{ avg}} \quad (4.16)$$

where Γ^* is the complex conjugate of Γ . Given the average components of vorticity for a

specific mode of excitation, one could compare the levels of vorticity for two different modes of excitation by comparing the values of average total vorticity at each mode. The measurements in Eqs. 4.13 - 4.16 are more accurately called the average vorticity squared. This average vorticity squared will subsequently be referred to as the average vorticity. It will be assumed from earlier arguments that the higher the values of total average squared vorticity, the greater the entrainment due to excitation at a particular mode.

At this point, it would be easy to simply give the results of integrating the above expressions, however, when first computing the square of the complex argument for the vorticity, an interesting feature of the expressions for the vorticity comes alight for two of the three components which bears discussion. A common term to each component of vorticity is:

$$\varepsilon f(\alpha, m, \text{eigenfunctions \& their derivatives}) e^{i(\alpha z + m\theta - \omega t)} . \quad (4.17)$$

The above common form can be expressed in complex notation resulting in expressions for the average values of vorticity as:

$$\Gamma_{r \text{ avg}} = (C_r + iD_r) e^{i(\alpha z + m\theta - \omega t)} \quad (4.18)$$

$$\Gamma_{\theta \text{ avg}} = G + (C_\theta + iD_\theta) e^{i(\alpha z + m\theta - \omega t)} \quad (4.19)$$

$$\Gamma_{z \text{ avg}} = (C_z + iD_z)e^{i(\alpha z + m\theta - \omega t)} \quad (4.20)$$

where

$$C_r = \varepsilon \alpha_I u_{\theta R} + \varepsilon \alpha_R u_{\theta I} - \frac{\varepsilon m}{r} u_{zI} \quad (4.21)$$

$$D_r = \varepsilon \alpha_I u_{\theta I} - \varepsilon \alpha_R u_{\theta R} + \frac{\varepsilon m}{r} u_{zR} \quad (4.22)$$

$$C_\theta = -\varepsilon u_{rR} \alpha_I - \varepsilon u_{rI} \alpha_R - \varepsilon \frac{du_{zR}}{dr} \quad (4.23)$$

$$D_\theta = \varepsilon u_{rR} \alpha_R - \varepsilon u_{rI} \alpha_I - \varepsilon \frac{du_{zI}}{dr} \quad (4.24)$$

$$G_\theta = -\frac{dU_z(r)}{dr} \quad (4.25)$$

$$C_z = \varepsilon \frac{du_{\theta R}}{dr} + \frac{\varepsilon m}{r} u_{rI} + \frac{\varepsilon}{r} u_{\theta R} \quad (4.26)$$

$$D_z = \epsilon \frac{du_{\theta I}}{dr} + \frac{\epsilon m}{r} u_{rR} + \frac{\epsilon}{r} u_{\theta I} . \quad (4.27)$$

In Eqs. 4.21 - 4.27, the R's and I's in the subscripts denote real and imaginary parts. Now, take a closer look at the the exponential argument. When split into real and imaginary components, it can be rewritten as:

$$\begin{aligned} e^{i(\alpha z + m \theta - \omega t)} &= e^{-\alpha_I z} e^{i(\alpha_R z + m \theta - \omega t)} \\ &= e^{-\alpha_I z} [\cos(x) + i \sin(x)] \\ &= e^{-i \alpha_I z} (E + i F) \end{aligned} \quad (4.28)$$

where

$$E = \cos(x) \quad (4.29)$$

$$F = \sin(x) \quad (4.30)$$

$$x = \alpha_R z + m \theta - \omega t . \quad (4.28)$$

The absolute value of the square of the vorticity components may now be expressed as:

$$\Gamma_r \Gamma_r^* = (C_r^2 + D_r^2) e^{-2\alpha_r z} \quad (4.32)$$

$$\Gamma_\theta \Gamma_\theta^* = [G_\theta + (C_\theta + ID_\theta)(E + iF) e^{-\alpha_r z}] \Gamma_\theta^* \quad (4.33)$$

$$\Gamma_z \Gamma_z^* = (C_z^2 + D_z^2) e^{-2\alpha_r z} \quad (4.34)$$

where $E^2 + F^2 = 1$ has been used in writing Eqs. 4.32 - 4.34.

In the above expressions for the radial and axial components of average vorticity, note that all temporal, frequency, and azimuthal dependance has disappeared. Although dependance upon the frequency is buried in the analysis leading to the eigenfunction terms (and their derivatives), Eqs. 4.32 and 4.34 are now functions of radial coordinate only. This means that if the average value of the radial or axial vorticity is desired, no integration with respect to time is necessary.

Looking at the average azimuthal vorticity, when the absolute value of the square is taken, the average azimuthal vorticity is still dependent upon time, azimuthal coordinate, and frequency. Multiplying the azimuthal vorticity by its complex conjugate, the following equation

results:

$$\Gamma_{\theta}\Gamma_{\theta}^* = G_{\theta}^2 + 2G_{\theta}e^{-\alpha_r z}[C_{\theta}\cos(x) - D_{\theta}\sin(x)] + [C_{\theta}^2 + D_{\theta}^2]e^{-2\alpha_r z}. \quad (4.35)$$

Since $\Gamma_{\theta}\Gamma_{\theta}^*$ is still dependent upon time, in order to get an average value for the azimuthal vorticity, $\Gamma_{\theta}\Gamma_{\theta}^*$ must be integrated over one period with respect to time and then divided by the period. It should again be evident that when integrating the above expression over one period, any term that is multiplied by a sine or a cosine, of some argument of time, will average to zero. Thus, the only terms left after performing the integration, are no longer dependent upon time. Consequently, not only is this integrated average azimuthal vorticity independent of time, it is also independent of azimuthal location and frequency of excitation. Thus, the average values of the three components of vorticity are:

$$\Gamma_{r\text{ avg}} = \Gamma_r\Gamma_r^* = [C_r^2 + D_r^2]e^{-2\alpha_r z} \quad (4.32)$$

$$\Gamma_{\theta\text{ avg}} = \frac{1}{T}\int_0^T \Gamma_{\theta}\Gamma_{\theta}^* dt = G_{\theta}^2 + [C_{\theta}^2 + D_{\theta}^2]e^{-2\alpha_r z} \quad (4.36)$$

$$\Gamma_{z\text{ avg}} = \Gamma_z\Gamma_z^* = [C_z^2 + D_z^2]e^{-2\alpha_r z}. \quad (4.34)$$

Substituting the values of the C's, D's and G in Eqs. 4.21 - 4.27 back into Eqs. 4.32, 4.34, and

4.36, the average values for the vorticity are found:

$$\Gamma_{r \text{ avg}} = \left[\left(\alpha_I u_{\theta R} + \alpha_R u_{\theta I} - \frac{m}{r} u_{zI} \right)^2 + \left(\alpha_I u_{\theta I} - \alpha_R u_{\theta R} + \frac{m}{r} u_{zR} \right)^2 \right] \epsilon e^{-2\alpha_I z} \quad (4.37)$$

$$\Gamma_{\theta \text{ avg}} = \left(\frac{dU_z(r)}{dr} \right)^2 + \left[\left(-u_{rR} \alpha_I - u_{rI} \alpha_R - \frac{du_{zR}}{dr} \right)^2 + \left(u_{rR} \alpha_I - u_{rI} \alpha_R - \frac{du_{zI}}{dr} \right)^2 \right] \epsilon e^{-2\alpha_I z} \quad (4.38)$$

$$\Gamma_{z \text{ avg}} = \left[\left(\frac{du_{\theta R}}{dr} + \frac{m}{r} u_{rI} + \frac{u_{\theta R}}{r} \right)^2 + \left(\frac{du_{\theta I}}{dr} - \frac{m}{r} u_{rR} + \frac{u_{\theta I}}{r} \right)^2 \right] \epsilon e^{-2\alpha_I z} . \quad (4.39)$$

Clearly, all three expressions for the average vorticity will grow exponentially to some function of the growth rate. The exponential term $e^{-2\alpha_I z}$ is common to all three components of average vorticity and only differs in the exponential growth rate of the velocity disturbances by a factor of e^2 . This factor of e^2 is introduced to the growth rate when the expression for one component of the vorticity is multiplied by its complex conjugate. It is interesting to see (from a mathematical point of view) that the growth rate is preserved through the calculations for the

time averaged vorticity.

It should also be noted that the term for the azimuthal component of vorticity has the constant of the derivative of the basic velocity profile squared added to the term that increases exponentially with the growth rate. It should be expected that the term for the basic velocity surfaces again in the analysis, taking the form of its derivative, because the basic velocity imposed on the flow field is always present and its effects should not be expected to disappear in subsequent calculations. Its effects on the total vorticity calculations disappear quickly as the exponential growth of the average vorticity quickly drowns out any contribution from the basic velocity derivative.

4.2.3 Multiple-Mode Excitation

When the effects of exciting the circular jet simultaneously at more than one mode are investigated, the equations determining the evolution of the vorticity field, Eqs. 4.13 - 4.15 need to be changed to allow for these effects. They become:

$$\Gamma_{r \text{ avg}} = \frac{1}{T} \int_0^T \left| \left(\sum_{k=1}^n \Gamma_{rk} \right)^2 \right| dt \quad (4.40)$$

$$\Gamma_{\theta \text{ avg}} = \frac{1}{T} \int_0^T \left| \left(\sum_{k=1}^n \Gamma_{\theta k} \right)^2 \right| dt \quad (4.41)$$

$$\Gamma_{z \text{ avg}} = \frac{1}{T} \int_0^T \left| \left(\sum_{k=1}^n \Gamma_{zk} \right)^2 \right| dt \quad (4.42)$$

where any number of modes (up to n) may be excited, and k is an index representing each individual mode being excited. In multi-mode excitation, the previously discussed independence of time, frequency and azimuthal coordinate no longer occurs. This means that the integration step in each of the above equations must be carried out. The mathematical consequence of the interaction of modes results in expressions containing time, frequency, and azimuthal location as variables. These terms result from trigonometric identities no longer simplifying the complex terms resulting from the squaring of the vorticity expressions. Due to this temporal dependency, the integration step in each of the above equations must be carried out.

Eqs. 4.40 - 4.42 are not easy to work with when more than several modes are simultaneously excited and therefore, some sort of pattern for each of the above equations was sought. After multiplying out the terms in the summation and integrating over one period with respect to time, a general formula became evident for each of the above three equations that made calculations considerably easier. In an attempt to limit the length of this document, only

the results will be presented. The average components of vorticity due to multiple mode excitation are:

$$\Gamma_{r \text{ avg}} = \sum_{k=1}^n \epsilon_k e^{-2\alpha_{Ik}z} \left[\left(\alpha_{Ik} u_{\theta Rk} + \alpha_{Rk} u_{\theta Ik} - \frac{m}{r} u_{zIk} \right)^2 + \left(\alpha_{Ik} u_{\theta Ik} - \alpha_{Rk} u_{\theta Rk} + \frac{m}{r} u_{zRk} \right)^2 \right] \quad (4.43)$$

$$\Gamma_{\theta \text{ avg}} = \left(\frac{dU_z(r)}{dr} \right)^2 + \sum_{k=1}^n \epsilon_k e^{-2\alpha_{Ik}z} \left[\left(-\alpha_{Ik} u_{rRk} - \alpha_{Rk} u_{rIk} - \frac{du_{zRk}}{dr} \right)^2 + \left(\alpha_{Rk} u_{rRk} - \alpha_{Ik} u_{rIk} + \frac{du_{zIk}}{dr} \right)^2 \right] \quad (4.44)$$

$$\Gamma_{z \text{ avg}} = \sum_{k=1}^n \epsilon_k e^{-2\alpha_{Ik}z} \left[\left(\frac{du_{\theta Rk}}{dr} + \frac{m}{r} u_{rIk} + \frac{u_{\theta Rk}}{r} \right)^2 + \left(\frac{du_{\theta Ik}}{dr} - \frac{m}{r} u_{rRk} + \frac{u_{\theta Ik}}{r} \right)^2 \right] \quad (4.45)$$

It is rewarding to see that again, there is no dependence upon time, frequency or azimuthal location. As was the case in simplifying the expression for the single mode average azimuthal component of vorticity, when using Eqs. 4.43 - 4.45, no integration step is necessary. It should be noted that when multiple modes are being excited at different periods, there is a common

period for the two or more modes. What that period may be is not important. The fact that such a period exists that the expression for vorticity may be integrated over, is important.

Several interesting features of the above equations should be pointed out. Eqs. 4.40 - 4.42 leave it unclear as to whether multi-mode vorticity may be calculated as the superposition of the combination of modes excited. However, Eqs. 4.43 - 4.45 make it apparent that, this is in fact an acceptable method of finding the total vorticity for multi-mode excitation. If the average vorticity fields have been determined for several individual modes of excitation, the following simple equations may be used to get the vorticity field for the corresponding multi mode excitation case:

$$\Gamma_{r \text{ avg}} = \sum_{k=0}^n \Gamma_{r \text{ avg } k} \tag{4.46}$$

$$\Gamma_{\theta \text{ avg}} = \sum_{k=0}^n \Gamma_{\theta \text{ avg } k} \tag{4.47}$$

$$\Gamma_{z \text{ avg}} = \sum_{k=0}^n \Gamma_{z \text{ avg } k} . \tag{4.48}$$

This would suggest that except in the region where the exponential term is close to one, i.e. in the extreme near field ($z < 0.15$), the disturbance with the greatest growth rate will have the greatest

effect on the flow regardless of how many modes are excited and which modes constructively interact with each other.

4.3 Results -- Vorticity Visualizations

4.3.1 Average Vorticity

Using vorticity as a measure of the effectiveness of excitation at a particular mode allows for visual interpretation of this measurement in the form of contour plots and iso-surface visualizations. Figures 4.1 - 4.5 show the contour plots of average vorticity calculated by Eqs. 4.46 - 4.48 for single mode and multi-mode excitation. The modes of excitation considered were modes 0, 1, 2, and 0 and 1 simultaneously. In order to compare the average vorticity levels for each case on a standard basis, the total disturbance level for each case was 5 percent of the basic axial centerline velocity. Just as was the case in the streakline plots, in cases of multiple mode excitation, each mode was excited at equal fractions of the total disturbance level. Although no scaling is present in these figures, the range of the calculations depicted is three nozzle radii from the centerline outward in the radial direction, and three jet radii outward in the axial direction with the jet centerline corresponding to an imaginary vertical line down the center of the plot.

Figure 4.1 shows the average vorticities for the axisymmetric mode ($m=0$). As inspection of Eqs. 4.3 - 4.5 would reveal, knowing that u_θ , the azimuthal velocity disturbance eigenfunction

is zero at any location in the flow field (and with $m=0$), it becomes apparent that the only component of vorticity resulting from the axisymmetric disturbance is due to the azimuthal component. The results shown are consistent with what one would expect: that the greatest levels of average vorticity occur in the shear layer (The regions approximately one jet radius from the centerline where the fast moving fluid in the jet interacts with the slow moving or non-moving ambient fluid surrounding the jet).

The four regions of growth that are evident in Fig.4.1 can be explained by inspecting the form of the radial eigenfunction and the derivative of the axial direction velocity disturbance eigenfunction. With the imaginary part of the radial eigenfunction (Fig. 3.3) reaching a negative maximum just before the jet radius ($r=1$) and the real part of the radial eigenfunction reaching a maximum just after the jet radius ($r=1$), the growth of the vorticity field just inside of the jet radius and just outside of the jet radius is easily explained. No vorticity is expected inside the shear layer as the velocity gradients are relatively small in this region, indicative of the lack of activity. The three dimensional view of the average vorticity (labeled “Surface Mesh”) in Fig. 4.1 shows how the vorticity levels grow in the axial direction due to the exponential spatial growth rate ($-\alpha_i$) .

Inspection of Figs 4.2 and 4.3 showing the average vorticity contour plots for modes $m=1$ and $m=2$ are more interesting than that of the axisymmetric mode. The main difference between the azimuthal (helical) modes and the axisymmetric mode, from an average vorticity standpoint, is the additional radial and axial components of vorticity present in the flow field. As was seen

in the streakline plots, the vortical structures rolling up in a manner such that they took on a three dimensional structure, are a direct result of the presence of the radial and axial components of vorticity. Again, for these two modes ($m=1$ and $m=2$), the concentrations of higher values of average vorticity appear just where they would be expected, in the shear layer region.

Multiple mode excitation yields results that would be expected from inspection of the results of single mode excitation for the average vorticity plots. Figure 4.4 shows the results of multi-mode excitation for the $m = 0$ and 1 case. As Eqs. 4.46 - 4.48 predict, multiple mode excited average vorticity results are simply the results of the individual modes superimposed upon one another. That is the results of mode $m = 0$, added to the results of mode $m = 1$, are what the results would be for modes $m = 0$ and 1. Since roll-up in the cross-plane (the r - z plane) is a result of the azimuthal component of vorticity (as is evident from the fact that in the axisymmetric mode ($m=0$), roll-up only occurs in the cross-plane), the vortical structures produced from multi-mode excitation are much stronger in the radial and axial directions than in the azimuthal direction.

4.3.2 Instantaneous Vorticity

The plots depicting the average vorticity fields were valuable for indicating what regions of the flow field experienced growth in vorticity when averaged over time, but gave no real indication of the location of instantaneous regions of high levels of vorticity or of the jet structure. For that reason, visualizations for the instantaneous vorticity field were generated to

supplement the earlier streakline plots. In order to pick interesting instances in time at which to observe at the instantaneous vorticity field, the streakline plots (Figs. 3.9 - 3.21) were examined. The times chosen to look at these instantaneous plots were $1.1T$ and $1.3T$ where $T = 2\pi/\omega$, is the period of excitation, and ω is the non-dimensional frequency of excitation. All of the images displayed begin a short distance from the jet exit and extend downstream for three nozzle radii.

The axisymmetric mode ($m=0$) was investigated first. Fig (4.5) shows a surface of constant vorticity for the mode $m = 0$ at time $t = 1.3T$. The level of vorticity displayed in this plot is 0.5 and corresponds to $1/80$ of the maximum vorticity value at three jet radii downstream. The level of vorticity chosen for the imaging is not of great importance. The specific level for any of the instantaneous surfaces of constant vorticity were chosen only to display the vortical structures present in the jet. As should be evident from Eqs. 4.3 - 4.5, the vorticity grows exponentially and thus, the highest levels of vorticity will appear farthest downstream. Unfortunately, these high levels of vorticity give little indication of the structures present in the flow. Therefore, lower levels of vorticity are looked at for all the instantaneous visualizations.

Figure 4.7 shows the beginning of the growth of one vortical structure near the jet exit and then another vortical structure forming further downstream. Comparison with Fig. 3.7, the streakline representation of the flow field at the same instant in time, shows the existence of similar structures at corresponding locations in the flow field. The axisymmetry, and the formation of vortex rings in complete structures that are periodic in nature should be noted.

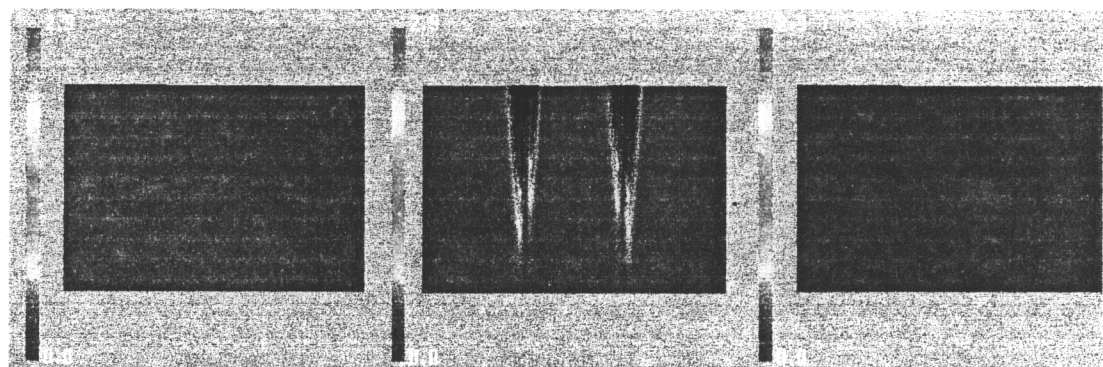
Next, the visualization of a surface of constant vorticity will be considered for the first azimuthal mode ($m=1$). Figure 4.6 shows the three components of instantaneous vorticity for the mode $m = 1$. From the streakline plots in a previous section, the phenomena of a helical vortical structure continuously evolving in the azimuthal direction was suggested. Clearly, the radial and axial components of vorticity display this continuous helical behavior. The azimuthal component, however, does not. While this helical behavior is not evident in the azimuthal component, it is obvious that the vorticity is concentrated in the shear layer. One reason that the helical behavior is not as evident in the azimuthal component of vorticity as it is in the radial and axial directions is that the constant term of the derivative of the basic axial flow (Eq. 4.4 governing the evolution of the azimuthal component of vorticity) has a major contribution to the vorticity in the very near field (before the disturbance quantities begin their exponential growth).

When the multi-mode cases for surfaces of constant vorticity are examined, more evidence of the nature of the roll-up, discussed in the streakline section, is seen. In a previous section, it was suggested, for the cases where the axisymmetric mode was excited simultaneously with one or more azimuthal (helical) modes, that roll-up still occurred in distinct, periodic, uneven, vortical ring-like structures. As was suggested in the axisymmetric case, if the azimuthal component of vorticity was entirely responsible for this streamwise directional roll-up, it would make sense that multiple mode excited jets exhibiting this periodic coherent structure development should be evident in the iso-surfaces of azimuthal vorticity. As can be seen in Figs. 4.10 - 4.12, this is definitely the case. The radial and azimuthal components of vorticity also show, to some extent, this phenomena of periodic distinct vortical structure formation (although

the most evidence appears in the iso-surfaces of the azimuthal component as would be expected).

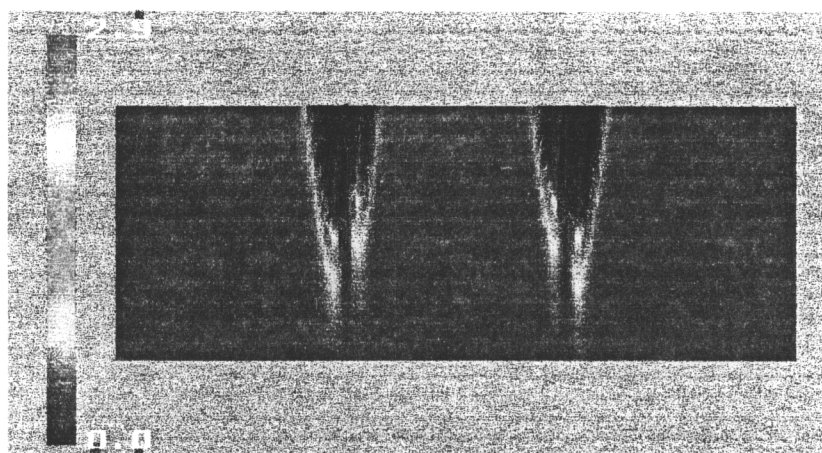
Linear stability theory predicts that the mode with the highest growth rate will cause the shear layer to expand the most rapidly. In Chapter 2, this mode was demonstrated to be the axisymmetric mode. It stands to reason, due both in fact to the physical geometry of the circular jet and to predictions of growth rate, that the azimuthal component would be responsible for greater entrainment than its radial and axial counterparts. This argument, based on the results of linear theory, is also in agreement with the results of experimental flow visualizations by Leipman and Gharib [1992].

Figure 4.1
 AVERAGE VORTICITY $M=0$



radial component azimuthal component axial component

Total Average
 Vorticity



Surface
 Mesh

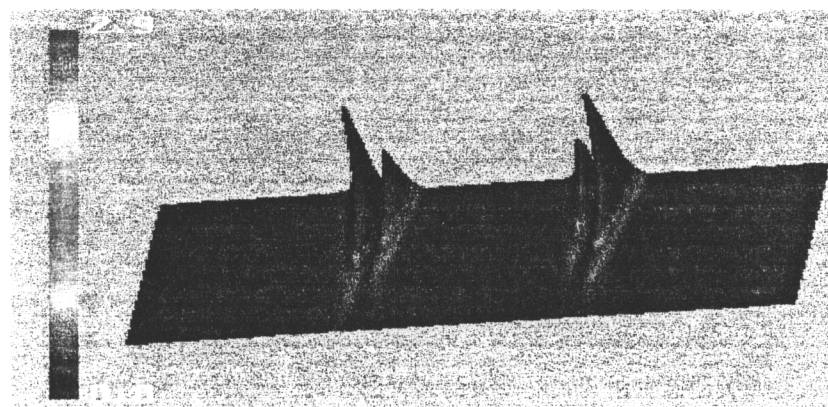
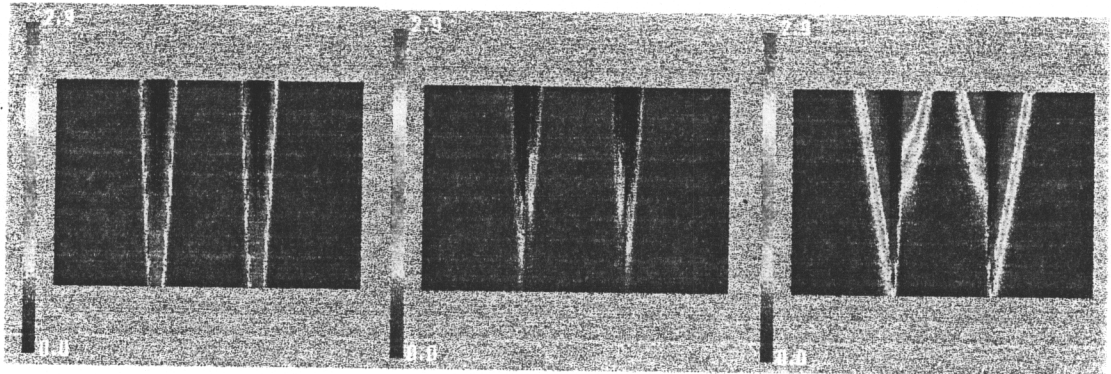
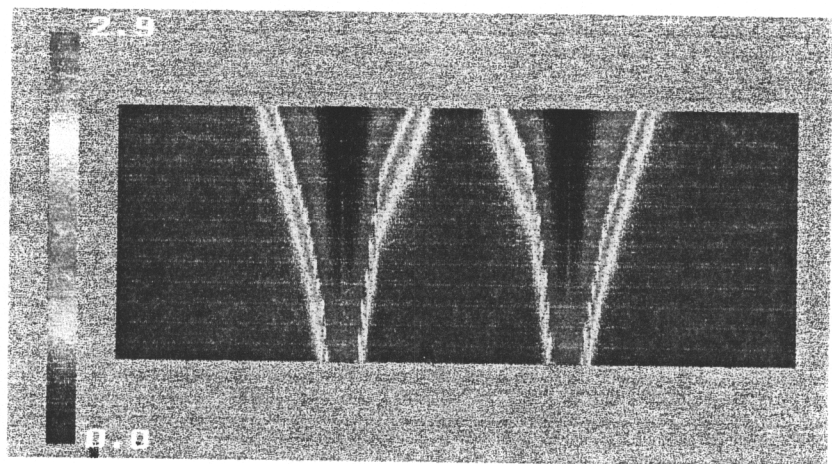


Figure 4.2
AVERAGE VORTICITY $M=1$



radial component azimuthal component axial component

Total Average
Vorticity



Surface
Mesh

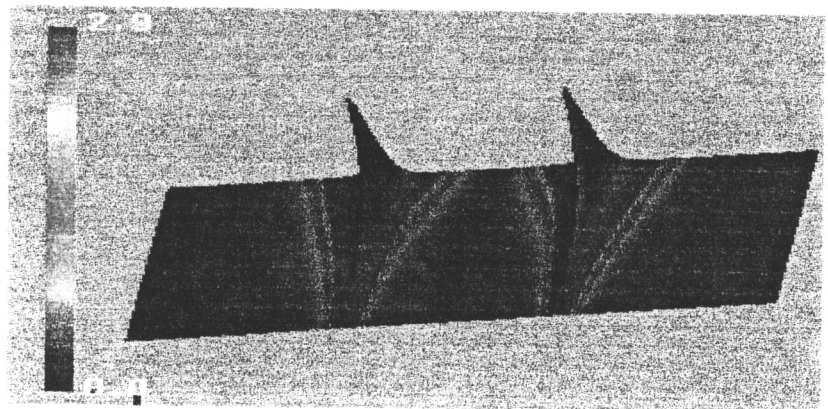
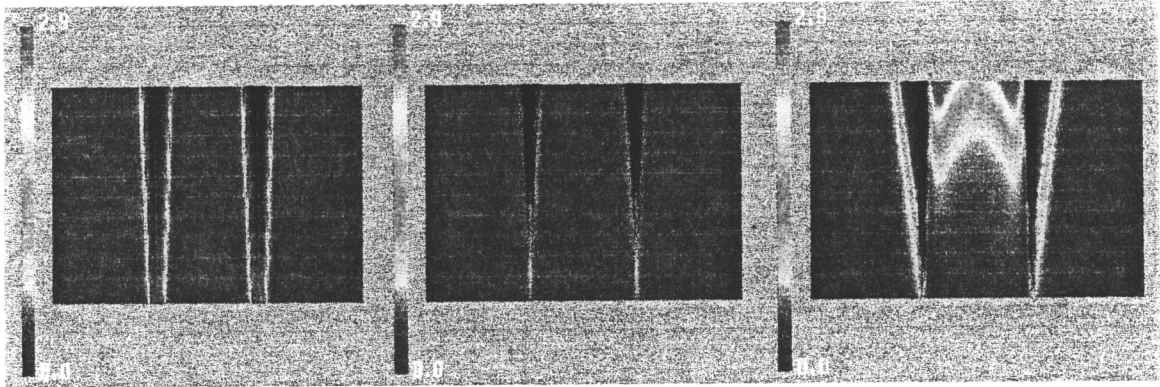
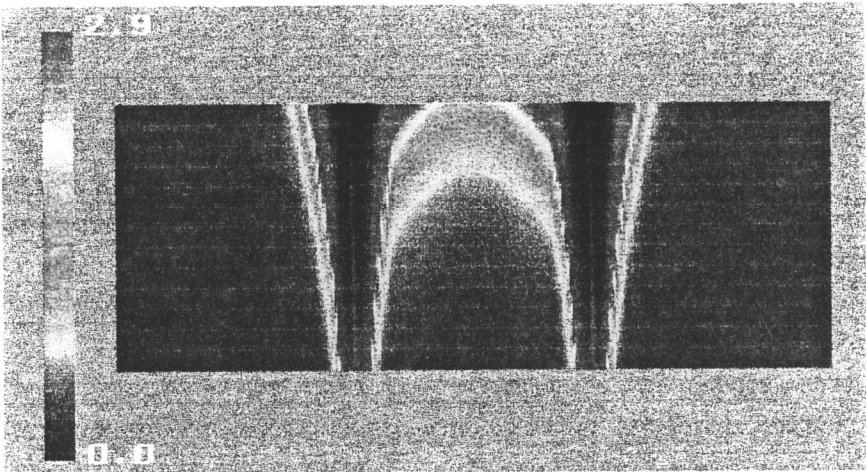


Figure 4.3
AVERAGE VORTICITY $M=2$



radial component azimuthal component axial component

Total Average
Vorticity



Surface
Mesh

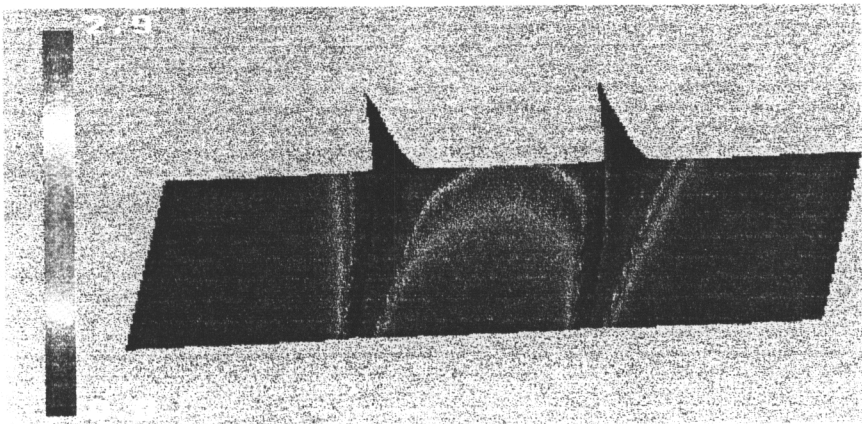
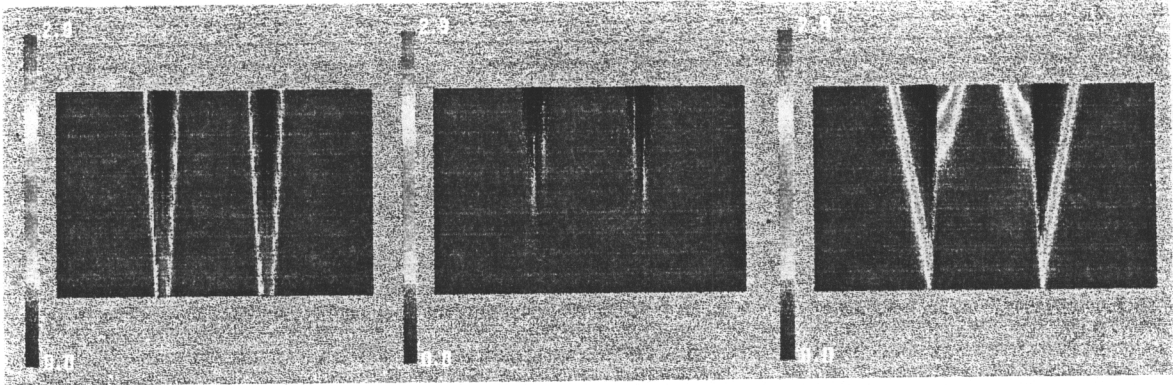
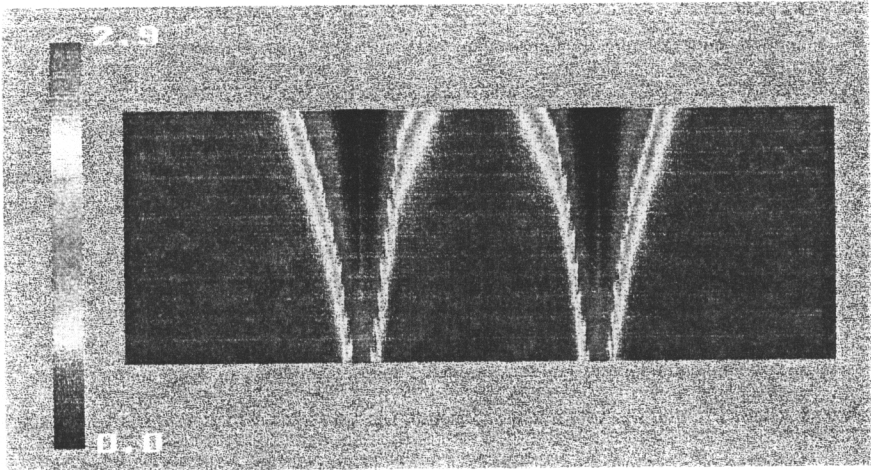


Figure 4.4
AVERAGE VORTICITY $M=0&1$



radial component azimuthal component axial component

Total Average
Vorticity



Surface
Mesh

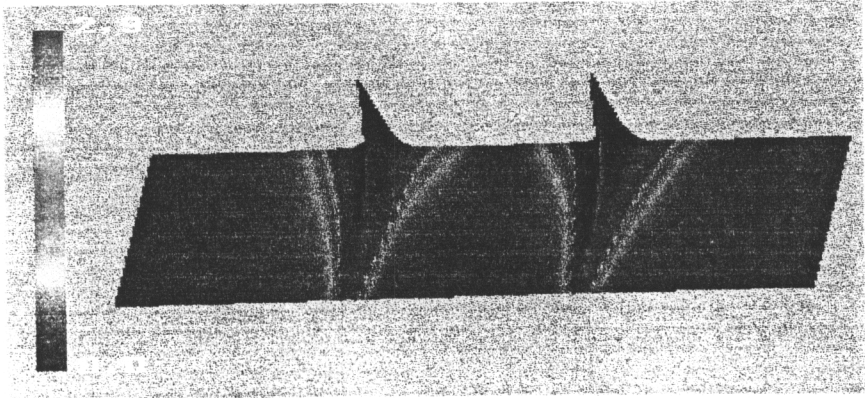


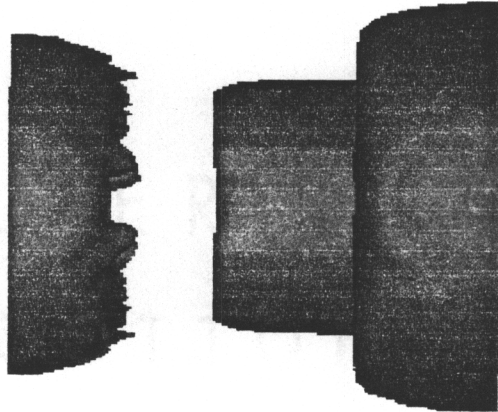
Figure 4.5

SURFACE OF CONSTANT VORTICITY

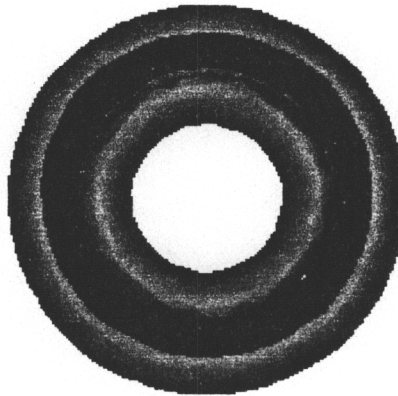
$M=0$

TIME=1.3T

Side
view



Front
view



Arbitrary
view

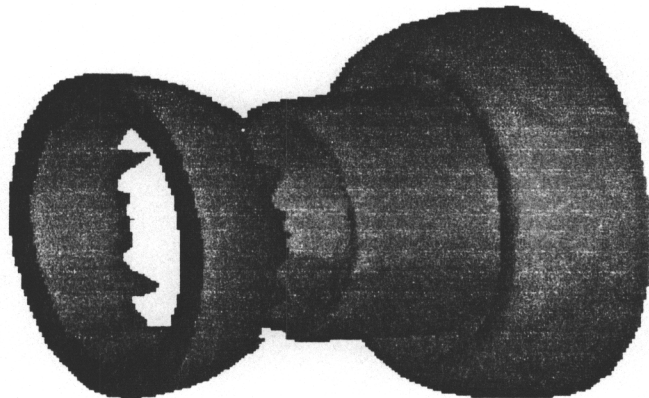


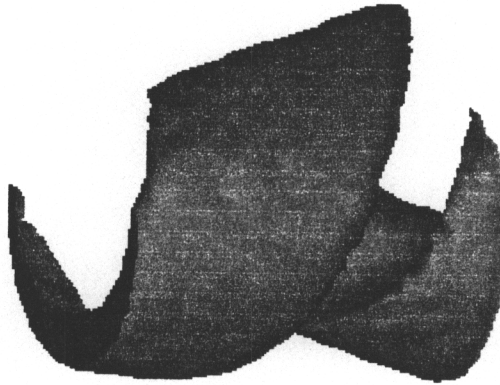
Figure 4.6

SURFACE OF CONSTANT VORTICITY

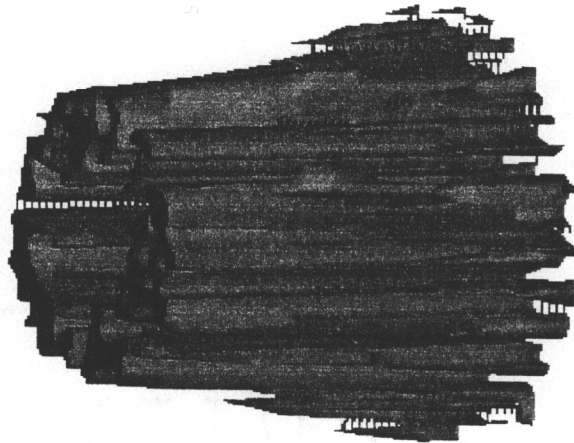
$M=1$

$TIME=1.3T$

Radial
Component



Azimuthal
Component



Axial
Component

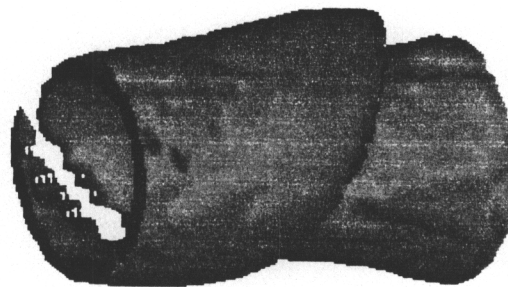


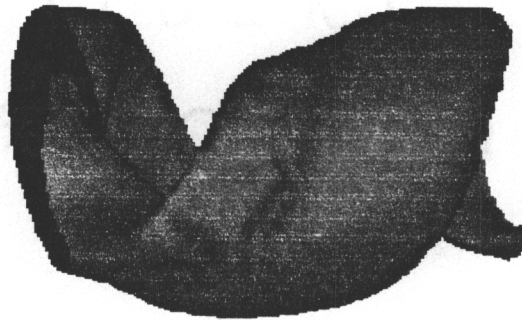
Figure 4.7

SURFACES OF CONSTANT VORTICITY

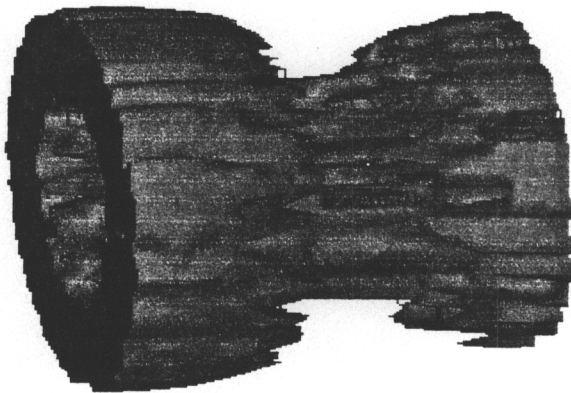
TIME=1.3T

M=0&1

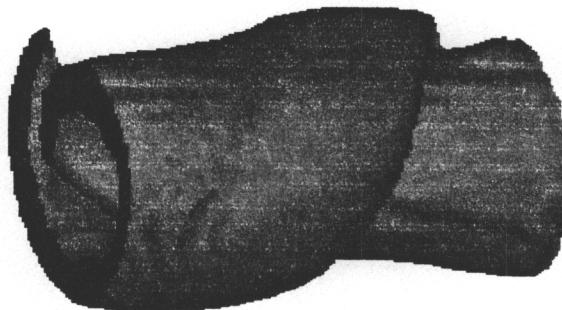
Radial
Component



Azimuthal
Component



Axial
Component



CHAPTER 5:

CONCLUSIONS AND FINAL REMARKS

5.1 Conclusions

Chapter 1 presented the goal of the current research effort as identifying mechanisms responsible for the entrainment of surrounding fluid into a non-reacting, circular, free jet using linear stability analysis and the results of streakline and vorticity visualizations. Integer, fractional, and multiple modes of excitation were examined.

The visualizations of instantaneous levels of vorticity showed the appearance of helical structures but were of little value in indicating the relative levels of entrainment due to various modes of excitation. A much more useful indicator was the average vorticity. With regard to the average vorticity, it was argued that for a given mode of excitation m , the mode with the largest growth rate will be the mode that results in the highest level of entrainment. As proven before (Huang [1994]), the axisymmetric mode ($m=0$) has the largest growth rate. Multiple mode excitation at modes other than the axisymmetric mode will clearly not be as effective as the axisymmetric mode alone in the entrainment process.

Finally, the importance of the azimuthal component of vorticity in the entrainment

process was identified. This component of vorticity was argued to be the most influential in the engulfment of the surrounding fluid into the jet. While finite amounts of vorticity in the radial and axial directions may help to more thoroughly mix the ambient fluid with the jet fluid once entrained into the jet stream, it is the azimuthal component of vorticity that is primarily responsible for that entrainment. With the axisymmetric mode of excitation resulting in the appearance of only azimuthal vorticity, and with the greatest growth rate of any other mode of excitation, it is clearly the mode of excitation that results in the highest levels of entrainment.

5.2 Possible Future Work

The work presented in this thesis by no means represented a comprehensive study of fractional and multiple mode excitation. This effort attempted only to identify the most important issues of these types of excitation from a theoretical standpoint. Suggestions for future work in the areas covered by this thesis consist of one main idea. An area that could produce some interesting and potentially valuable insight to the early stages of the stability of circular jets is the effects of the interaction of modes beyond what investigations were conducted in the current effort. Areas left unaddressed were effects of the interaction of modes at different frequencies of excitation; the role of initial phase relationship in multiply excited modes at the same excitation frequency; and comparison of counter-propagating or spinning modes of excitation with the experimental results of Strange [1983], Cohen and Wynanski [1987], and Ding [1995]. The investigation of spinning mode excitation from a linear stability analysis

approach would result in predictions of instantaneous regions of high levels of vorticity in a manner consistent with the axis switching phenomena seen to occur in elliptical jets.

REFERENCES:

1. Batchelor, G. K., and Gill, A. E., "Analysis of the Stability of Axisymmetric Jets," *JFM*, v.14, pp. 529-551, 1962.
2. Bayly, B. J., Orszag, S. A., and Herbert, T., "Instability Mechanisms in the Shear Flow Transition," *Ann. Rev. Fluid Mechanics*, v.20, pp. 359-391, 1988.
3. Betchov, R. and Criminale, W. O., *Stability of Parallel Flows*, Academic Press, 1967.
4. Blair, J. R., *Near Field Behavior of Reacting Free Jets*, Masters Thesis, Virginia Polytechnic Institute and State University, 1995.
5. Browand, F. K., and Laufer, J., "The Role of Large Scale Structures in the Initial Development of Circular Jets," *Proc. of 4th Symposium on Turb. In Liquids*, University of Missouri - Rolla, Sept. 1975, pp. 333-344.
6. Brown, G. L., and Roshko, A., "On Density Effects and Large Structure in Turbulent Mixing Layers," *JFM*, v.64, pp. 775, 1974.
7. Cohen, J., and Wygnanski, "The Evolution of Instabilities in the Axisymmetric Jet. Part 1. The Linear Growth of Disturbances Near the Nozzle," *JFM*, v.176, pp. 191-219, 1987.
8. Cohen, J., and Wygnanski, "The Evolution of Instabilities in the Axisymmetric Jet. Part 2. The Interaction of Two Waves," *JFM*, v.176, pp. 221-235, 1987.

9. Corke, T. C., and Kusek, S. M., "Resonance in Axisymmetric Jets with Controlled Helical Mode Input," *JFM*, v.249, pp. 307-336, 1993.
10. Crow, S. C., and Champagne, F. H., "Orderly Structure in Jet Turbulence," *JFM*, v.48, pp. 547-591, 1971.
11. Ding, C., *Methodologies for Active Control of Free Shear Flows*, Ph.D. Dissertation, Virginia Polytechnic Institute and State University, 1995.
12. Drazin, P. G., and Reid, W. H., *Hydrodynamic Stability*, Cambridge University Press, 1981.
13. Freymuth, P., "On Transition in a Separated Laminar Boundary Layer," *JFM*, v.25, pp. 983-700, 1966.
14. Grosch, C. E., and Jackson, T. L., "Inviscid Spatial Stability of a Three-Dimensional Compressible Mixing Layer," *JFM*, v.231, pp.35-50, 1991.
15. Gutmark, E., and Ho, C. M., "Preferred Modes and the Spreading Rates of Jets," *Phys. Fluids*, v.26, No.10, pp. 2932-2938, 1983.
16. Hasan, M. A., and Hussain, A., "The Self Excited Axisymmetric Jet," *JFM*, v.115, pp. 58-89, 1982.
17. Ho, C. M., and Huang, L. S., "Subharmonics and Vortex Merging in Mixing Layers," *JFM*, v.119, pp. 443-432, 1982.
18. Ho, C. M., and Huerre, P., "Perturbed Free Shear Layers," *Ann. Rev. of Fluid Mechanics*, v.16, pp. 365-424, 1984.

19. Huang, S. L., *Linear Stability Analysis of Non-Reacting and Reacting Elliptical Jets*, Ph.D. Dissertation, Virginia Polytechnic and State University, 1994.
20. Lessen, M., and Singh, P. J., "The Stability of Axisymmetric Free Shear Layers," *JFM*, v.60, Part 3, pp. 433-457.
21. Lin, S. J., and Corcos, G. M., "The Mixing Layer: Deterministic Modes of a Turbulent Flow III. The Effects of Plain Strain on the Dynamics of Streamwise Vortices," *JFM*, v.141, pp. 439-482, 1984.
22. Leimpan, D. and Gharib, M., "The Role of Streamwise Vorticity in the Near-Field Entrainment of Round Jets," *JFM*, v.245, pp. 643-668, 1992.
23. Long, T. A., and Petersen, R. A., "Controlled Interactions in a Forced Axisymmetric Jet. Part 1. The Distortion of the Mean Flow," *JFM*, V.235, pp. 37-55, 1992.
24. Mattingly, G. E., and Chang, C. C., "Unstable Waves on an Axisymmetric Jet Column," *JFM*, v.65, pp. 541, 1974.
25. Michalke, A., "On Spatially Growing Disturbances in an Inviscid Shear Layer," *JFM*, v.65, pp. 521-544, 1965.
26. Michalke, A., "*Instability of a Compressible Circular Free Jet with Consideration of the Influence of the Jet Boundary Layer Thickness*," NASA Translation, 1975.
27. Michalke, A., and Hermann, G., "On the Inviscid Instability of a Circular Jet with External Flow," *JFM*, v.114, pp. 345-359, 1982.
28. Michalke, A., "Survey on Jet Instability Theory," *prog. Aerospace Sci.*, v.21, pp. 159-199,

1984.

29. Monkeitz, P. A., and Pfizenmaier, E., "Mixing by 'Side Jets' in strongly Forced and Self-Excited Round Jets," *Phys. Fluids A*, v.3, No.5, pp. 1356-1361, 1991.
30. Mutter, T. B., *Numerical Simulations of Elliptical Jets: A study of Jet Entrainment*, Masters Thesis, Virginia Polytechnic Institute and State University, 1994.
31. Petersen, R. A., and Samet, M., "On the Preferred Mode of Jet Instability," *JFM*, v.194, pp 153-173, 1988.
32. Plaschko, P., "Helical Instabilities of Slowly Divergent Jets," *JFM*, v.92, pp. 209-215, 1979.
33. Schubauer, G. B., and Skramstad, H., "Laminar Boundar Layer Oscillations and Transition on a Flat Plate," *J. Res. Nat. Bur. Standards*, v.39, pp. 251-292, 1947.
34. Sherman, F., "Viscous Flow," McGraw-Hill, 1990.
35. Strange, P. J. R., and Crighton, D. G., "Spinning Modes on Axisymmetric Jets. Part 1." *JFM*, v.134, pp. 231-245, 1983.
36. White, F. M., *Viscous Fluid Flow*, 2nd Ed., McGraw-Hill, 1991.

APPENDIX A:

FRACTIONAL MODE EXCITATION

Modeling of fractional modes of excitation using linear stability analysis is a very difficult task. The linear stability analysis eigenvalue problem does not admit a fractional value for the mode of excitation m , because a discontinuity exists in the azimuthal direction. It is due to the questionable methods of modeling fractional mode excitation that the results of this investigation may also be debatable. It is the authors opinion that the results of the fractional mode analysis investigated in this effort are acceptable provided that the locations of the jet being explored do not approach the jet center. As all of the results of the fractional mode excitation stem from this partial mathematical analysis, they will be presented in this appendix.

The extent of study on fractional mode excitation has been limited to experimental work. Furthermore, this experimental fractional mode excitation has only dealt with the spinning modes of excitation. Spinning modes consist of counter-propagating modes of equivalent azimuthal mode number. Cohen and Wygnanski [1987] extended the work of Strange [1983] to show that the standing wave excitation produced by spinning modes allows for control of the directional jet expansion. Iso-velocity contours predict elliptic evolution of the jet for $m = \pm 1$ excitation, triangular evolution for $m = \pm 1.5$ excitation, and square evolution for $m = \pm 2$ excitation.

Studies of active control of free shear flows were conducted by Ding [1995]. These studies focused on control of the far field. Ding found that by exciting the jet at non-integer and counter-propagating azimuthal modes, marked changes in the streamwise evolution of the jet could be achieved. Increased entrainment of the surrounding air by somewhat more than two-fold was demonstrated for the non-integer and counter-propagating azimuthal modes when compared with the unexcited jet.

Modeling of the Fractional Modes

The linear stability tool of Huang [1994] was adapted to allow for fractional mode excitation. One of the aspects that wasn't addressed earlier, was the difference between integer and fractional modes of excitation, and their significance. In this section, both the significance of integer and fractional mode excitation will be addressed and the two different approaches to solving the linear stability eigenvalue problem will be discussed.

In integer mode excitation, the phase difference between any one actuator and either the previous actuator or the next is the same. This result from the geometry of the jet exit results in the creation of a continuous disturbance at any streamwise cut through the jet. However the same cannot be said of jets excited at fractional modes. Fractional mode excitation results in a discontinuous disturbance as when one spatial cycle has been completed, an incomplete temporal cycle exists. For example, the $m = 3/2$ case requires one and one-half spatial cycles to complete

one temporal cycle.

This discontinuity in the excitation at 2π is the source of a mathematical difficulty which will be discussed shortly. For the experimentalist, however, this discontinuity poses no difficulty. This is because only a limited number of actuators are used (usually six or eight) in experiments. Thus, what is seen by mathematician as a discontinuity is only a rapid (azimuthal) change for the experimentalist which can easily be accommodated. This case will be taken up again after the discussion of the procedure for the calculation of the eigenfunctions for fractional modes of excitation.

From an analytical point of view, approximating the boundary conditions in the linear stability analysis using modified Bessel functions changes significantly from integer to fractional mode excitation. While the curves of fractional order modified Bessel functions appear as one would expect, (Fig A1) fitting perfectly between their corresponding integer order modified Bessel functions, the mathematical expressions of their forms and the methods of computing them are very different.

The expressions for modified Bessel functions of fractional modes of excitation are generally given in terms of a series of hyperbolic functions. Since the only fractional orders being investigated in this effort were the half mode ($m=1/2$) and the three-halves mode ($m=3/2$), these expressions were hard coded into the linear stability eigenfunction solving routine. Both

the modified Bessel functions of the first and second kind and their derivatives were needed to solve the eigenvalue problem. Thus, the code of Huang [1994] was changed and the Bessel functions and their derivatives were all input as subroutines, specifically:

$$I_{\frac{1}{2}}(x) = \sqrt{\frac{2}{\pi x}} \sinh(x) \quad (\text{A1})$$

$$\frac{d}{dx} I_{\frac{1}{2}}(x) = \sqrt{\frac{2}{\pi}} x \cosh(x) - \sqrt{\frac{1}{2}} \pi x^{-\frac{3}{2}} \sinh(x) \quad (\text{A2})$$

$$I_{\frac{3}{2}}(x) = \sqrt{\frac{2}{\pi x}} \left[\cosh(x) - \frac{\sinh(x)}{x} \right] \quad (\text{A3})$$

$$\frac{d}{dx} I_{\frac{3}{2}}(x) = \sqrt{\frac{2}{\pi x}} \left\{ \left(1 + \frac{3}{2x^2} \right) \sinh(x) - \frac{3 \cosh(x)}{2x} \right\} \quad (\text{A4})$$

$$K_{\frac{1}{2}}(x) = \sqrt{\frac{2}{\pi x}} [\cosh(x) - \sinh(x)] \quad (\text{A5})$$

$$\frac{d}{dx} K_{\frac{1}{2}}(x) = \sqrt{\frac{\pi}{2}} (x^{-\frac{1}{2}} + \frac{1}{2} x^{-\frac{3}{2}}) [\sinh(x) - \cosh(x)] \quad (\text{A6})$$

$$K_{\frac{3}{2}}(x) = \sqrt{\frac{\pi}{2x}} [\cosh(x) - \sinh(x)] (1 + \frac{1}{x}) \quad (\text{A7})$$

$$\frac{d}{dx} K_{\frac{3}{2}}(x) = \sqrt{\frac{\pi}{2}} (x^{-\frac{1}{2}} + \frac{3}{2} x^{-\frac{3}{2}} + \frac{3}{2} x^{-\frac{5}{2}}) [\sinh(x) - \cosh(x)] . \quad (\text{A8})$$

The growth rates for a number of modes were calculated over a range of non-dimensional frequencies (Fig. A2). As expected, the growth rate curves for the fractional modes, $m=1/2$, and $m=3/2$, fell between the curves for $m=0$ and $m=1$, and between $m=1$ and $m=2$, as expected. The most amplified frequency of the mode, $m=1/2$, fell around $\omega=1.4$. Since the most amplified frequencies for $m=0$ and $m=1$ were found to be approximately 1.4 (Huang [1994]), the most amplified frequency for the half mode would be expected to be the same. The most amplified frequency for the three-halves mode was found to be approximately 1.3. This result is also consistent with what would be expected based on the results of integer mode growth rates. The validity of the integer mode growth rates was verified by the results of Huang [1994]. They were also found to be in nearly exact agreement with results obtained by Michalke [1981].

Another characteristic that was verified in the analysis of fractional modes was the trend of higher azimuthal modes becoming the fastest growing modes as excitation frequency shifted downward. Figure 3.4 shows that around a non-dimensional frequency of 1.2, the half mode has the highest growth rate of all the modes. Near a non-dimensional frequency of 0.9, the first azimuthal mode takes on the largest growth rate. This trend of the shifting of the mode with the highest growth rate, continues as the frequency decreases. The fact that the frequency dependant growth rates of the fractional modes conform to the verified integer mode trends is taken to be a confirmation of the fractional mode results.

Further confirming the fractional mode analysis are the axial velocity disturbance eigenfunctions (Figs. A3 - A5) (at least at locations away from the jet center). The axial direction velocity disturbance eigenfunctions go to zero at both the jet center and far from the jet center for both the half and the three-halves modes of excitation just as expected. It is disturbing however, that the radial velocity disturbance eigenfunction and the azimuthal velocity disturbance eigenfunction for $m=1/2$, exhibit asymptotic behavior as both the real and imaginary parts tend to plus and minus infinity as they approach the jet center.

Another interesting trend can be identified in the real part of the axial direction velocity disturbance eigenfunction. Figure A6 shows these eigenfunctions for modes zero, one-half, one, three-halves, and two. This figure shows the results of the integer order modes of excitation shown in Fig. 3.8 along with the results from the fractional mode analysis (not previously displayed). The clear trend regarding the location of the relative minima and maxima with

respect to one another for a given eigenfunction discussed earlier is consistent with the results from the fractional modes of excitation. The intermediate minima and maxima for the real part of the velocity disturbance eigenfunction for the mode $m = 0$ grow in their relative positions to the absolute minimum and maximum, as the mode of excitation increases until finally, at mode $m = 2$, the absolute minimum and maximum occur between a local minimum and a local maximum. While this is the most obvious trend in the eigenfunctions of both the integer and fractional modes of excitation, other such trends do appear in the velocity disturbance eigenfunctions in the radial and azimuthal directions. It is these trends along with results consistent with expectations and results from integer modes of excitation that allow the author to argue for the accuracy of the fractional mode results at locations away from the jet center.

Streakline Visualizations

The original streakline code used to calculate the streaklines was written by Huang [1994], however, it was only intended to calculate the streaklines for the axisymmetric ($m=0$) mode. This code was altered by the author to allow for azimuthal variation of the streaklines, and also to allow for the calculation of streaklines developing due to fractional mode excitation. For each fractional mode investigated ($1/2$ and $3/2$), six streakline plots were calculated over a range of times, measured in forcing periods, from 0.5 forcing periods, up to 1.5 forcing periods. The plots show the streaklines at times $0.5T$, $0.7T$, $0.9T$, $1.1T$, $1.3T$, and $1.5T$, where $T = 2\pi/\omega$ is the forcing period for a particular mode of excitation. Thus, the developing streaklines were

calculated over one forcing period and should provide all the information that could be gathered from any streakline study of the flow.

Calculation of the streaklines for fractional modes (Figs. A7 and A8) show that the helical growth rate of the continuous vortical structure appears as would be expected in relation to those of modes $m=1$ and $m=2$, but only result in a continuous plot as long as the calculations do not carry the particle trajectory across the axial plane (θ - z plane) where $\theta=0+\epsilon$ on one side and $\theta=2\pi-\epsilon$ on the other, (ϵ is some infinitesimal amount). Obviously, the disturbance at $\theta=0+\epsilon$ and the disturbance at $\theta=2\pi-\epsilon$ are two different values any time the mode m is equal to some non-integer value. Thus, for these plots, streaklines that cross this axial plane of azimuthal discontinuity are not displayed as they predict non-physical results.

The above discussion of the calculation of the streaklines crossing the plane of azimuthal discontinuity does not mean that the discontinuity in the calculation reflects a discontinuity in the flow field. Clearly, in a physical sense, as one passes through the angle 2π , there is no sudden jump back to zero. The azimuthal angle continues increasing, however this effect cannot be displayed (nor is it necessary to display it) and would require considerable additional attention to the streakline particle tracking. Although not shown, the helical vortical structures seen resulting from fractional mode excitation are continuous. It is the disturbance in the cross plane (the r , θ plane) of fractionally excited jets that is not (continuous).

In Figs. A7 and A8, for excitation at two modes, modes 0 and $\frac{1}{2}$ and modes 0 and 1, the

resulting delay in roll-up from one side to the side opposite, is not nearly as pronounced as the delay in roll-up due to excitation at modes zero, one-half, and one (Fig. A9). The result that roll-up occurs unevenly is considerably more evident in the triple mode excitation case than in the double mode excitation cases is expected. In fact, the stronger azimuthal mode excitation tendencies are a direct result of the fact that two-thirds of the disturbance energy comes from the azimuthally excited modes: $m=0$ and $m=1/2$. In the double mode excitation cases, only half of the disturbance energy is put into the azimuthally excited mode, either $m=1/2$ or $m=1$; the other half of the energy going into the axisymmetric mode. Since the axisymmetric case contributes no energy to azimuthal variation, putting more energy into the azimuthal modes of the multiple-mode excited jet would lead to increased azimuthal variation in the rolling-up of the shear layer. Again this is more evident in the case where two-thirds of the disturbance energy goes into the azimuthally excited modes and only one-third of the energy goes toward exciting the axisymmetric mode.

Average Vorticity Plots

In the average vorticity investigation, the fractional modes of excitation yield results that seem to be expected in regions away from the centerline of the jet, but unfortunately predict unrealistic behavior near the centerline. Figs. A11 and A12 show the average vorticity values for mode $m = 1/2$ and $m = 3/2$. The expected growth in the shear layer occurs for all three components of vorticity, however, in the axial direction, the linear stability analysis for fractional

mode excitation predicts the growth of vorticity at the jet center; an unrealistic result (which is worse for the $m = 1/2$ case than for the $m = 3/2$ case).

Explanation for the presence of vorticity near the jet center is not difficult. This centerline vorticity results from Eq. 4.5, the equation for the axial component of vorticity. The terms responsible for this unrealistic growth are the terms containing the reciprocal of the radius ($1/r$). As the radius approaches zero, the two terms in E.Q. 4.5 including this reciprocal radius will increase without bound unless the rest of the term also tends to zero, or if the values for $u_r(r)$ equal $u_\theta(r)$. One look at the velocity disturbance eigenfunctions for the radial and azimuthal directions for modes $m = 1/2$ and $m = 3/2$ will suggest that the above conditions for centerline vorticity to approach zero (as would be expected) will not be satisfied. Thus, the source of this prediction of artificial vorticity near the jet center lies in the linear stability analysis. Since the analysis proves consistent with experiment for the integer modes of excitation, the boundary conditions must be at fault. Despite this shortcoming, close inspection of the velocity disturbance eigenfunctions for all of the modes investigated ($m = 0, 1/2, 1, 3/2$, and 2) show trends that are consistent for both the integer and fractional modes of excitation.

Instantaneous Vorticity

Figure A13 shows constant surfaces of vorticity for the mode $m = 3/2$. What can be seen from this visualization, is the helical nature of the half mode. As was the case for the streakline

visualizations, all of the azimuthal modes investigated (0, 1/2, 1, 3/2, and 2) displayed this continuous helical vortical structure. There is also greater evidence of the continuous helical structure in the azimuthal component of instantaneous vorticity than in the other modes azimuthal modes of excitation. This is attributed to the choice of the time (1.1T) at which the vorticity field was computed.

In all three cases of multi-mode excitation that were examined, $m = 0$ and 1/2, $m = 0$ and 1, and $m = 0$, 1/2, and 1, (Figs. A14 and A15), the azimuthal component of vorticity shows evidence of periodic vortex rings forming in the streamwise direction. This confirms the suggestions by the author that evidence exists of such structure formation occurring from the streakline visualizations.

At least some of the difficulties might be resolved by recognizing that the fractional mode excitation might not be adequately modeled by normal mode representation of the disturbances. This is because the resulting disturbance is discontinuous over 2π for a given fractional mode of excitation. For the experimentalist, a real jet has no problem accommodating this disturbance, however, from a mathematical point of view, this discontinuous disturbance may violate the assumption of normal modes as several modes would be required to model the disturbance properly.

Figure A1

Modified Bessel Functions of Increasing Order

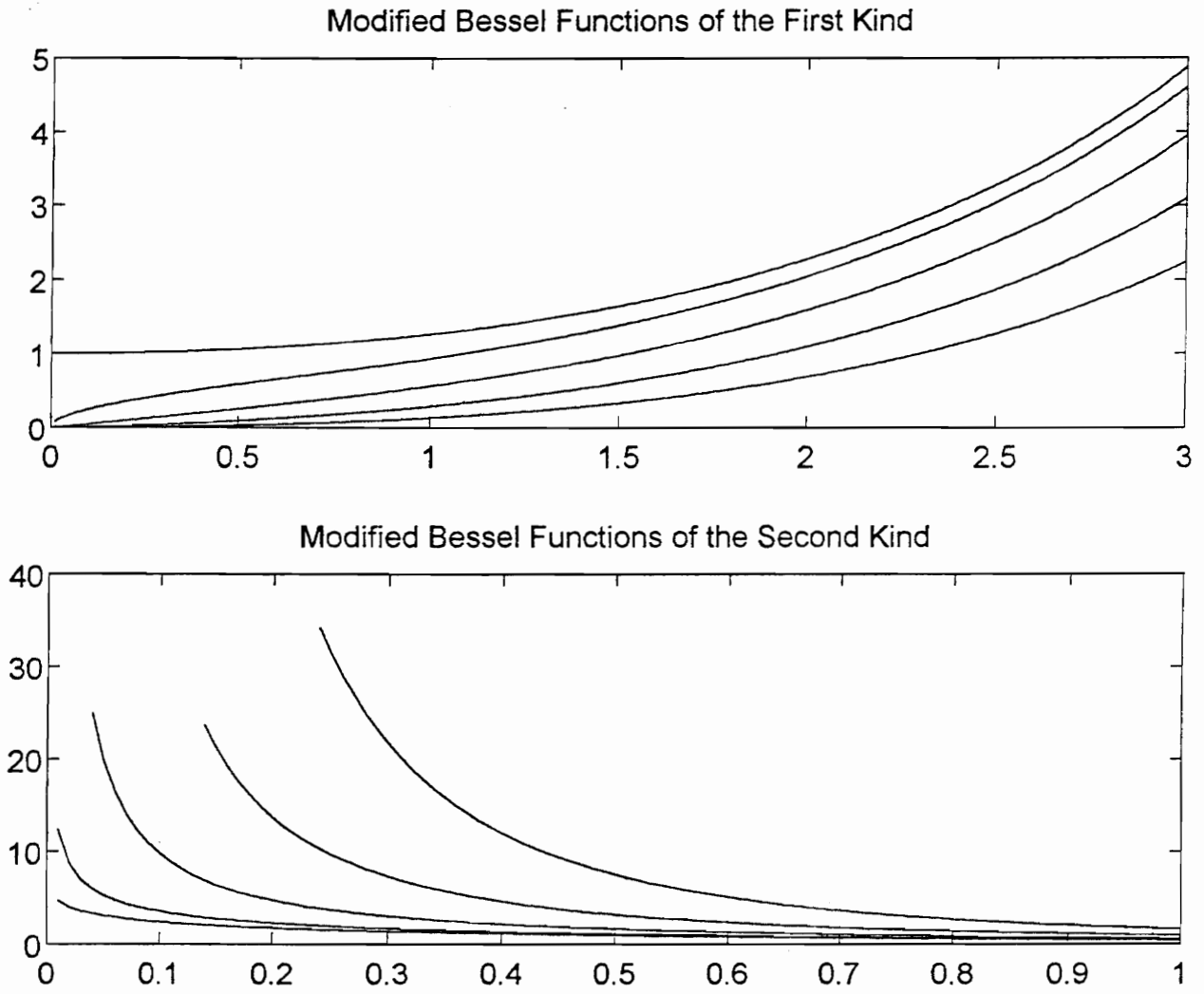


Figure A2

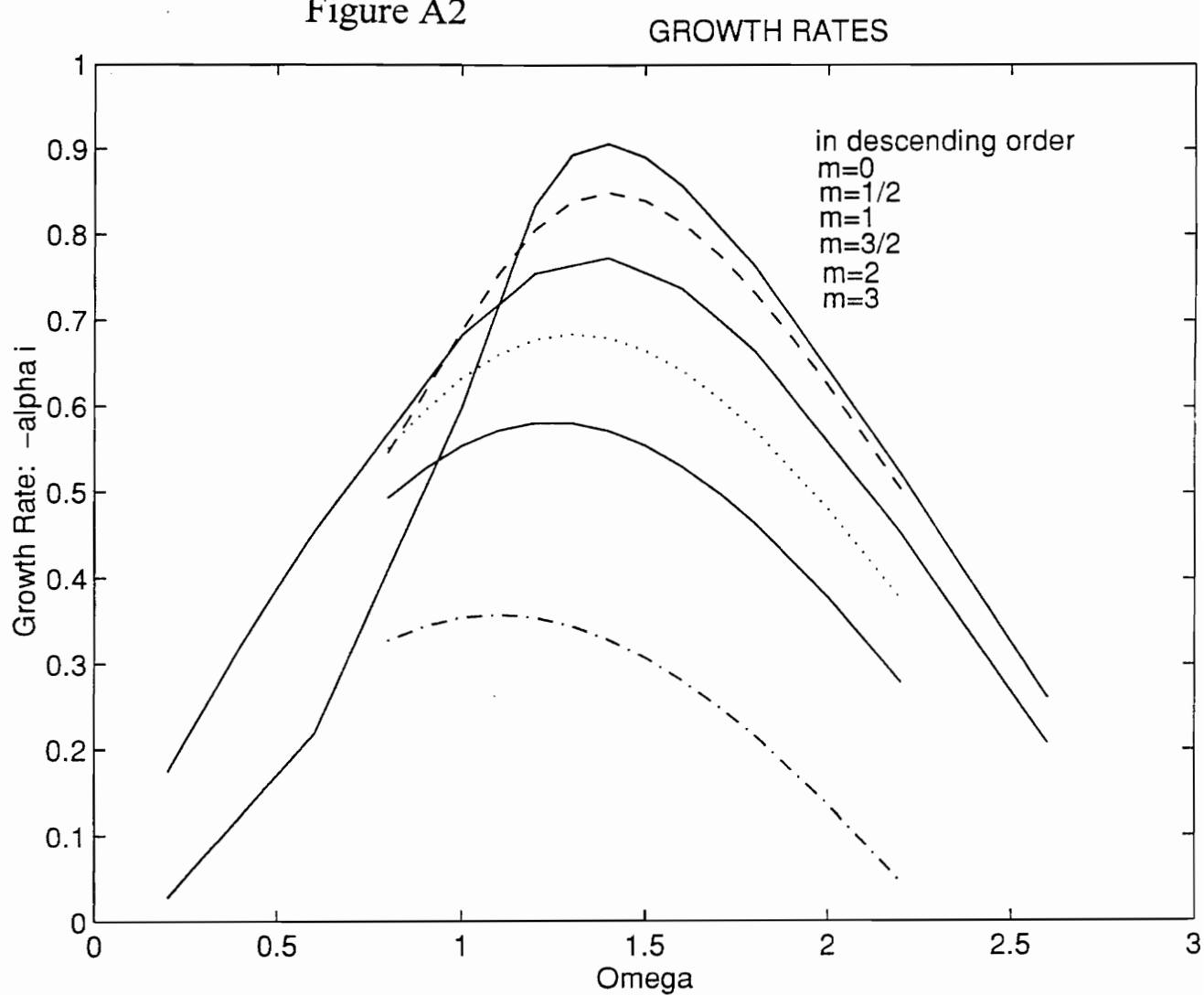
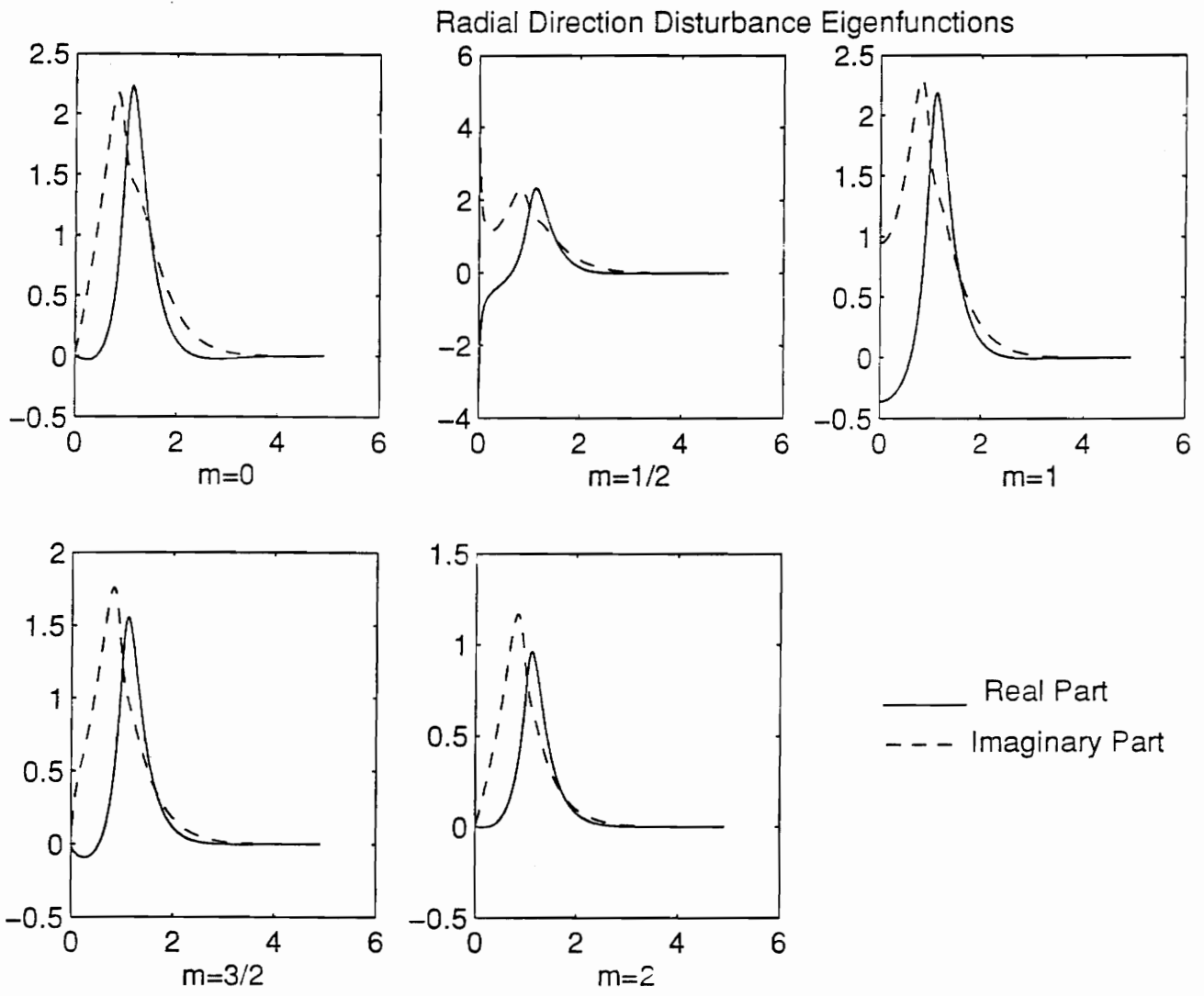
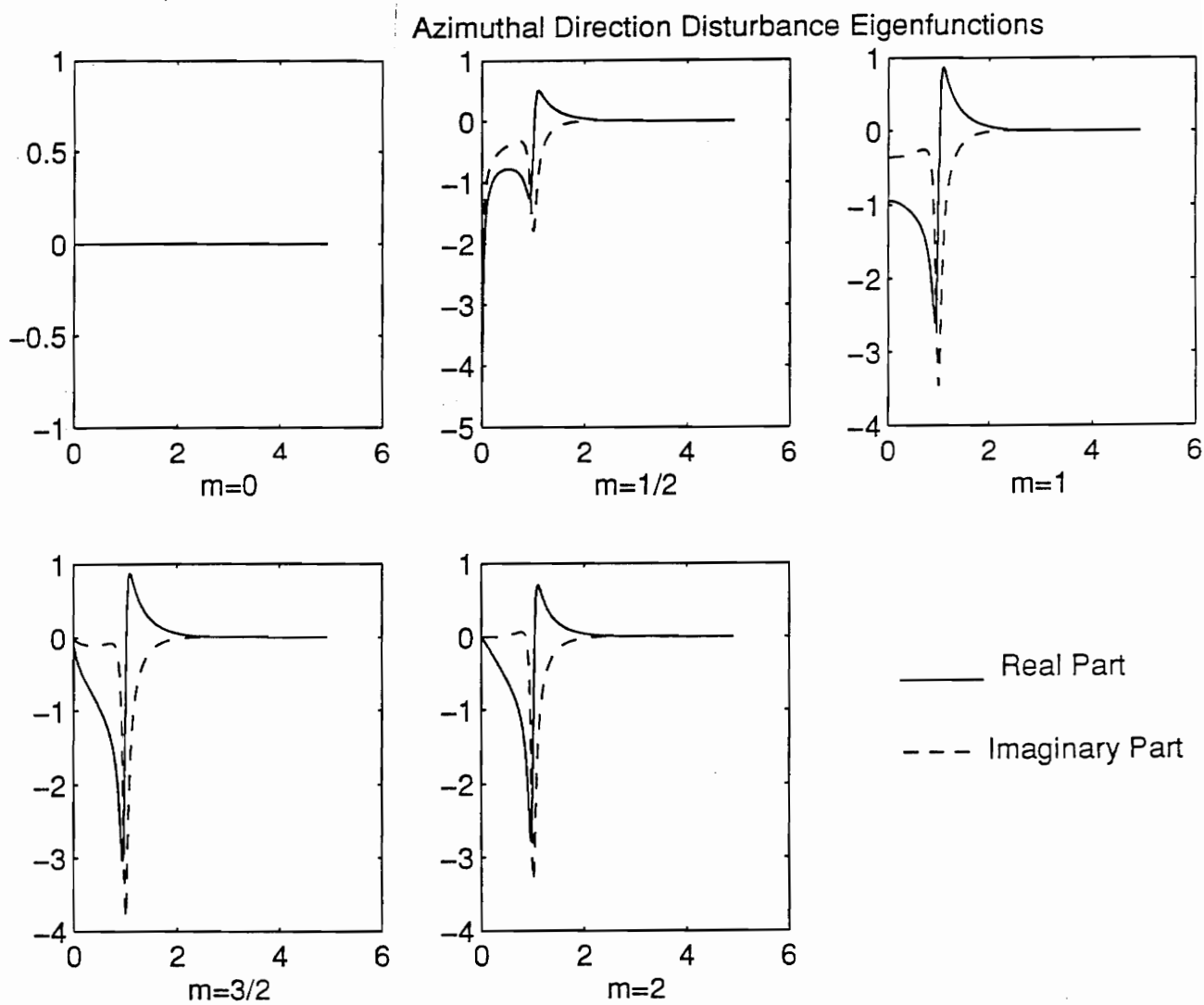


Figure A3



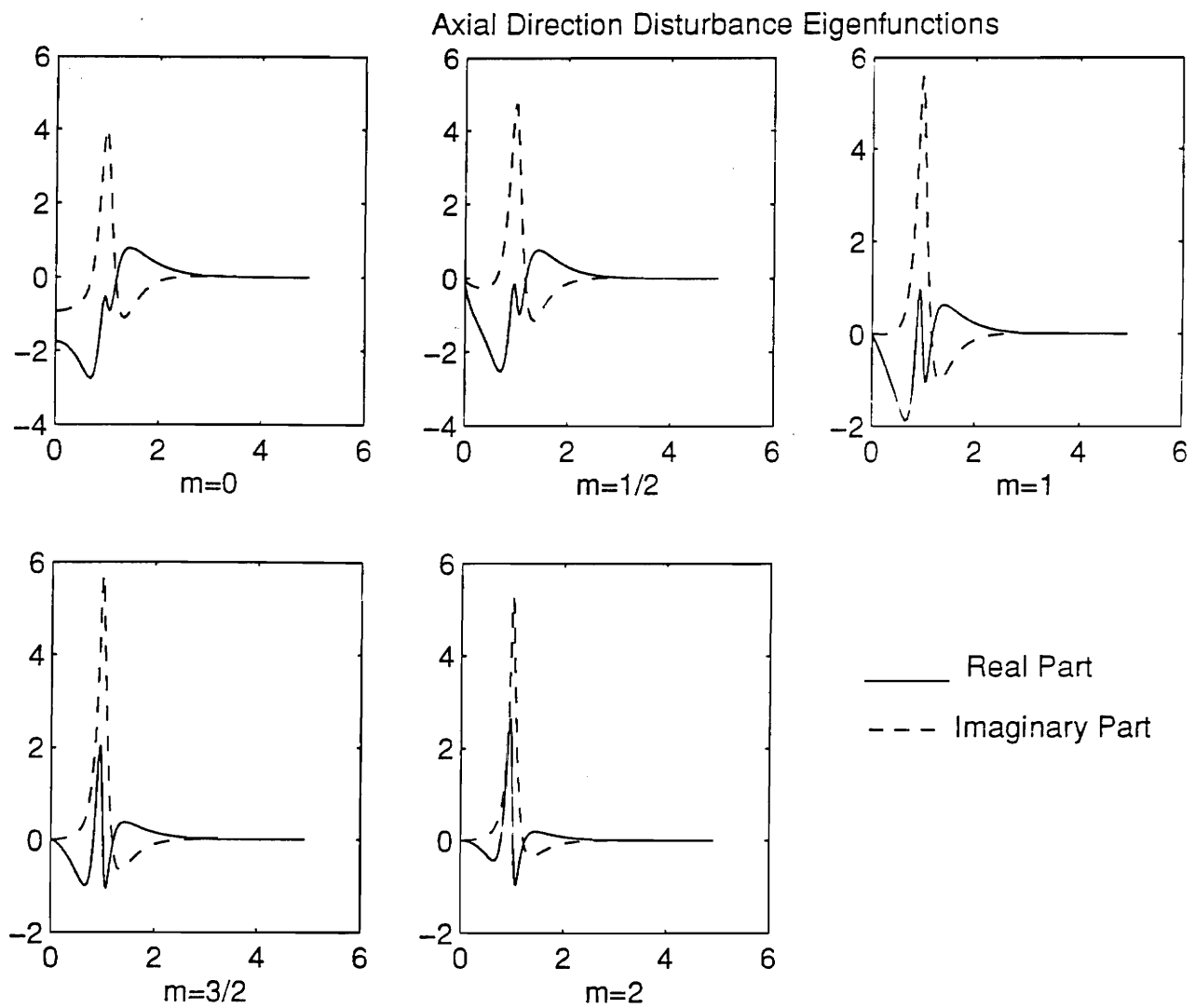
axes: radial coordinate vs. magnitude

Figure A4



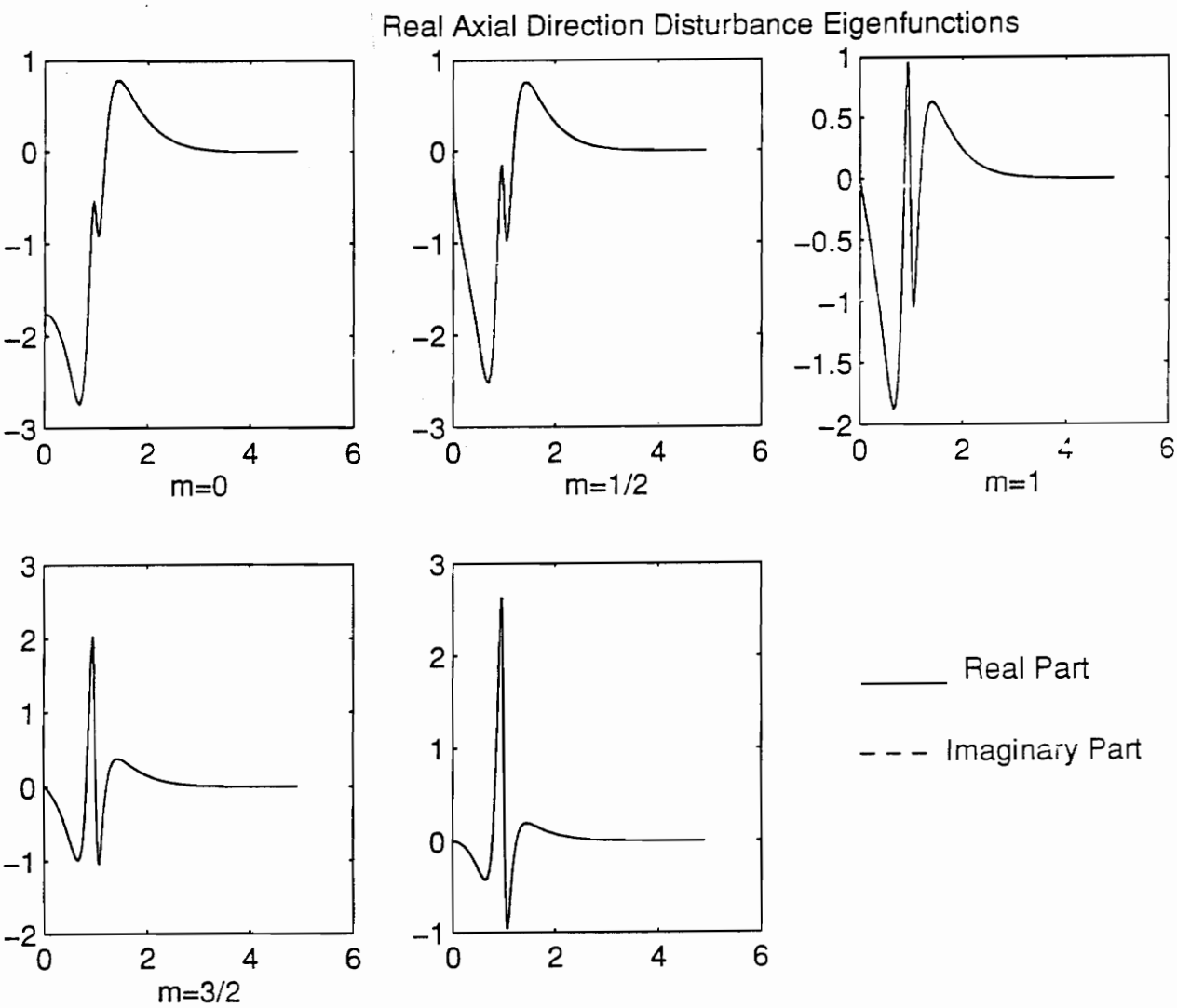
axes: radial coordinate vs. magnitude

Figure A5



axes: radial coordinate vs. magnitude

Figure A6



axes: radial coordinate vs. magnitude

Figure A7

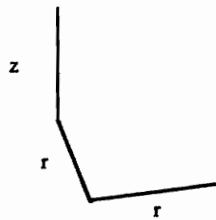
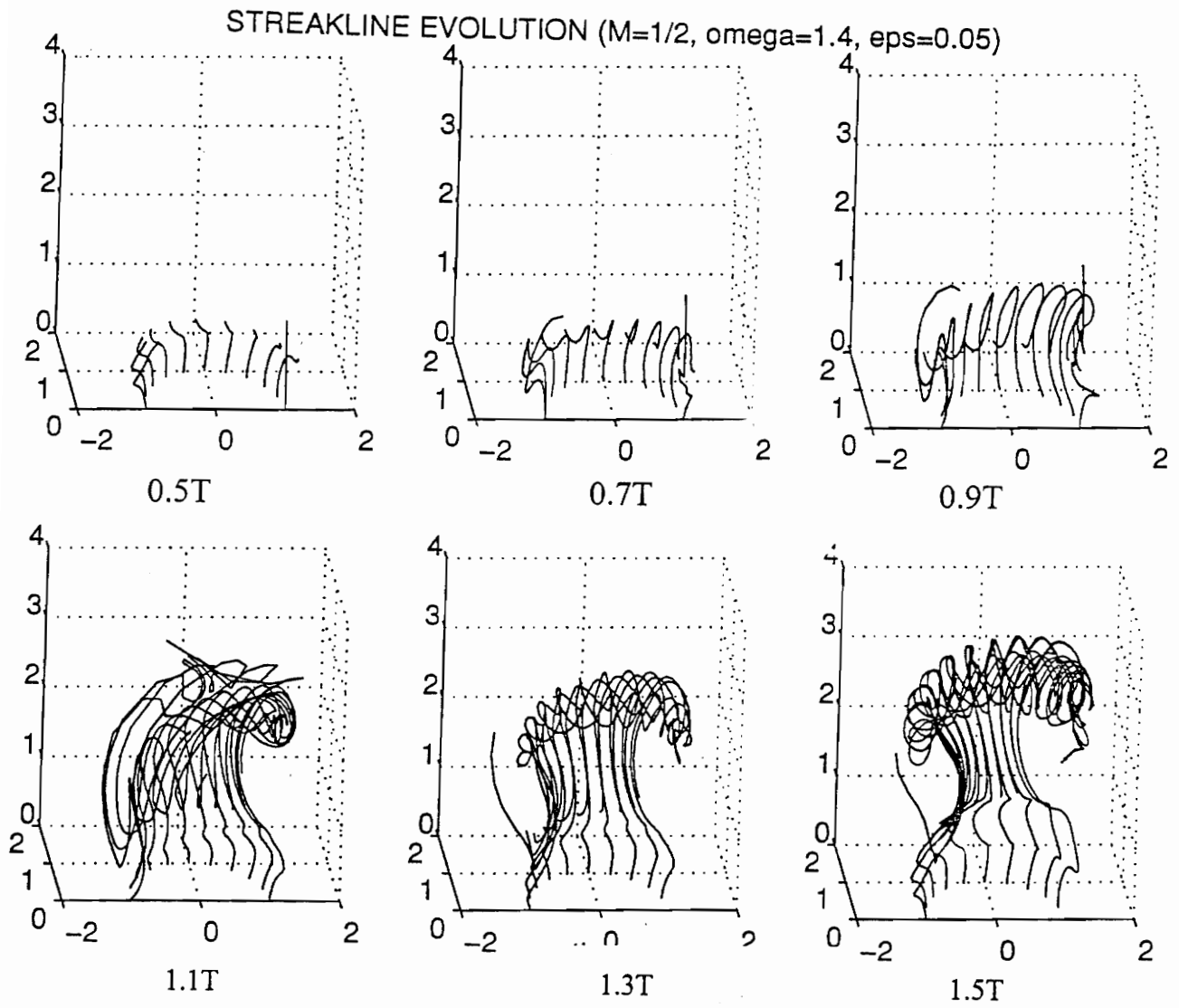


Figure A8

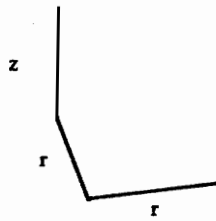
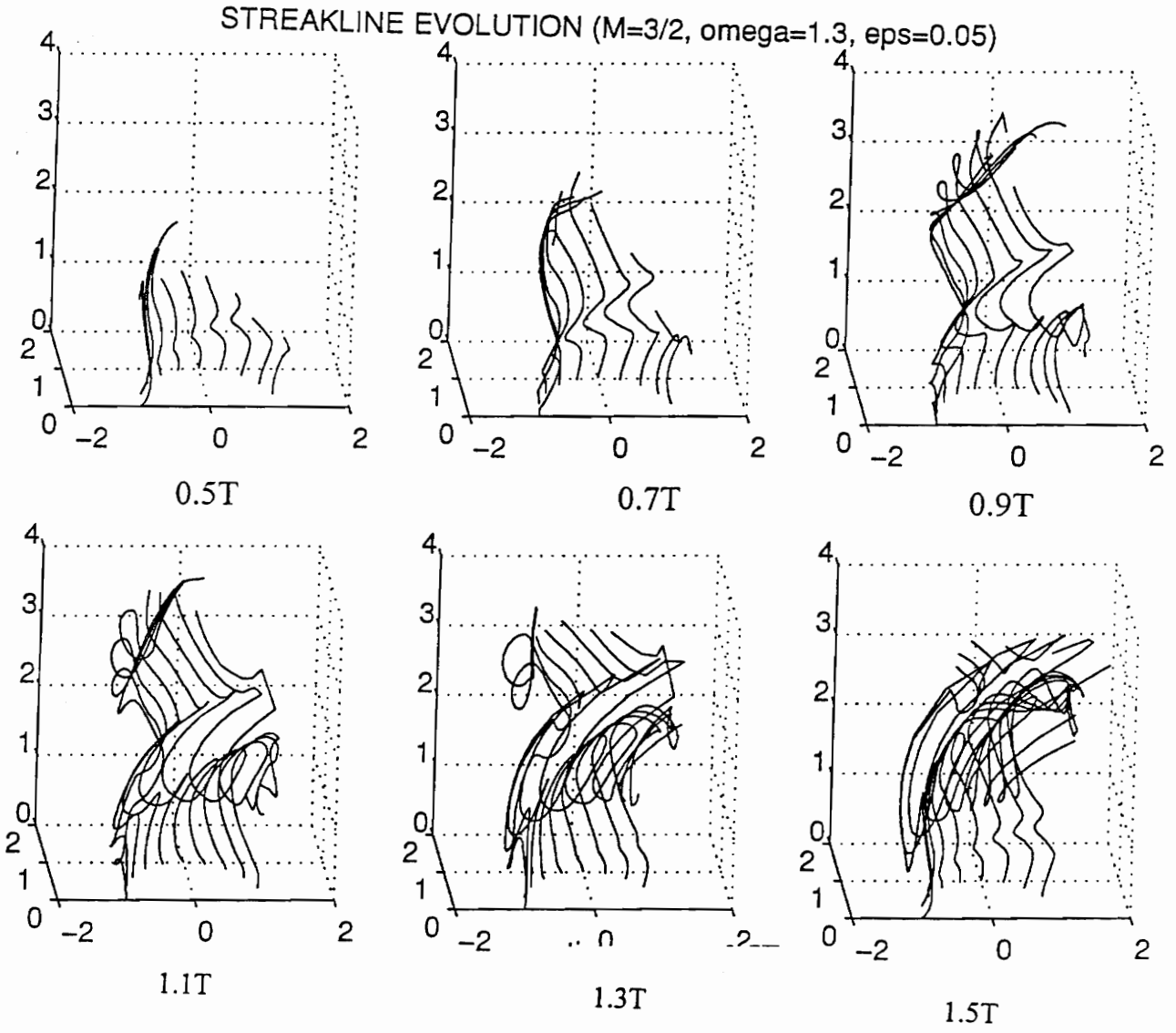


Figure A9

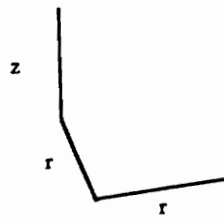
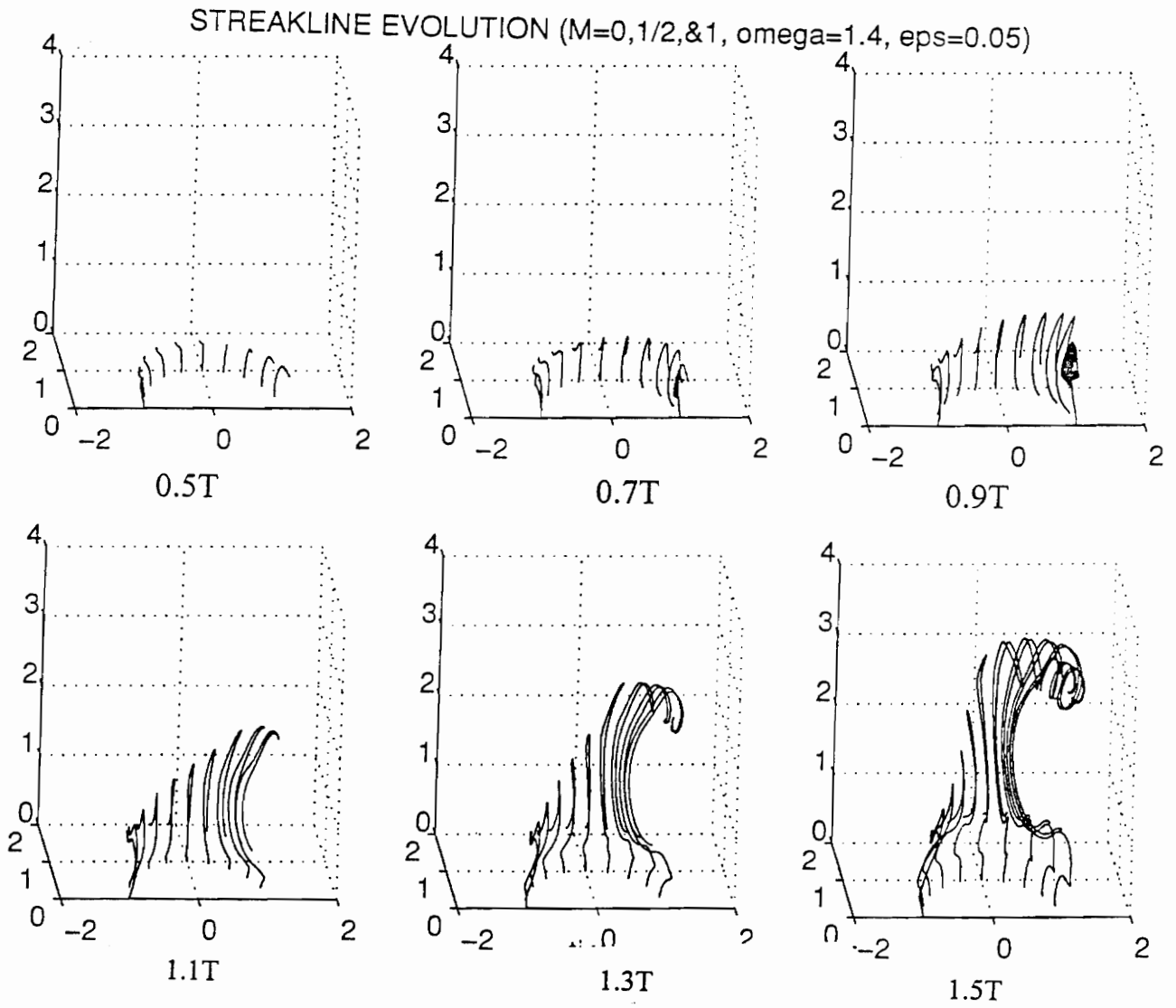


Figure A10

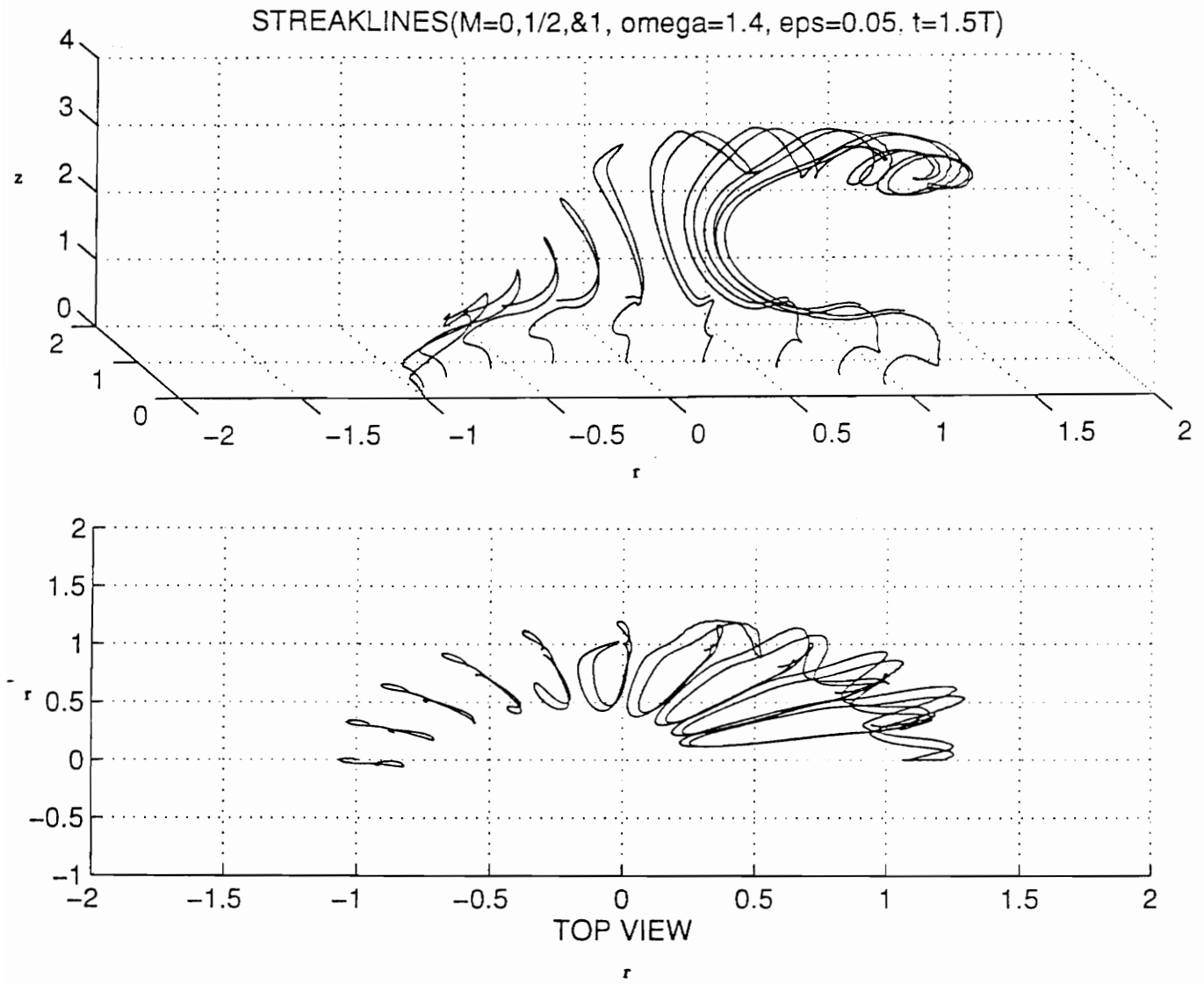


Figure A1

Modified Bessel Functions of Increasing Order

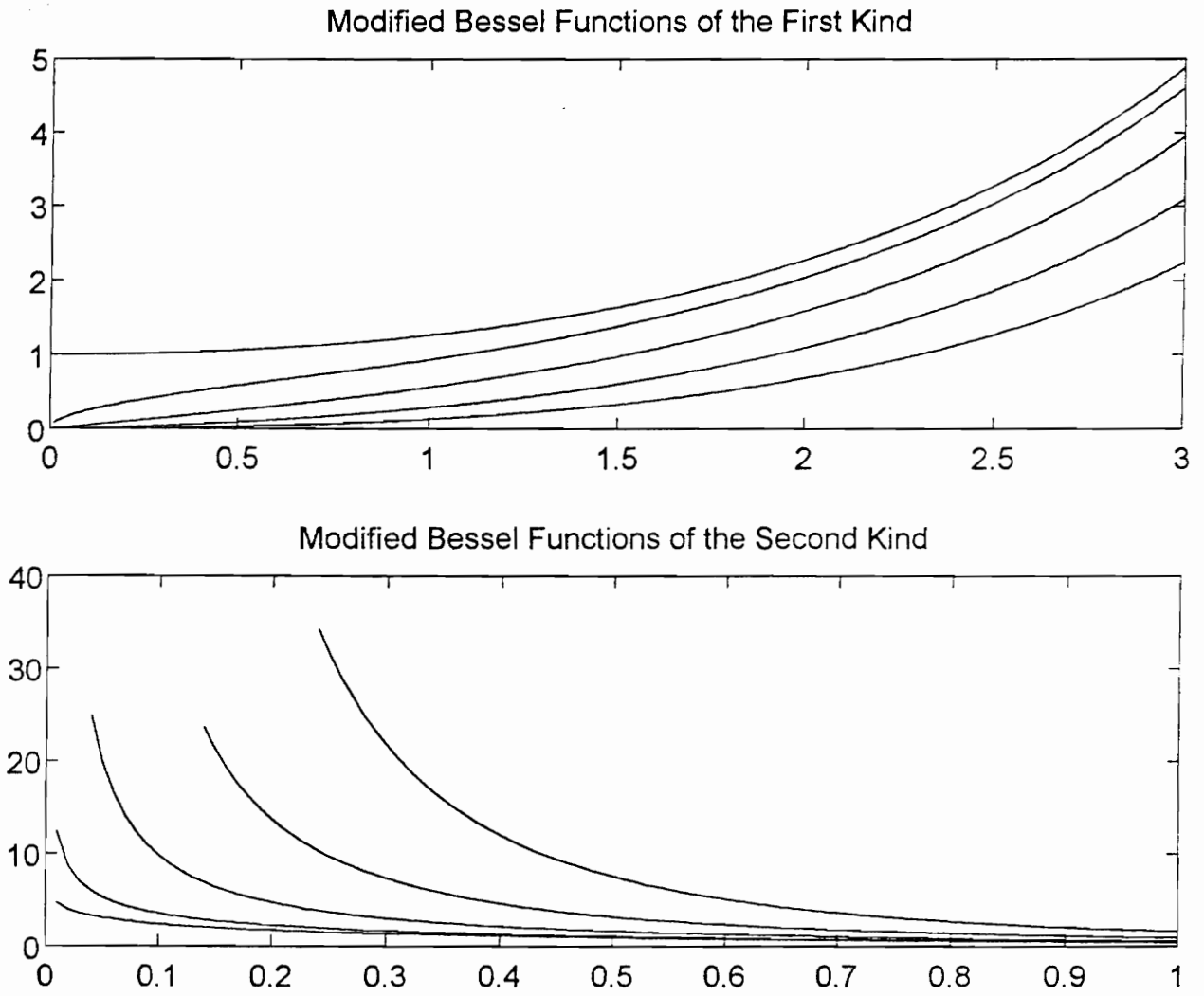


Figure A2

GROWTH RATES

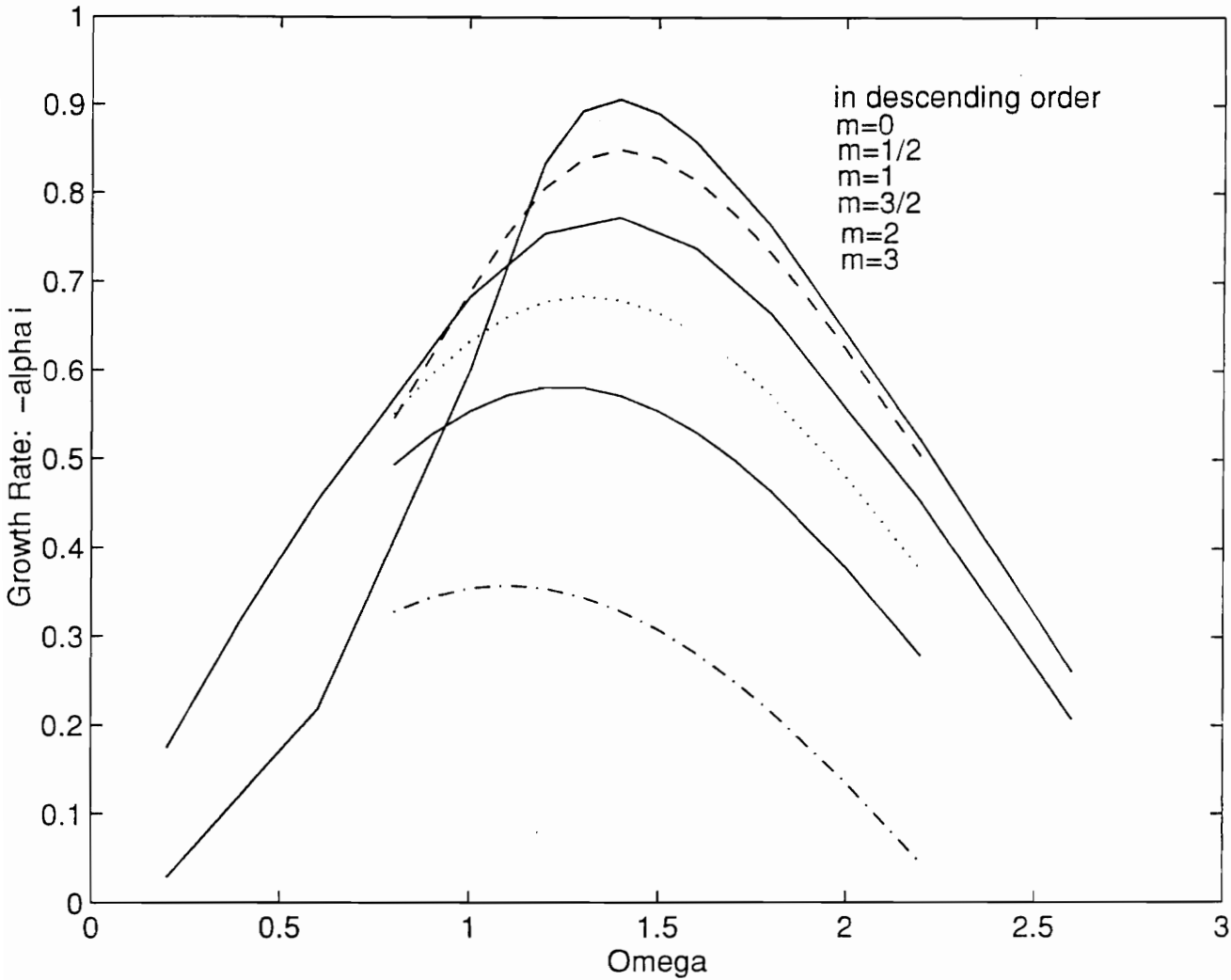
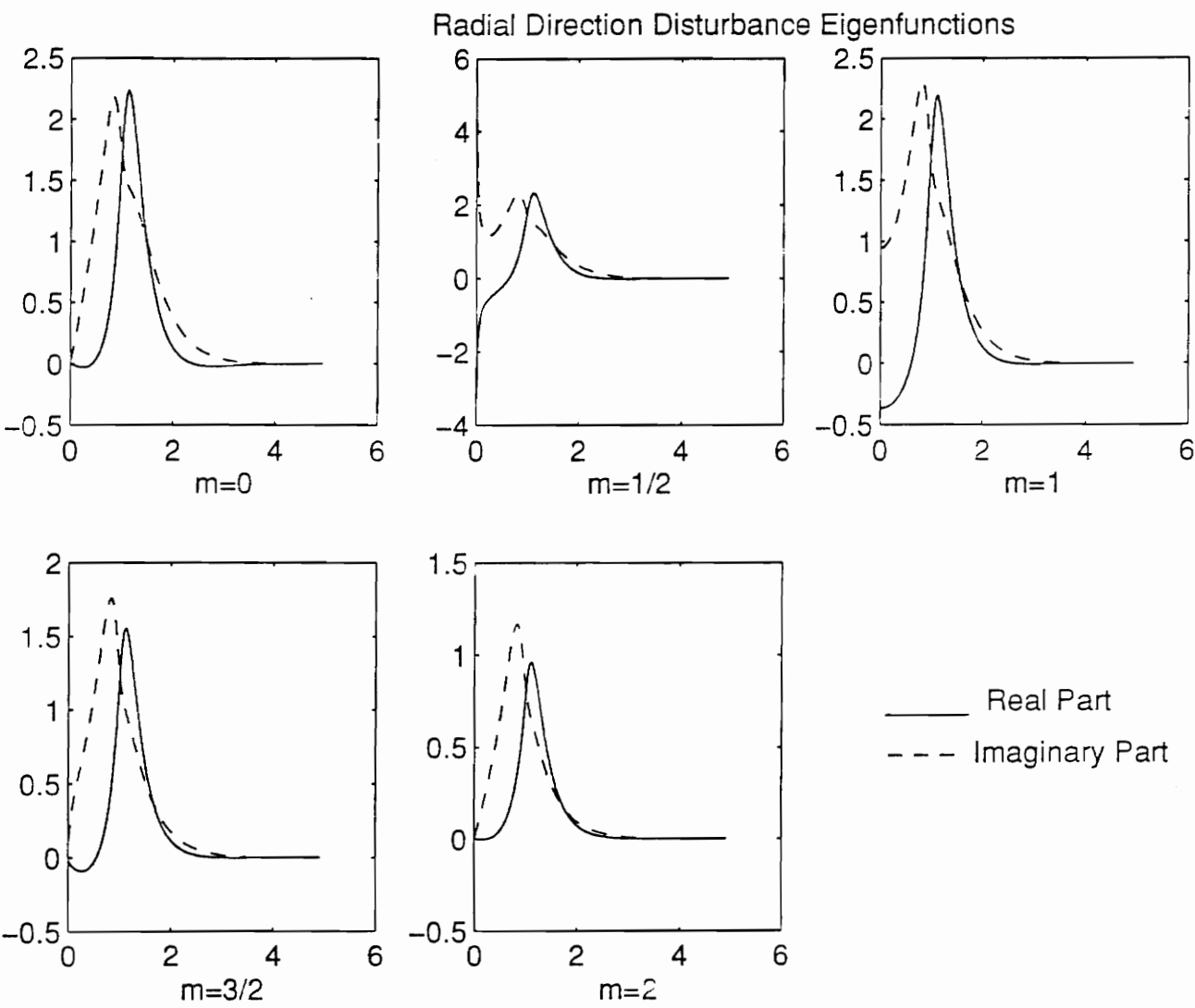


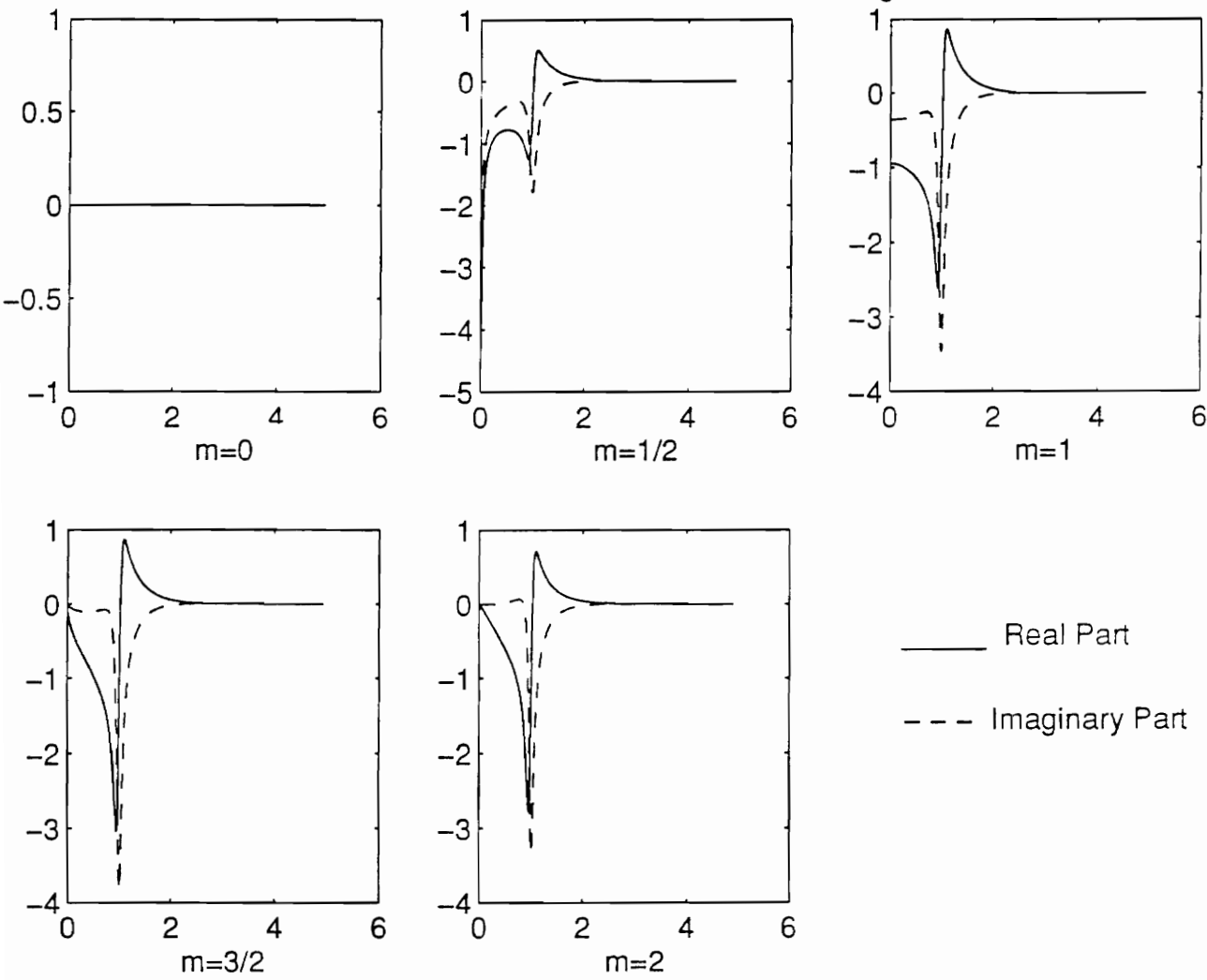
Figure A3



axes: radial coordinate vs. magnitude

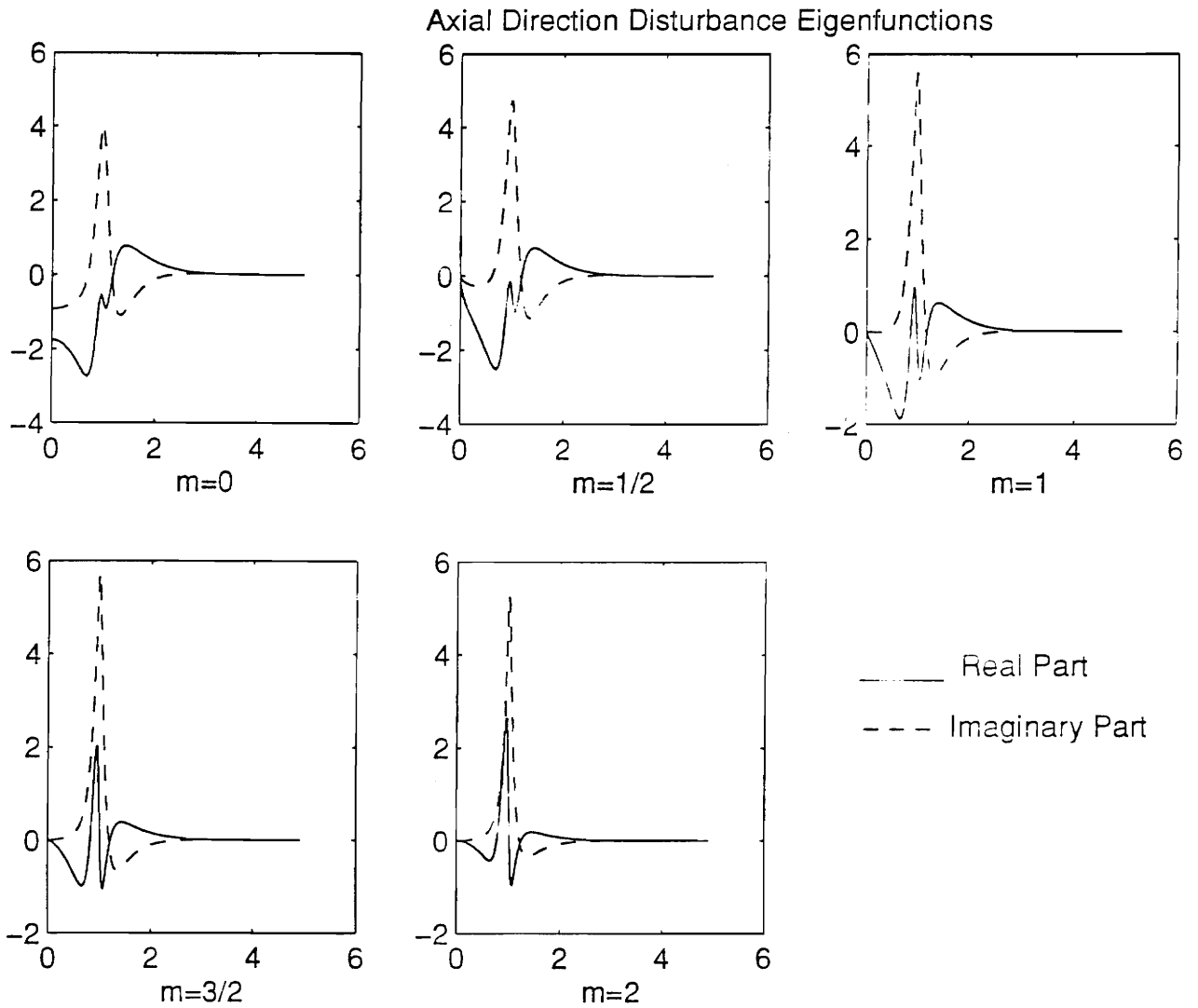
Figure A4

Azimuthal Direction Disturbance Eigenfunctions



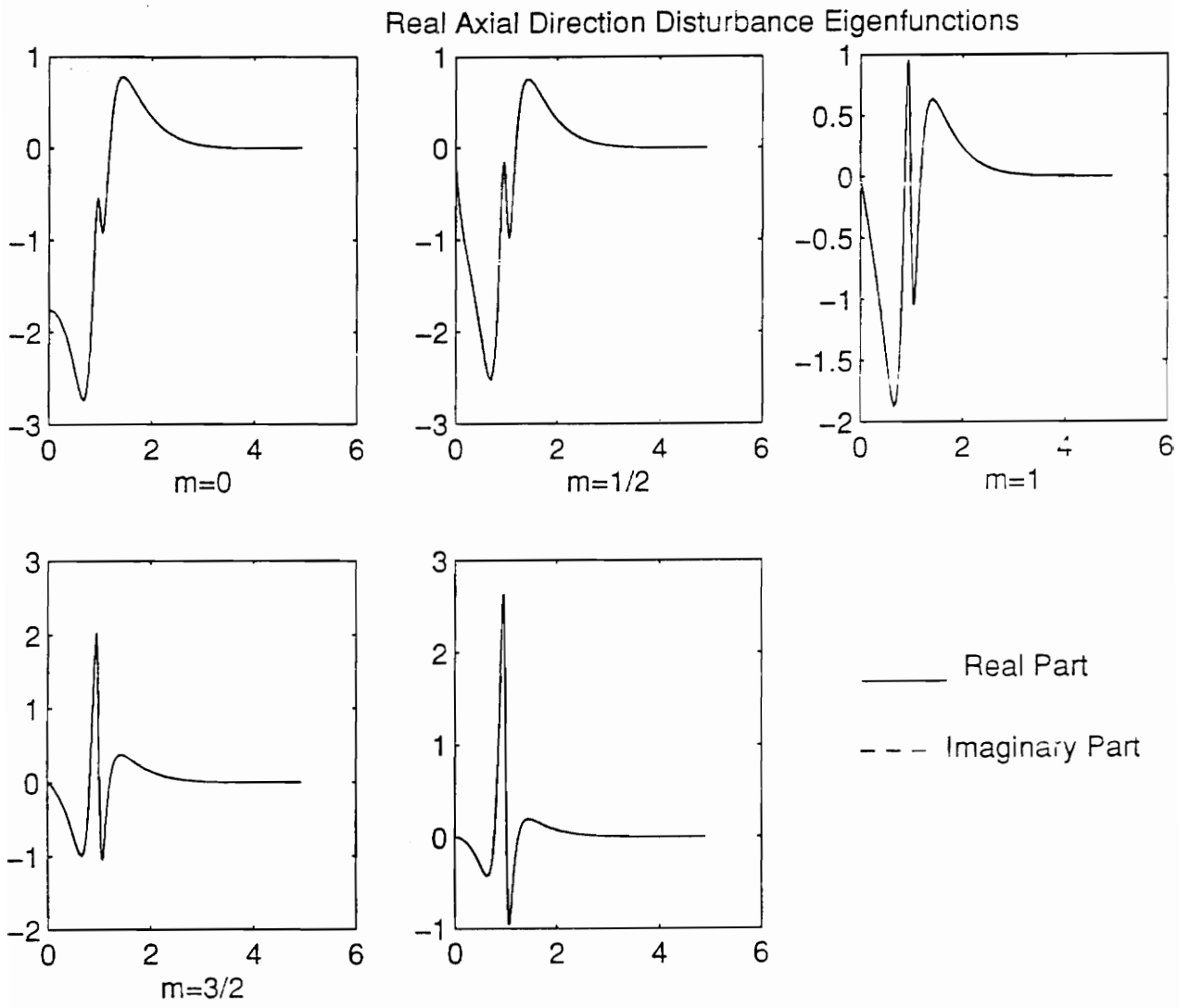
axes: radial coordinate vs. magnitude

Figure A5



axes: radial coordinate vs. magnitude

Figure A6



axes: radial coordinate vs. magnitude

Figure A7

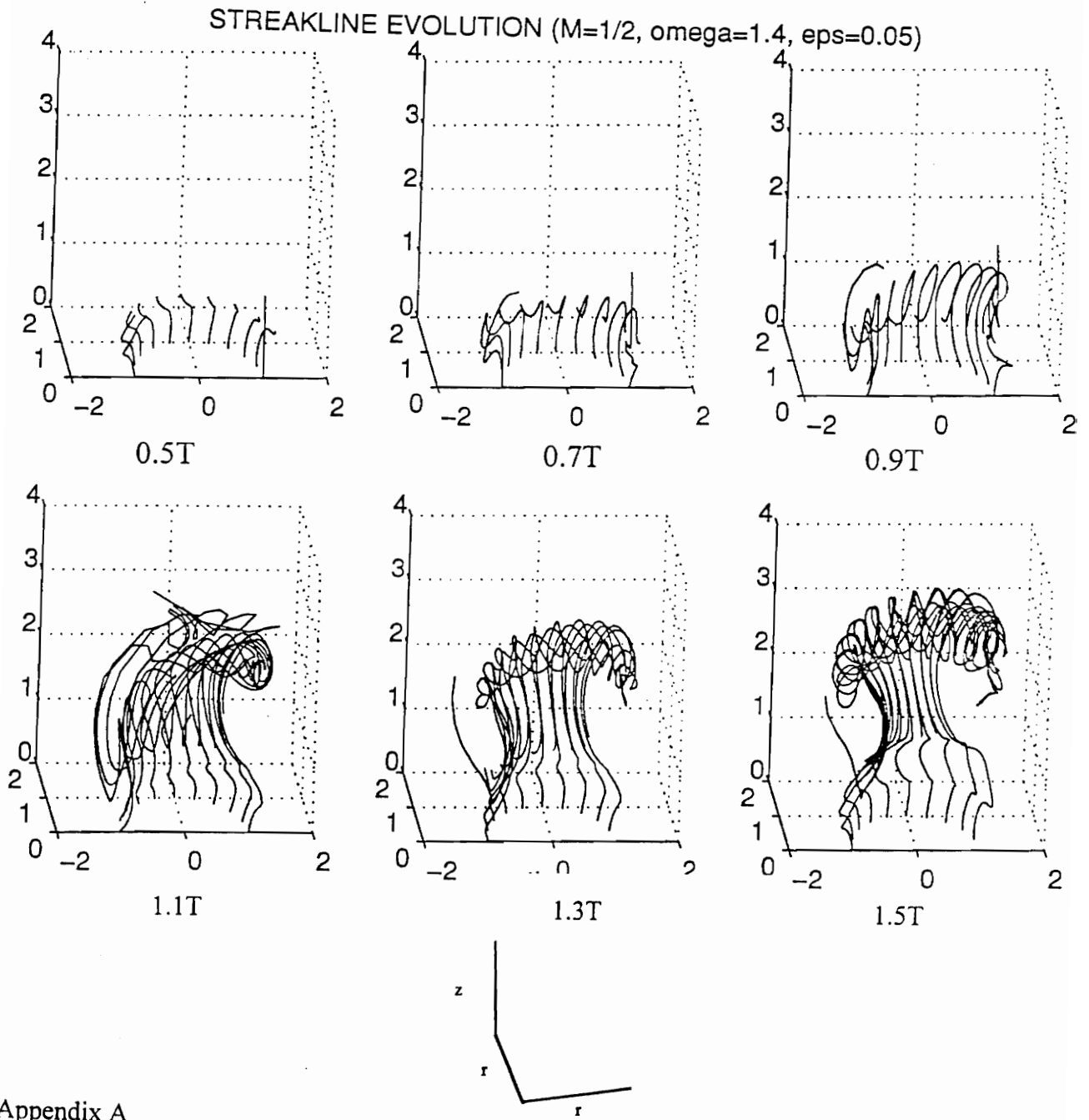


Figure A8

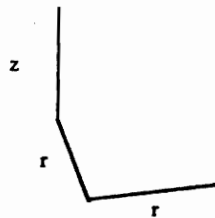
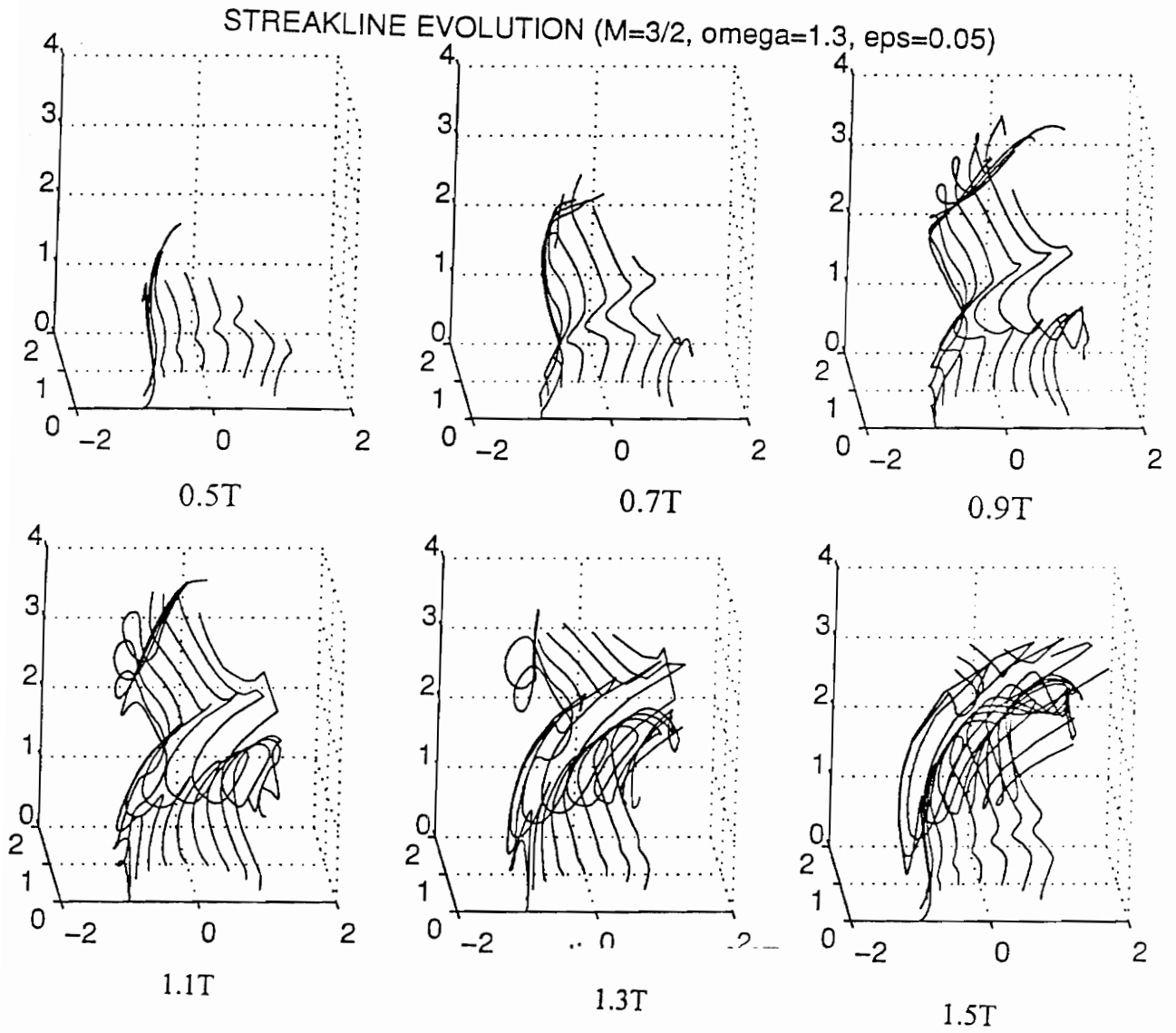


Figure A9

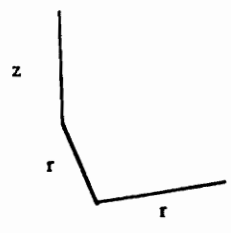
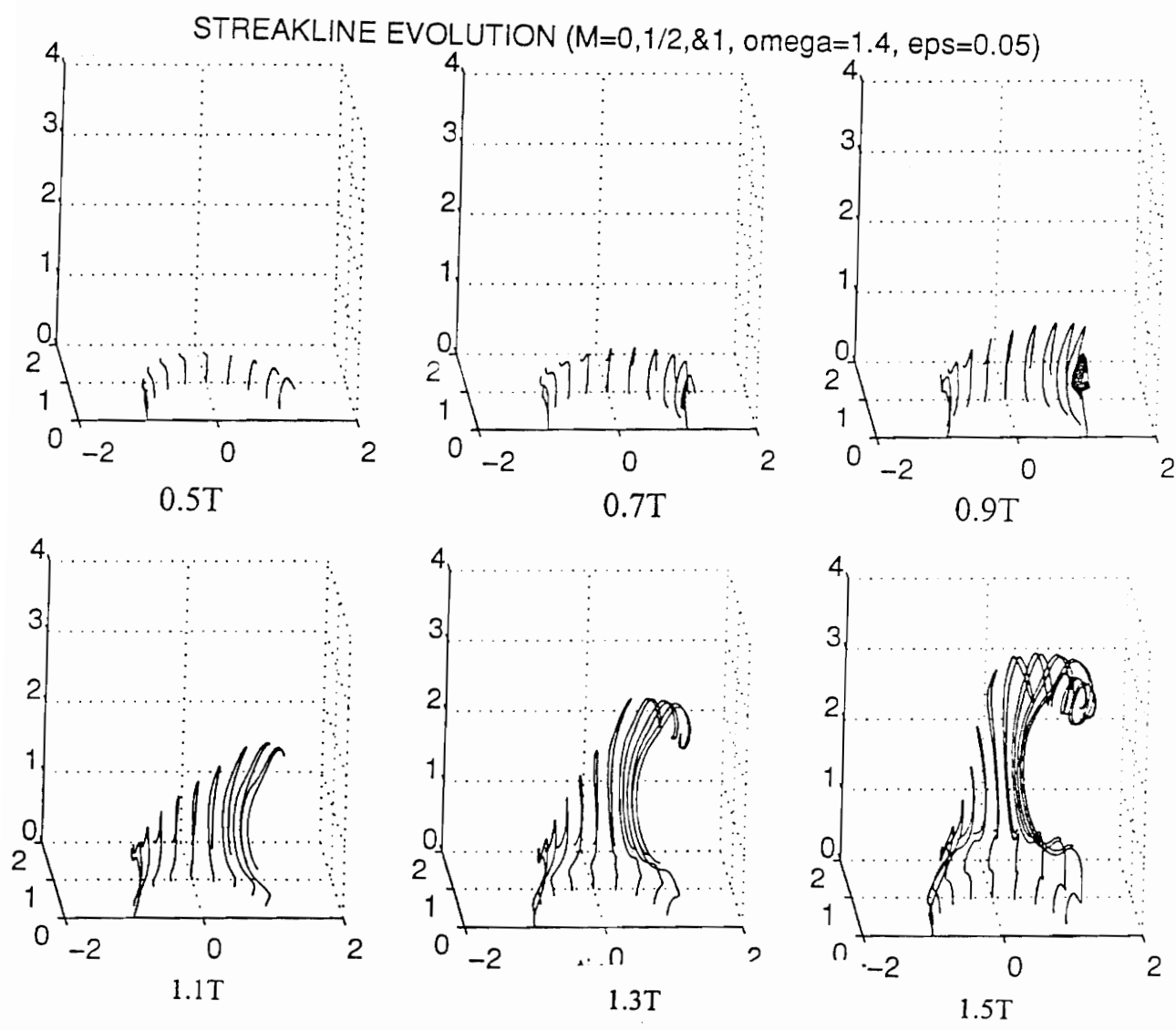


Figure A10

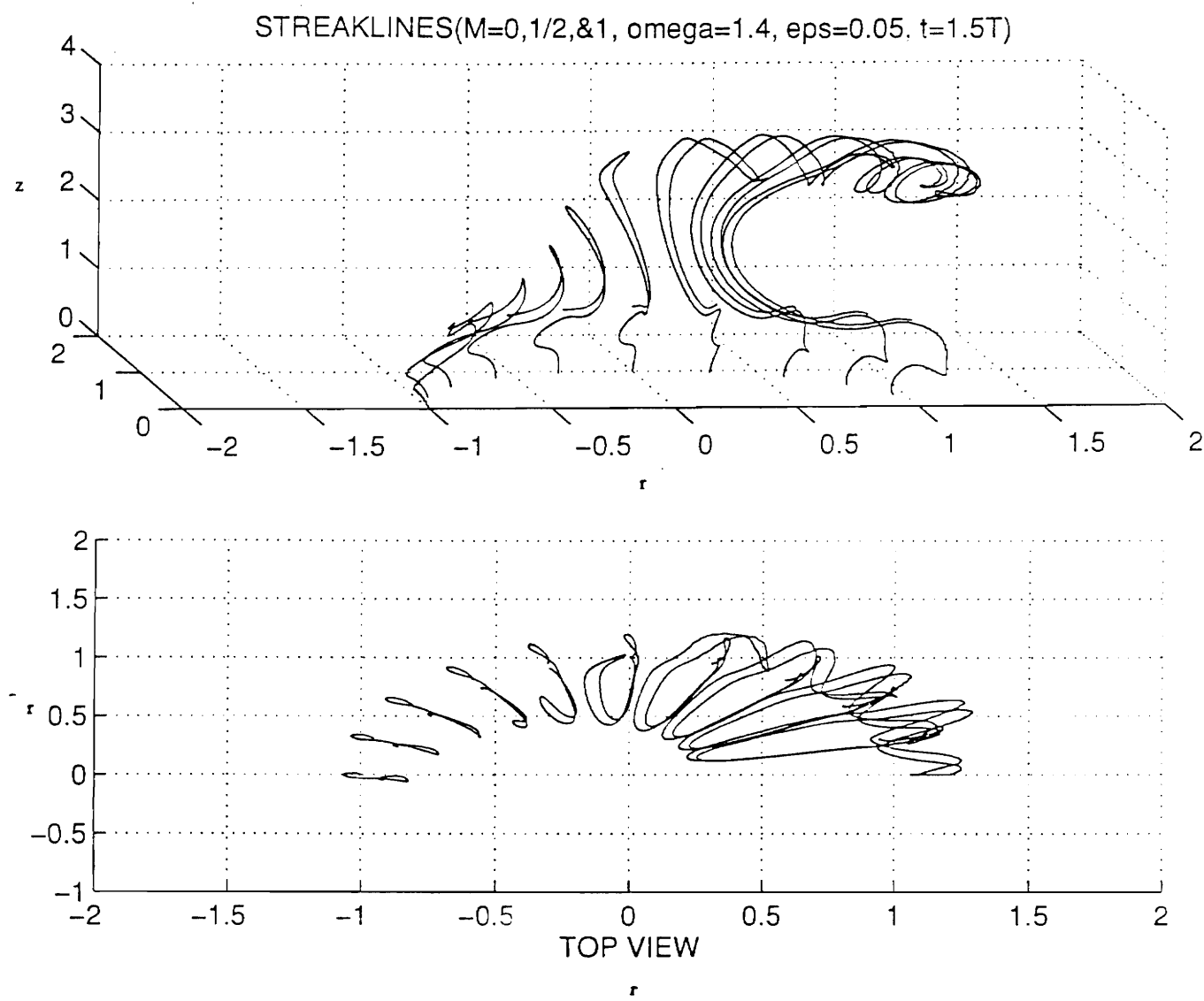
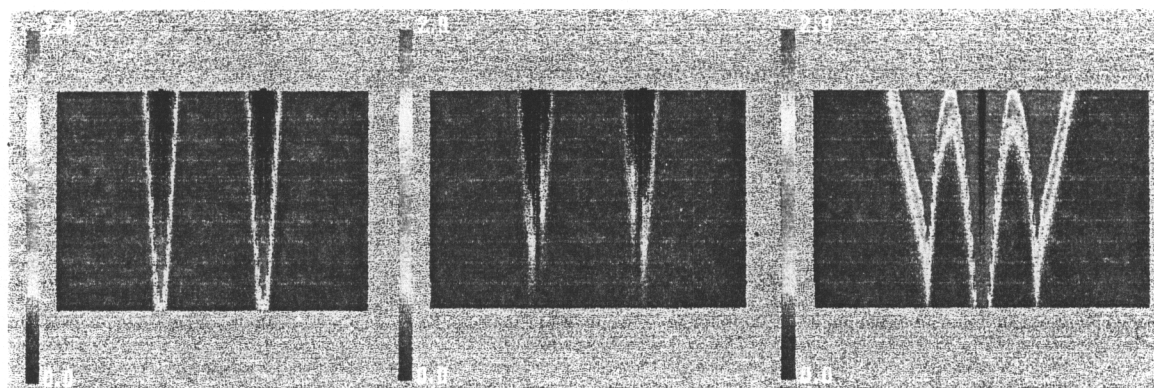
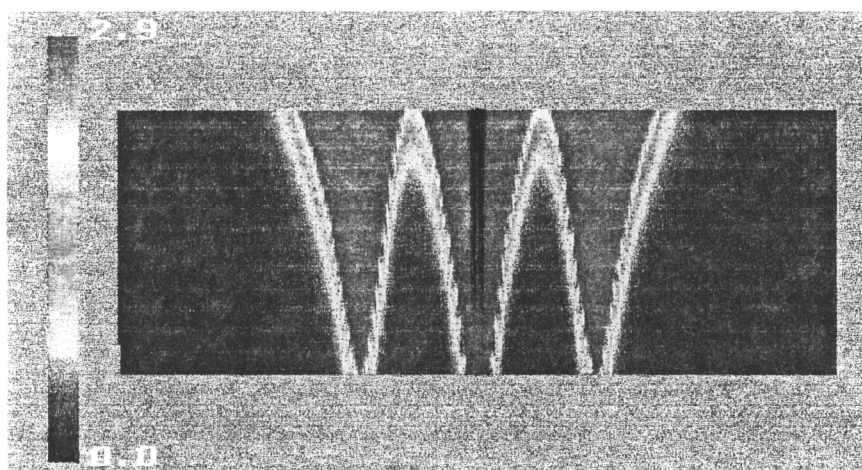


Figure A11
AVERAGE VORTICITY **M=1/2**



radial component azimuthal component axial component

**Total Average
Vorticity**



**Surface
Mesh**

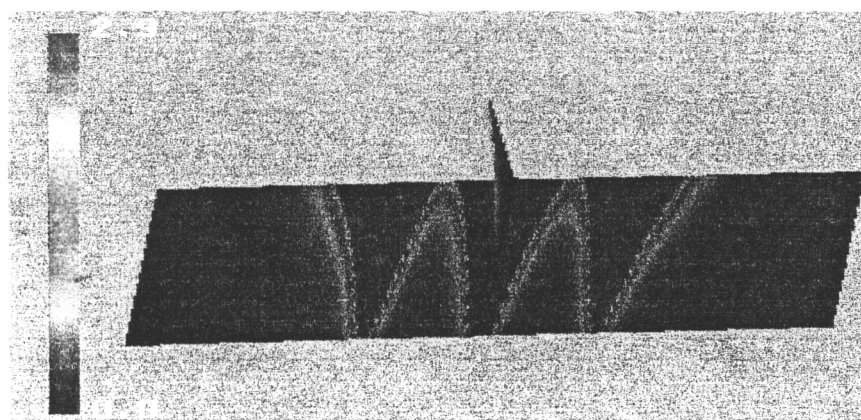
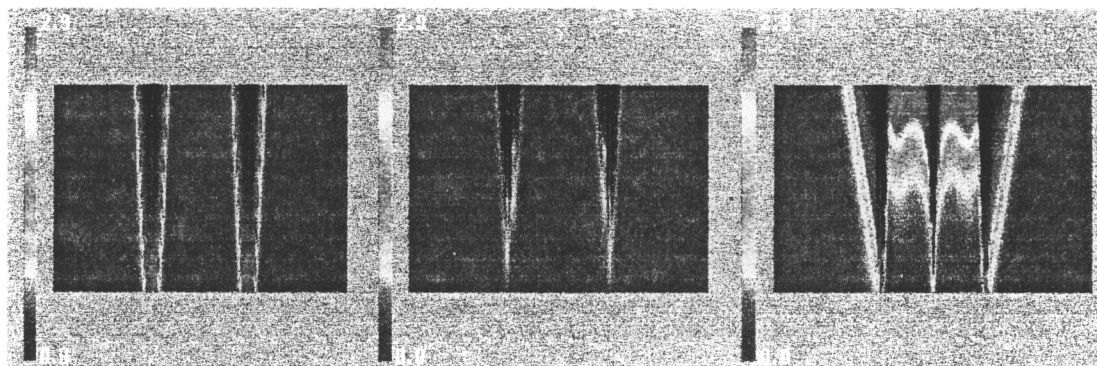
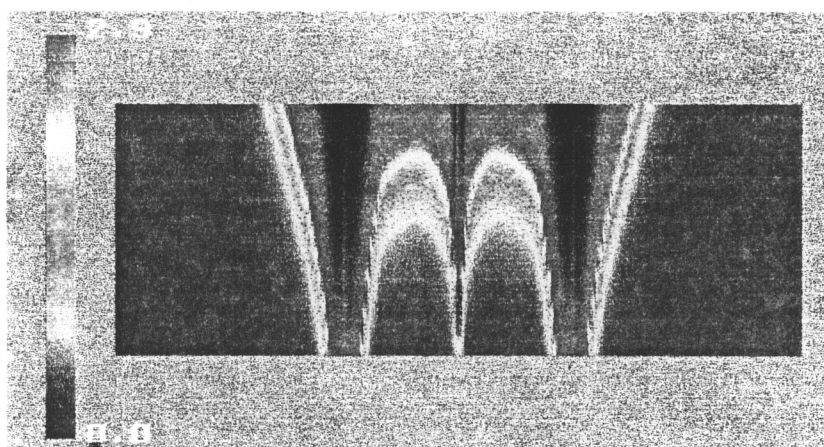


Figure A12
AVERAGE VORTICITY **M=3/2**



radial component azimuthal component axial component

**Total Average
Vorticity**



**Surface
Mesh**

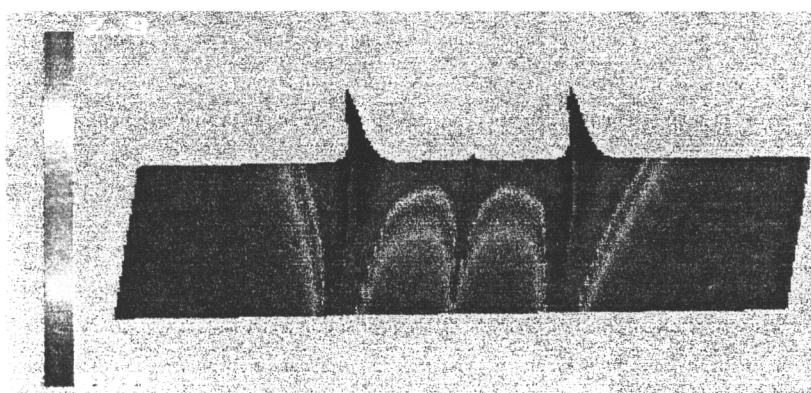


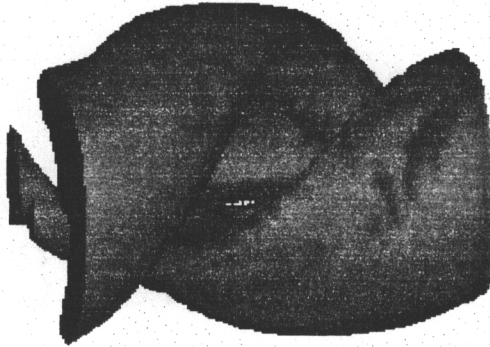
Figure A13

SURFACE OF CONSTANT VORTICITY

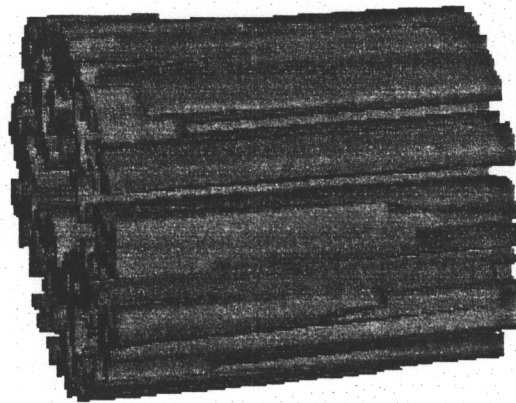
$M=3/2$

TIME=1.1T

Radial
Component



Azimuthal
Component



Axial
Component

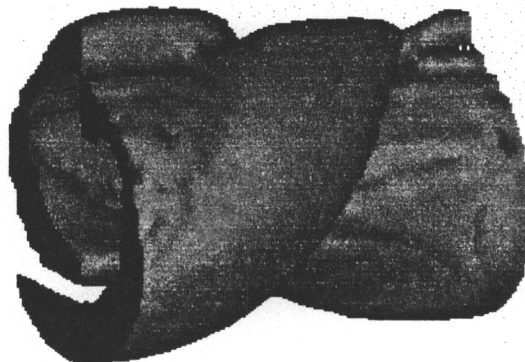
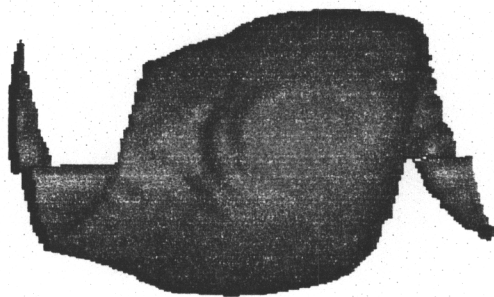
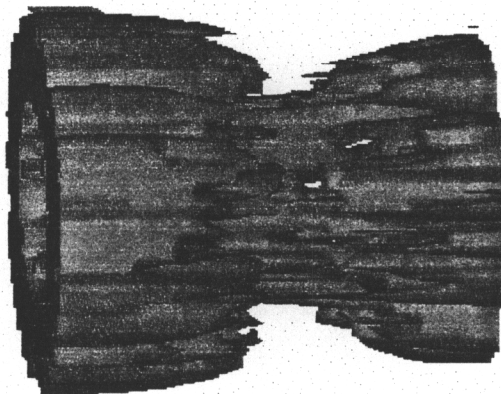


Figure A14
SURFACES OF CONSTANT VORTICITY
TIME=1.3T M=0&1/2

Radial
Component



Azimuthal
Component



Axial
Component

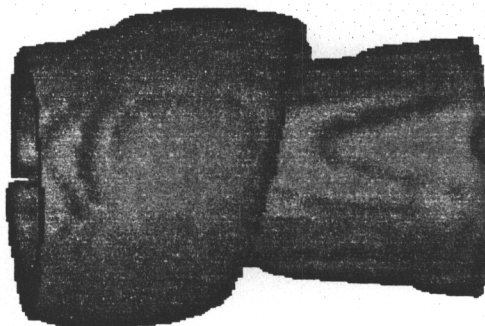


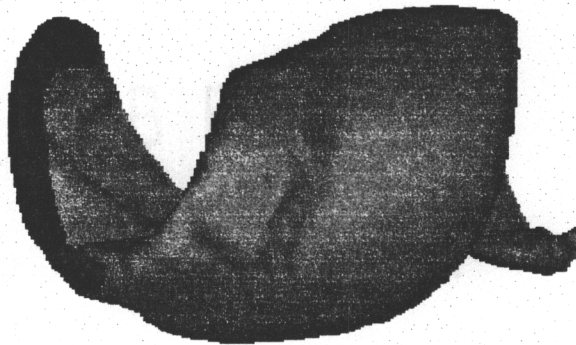
Figure A15

SURFACES OF CONSTANT VORTICITY

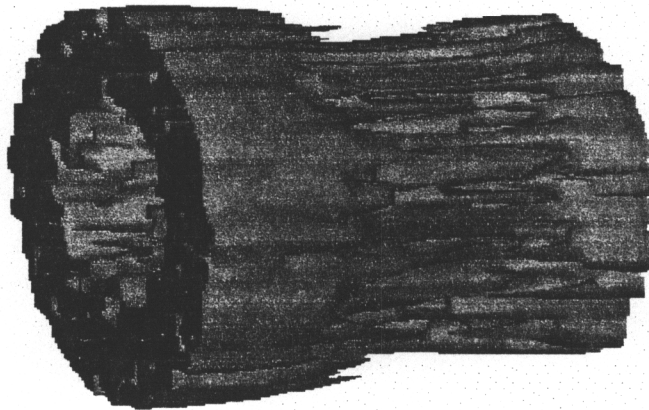
TIME=1.3T

M=0, 1/2, & 1

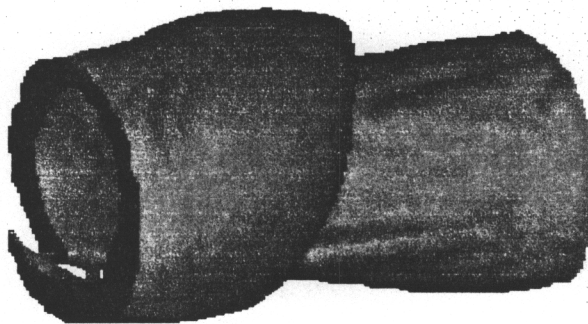
Radial
Component



Azimuthal
Component



Axial
Component



VITA:

The Author was born on April 13, 1972, to James W. and Marcia P. Leimkuhler in Woodbury, New Jersey. He lived in Princeton Junction, New Jersey until 1980, when he and his family moved overseas to Saudi Arabia for five years. In 1985, he returned to Princeton Junction, where he attended West Windsor-Plainsboro High School. Upon graduating in 1990, the Author enrolled in Ohio University earning a Bachelor of Science degree in mechanical engineering, and graduating in the class of 1994. In the Fall of that same year, the Author began his graduate education at Virginia Polytechnic Institute and State University. Upon completion of his Master of Science, he will begin a career in mechanical engineering at Westinghouse Electronic Systems Group in Baltimore, Maryland.

Matt Leimkuhler